Non-Classical Studies for Cyclic Preferential Crystallization of a Stable Racemic Compound

Lina Harfouche

Normandie Université

THÈSE EUROPÉENNE

Pour obtenir le diplôme de doctorat européen

Spécialité chimie des matériaux

Préparée au sein de l'Université De Rouen Normandie

Non-Classical Studies for Cyclic Preferential Crystallization of a Stable Racemic Compound

Présentée et soutenue par
Lina HARFOUCHE

Thèse soutenue publiquement le 26 Mai 2020 devant le jury composé de		
Mme. M. Ermelinda S. EUSÉBIO	Professor, University of Coimbra, Portugal	Rapporteur
M. Tom LEYSSENS	Professor, Université catholique de Louvain, Belgium	Rapporteur
M. Arnaud GRANDEURY	PhD, Senior Scientist, Novartis, Switzerland	Examinateur
M. Gérard COQUEREL	Professor, Université de Rouen, France	Examinateur
M. Clément BRANDEL	PhD, Assistant professor, Université de Rouen, France	Examinateur
M. Yohann CARTIGNY	PhD, Assistant professor, Université de Rouen, France	Examinateur

Thèse dirigée par Prof. Samuel PETIT et Dr. Yohann CARTIGNY, Laboratoire Sciences et Méthodes Séparatives (EA 3233 SMS)

UNIVERSITÉ DE ROUEN NORMANDIE

ED PSIME

SMS Sciences et Méthodes Séparatives

core Continuous Resolution and Deracemization of Chiral Compounds by Crystallization

funding Scheme
Marie Skłodowska-Curie Innovative Training Network
Call part identifier: H2020-MSCA-ITN-2016
Project Number: 722456 CORE

With love,

To My Godson,

Anthony

ACKNOWLEDGEMENTS

First, I would like to express my sincere gratitude to my supervisors, Prof. Samuel Petit and Dr. Yohann Cartigny for their patience, motivation, enthusiasm, and knowledge. Their encouragement, support and guidance gave me confidence and provided me with the motivation I needed to overcome challenges. I have been fortunate to work with you and benefit from your expertise.

I wish to express my appreciation to Dr. Clément Brandel for the continuous support of my PhD study and research. He guided and encouraged me to be more rigorous. Thank you for your persistent help.

I extend my sincere gratitude to Prof. Gérard Coquerel, the Head of the SMS Laboratory. He is a responsible and resourceful professor. I appreciate his valuable guidance through the many interesting and helpful discussions.

I am also grateful to Dr. Nicolas Couvrat and Dr. Morgane Sanselme, for all their kindness and help. They are highly motivated, and they have many interesting ideas and suggestions.

I gratefully acknowledge the funding received for my PhD from the 'Marie Skłodowska-Curie Innovative Training Network'.

During my PhD project, I had the great pleasure to work with very dedicated, and talented colleagues at the SMS lab, Strathclyde University, Max Planck Institute, Corbion and last but not least, the "CORE family" (the list is long, but you know yourselves). To all of them: I am grateful for your part in my journey, for the nice memories we have together and for the rewarding discussions.

I am deeply grateful to my parents, my sister and all my family. You always believed in me - not only during my PhD, but during my whole life. Thanks for your endless love, infinite support, and constant encouragement.

Finally, I wish to thank my love Lavinius. Your relentless love and support were my source of inspiration and made this journey easier. Thanks for your encouragement and support, in success as well as in failure. Thanks for keeping me smiling and happy every day.

TABLE OF CONTENTS

LIST OF FIGURES

LIST OF TABLES

LIST OF ABBREVIATIONS AND SYMBOLS

API	Active pharmaceutical ingredient
AS3PC	Auto seeded polythermic programmed preferential crystallization
C_o	Initial concentration
DCM	Dichloromethane
DMF	Dimethylformamide
DMSO	Dimethyl sulfoxide
DPL	Diprophylline
DSC	Differential scanning calorimetry
ee	Enantiomeric excess
EtOH	Ethanol
FDA	Food and Drug Administration
FTIR	Fourier-transform infrared spectroscopy
G	Free energy
h	Hours
C-HPLC	Chiral high-performance liquid chromatography
IPA	Isopropyl alcohol
MeOH	Methanol
min	Minutes
mL	Milliliter
mp	Melting point
MSZW	Metastable zone width
MTBE	Methyl tert-butyl ether
$O.P._{c.s}$	Optical purity of the collected solid
P3D	3-(2-Propylphenoxy)-propane-1,2-diol
PC	Preferential crystallization
PE	Pure enantiomer of proxyphylline
Pr	Productivity
PXL	Proxyphylline

R	Universal gas constant
R/*S*	The enantiomeric form
RS	The racemic form
*s**	Solubility
S3PC	Seeded polythermic programmed preferential crystallization
SA	Salicylic acid
SCM	Super cooled melt
SCXRD	Single crystal X-ray diffraction
s.d.	Standard deviation
SHG	Second harmonic generation
SIPC	Seeded isothermal preferential crystallization
T	Temperature
T_B	Highest temperature of the AS3PC process (a suspension is obtained)
T_F	Lowest temperature of the preferential crystallization process
T_{Homo}	Temperature of homogenization of the system
$t_{(process)}$	Time between seeding the medium and filtration
$V_{solvent}$	[L] The solvent volume
T_c	Crystallization temperature
T_t	Transition temperature
T_f^{onset}	Melting (fusion) temperature
t_i	Induction time
THF	Tetrahydrofuran
vdW	van der waals
$W_{C.S.}$	Weight of collected solid
$W_{P.E.}$	Weight of pure enantiomer
W_{seeds}	Weight of seeds
X_{mol}	Mole fraction
Y_{exp}	Experimental yield
Y_{theo}	Theoretical yield

β	Supersaturation
ΔH_{fus}	Molar enthalpy of fusion
^{o}C	Degrees Celsius
^{1}H NMR	Proton nuclear magnetic resonance

GENERAL INTRODUCTION

In the pharmaceutical industry, around 56% of the marketed drugs are chiral compounds.[1] Around 80% are formulated as racemic mixtures, *i.e.* equimolar mixtures of both enantiomers.[2] The US Food and Drug Administration (FDA) recommends the assessment of the biological activity of each antipode since their biological activities (*e.g.* toxicity) can be different.[3] Due to these requirement, the interest of obtaining pure enantiomers of chiral drugs is growing rapidly. The goal is to obtain effective and safer drugs.[4] The single-enantiomer drug sales reached $225 billion dollars worldwide in 2005.[5] It was estimated that this class of drugs would grow at an average annual rate of 11.4%.[6] This leads us to the research objective of the CORE Network to jointly construct an industrial toolbox on continuous resolution that provides next generation tools, approaches and methods to industry. This thesis will provide a novel approach for the use of continuous enantioselective crystallization processes on racemic compounds.

Different methods exist for the separation of enantiomers, and can be classified in four categories:

i. Chiral enzymatic separation using stereoselective biological activity.[7]
ii. Separation of racemic compounds using columns with chiral stationary phases (chiral chromatography).[8]
iii. Direct asymmetric synthesis of optically pure compounds using catalyst or chiral precursors.[9]
iv. Crystallization methods, sometimes combined with the racemization of the undesired enantiomer (*i.e*. the distomer),[10] are further classified into two subcategories:
    a. A straightforward method used to separate enantiomers without any external additives, known as Preferential Crystallization (PC).
    b. An indirect method based on using chiral or non-chiral additives or solvents, such as formation of a diastereomeric salts or solvates or cocrystals.

Between the methods, crystallization techniques are preferred at industrial scale. They offer high selectivity, low cost, easy recycling of the solvent, low waste streams, and efficiency. These techniques are also environmentally friendly.

It is stated that PC is only applicable if the racemic mixture crystallizes as a conglomerate[11] (*i.e.* a physical mixture of homochiral particles, each enantiomer crystallizes separately). Direct PC in stable racemic compound forming systems (*i.e.* the crystal contains a lattice with a regular arrangement of both enantiomers in equal amounts) is therefore challenging in view of the much higher probability to form a racemic compound versus conglomerate.

The aim of this research is to investigate the possibility of using PC for the separation of enantiomers in a stable racemic compound system. PC will be used via two novel approaches:

i. Via a metastable conglomerate. An example in literature has shown that it is possible to perform PC in a stable racemic compound system by selecting the suitable solvent that enables access to an unforeseen metastable conglomerate.[12] The encouraging data enables to envisage that PC could be performed in more systems than previously thought.
ii. Via the use of a cocrystal obtained through the conversion of the racemic compound into a conglomerate system.

First, the fundamental prerequisites of this work, together with a literature review and a presentation of the work strategy, are presented in **Chapter 1**.

The solid-state characterization and the chiral resolution of PXL by PC under kinetic control is described in **Chapter 2** and **3** respectively. A screening methodology of different critical parameters needed to successfully apply PC on racemic compounds is also presented.

The results obtained during the cocrystal screening of PXL are presented in **Chapter 4**. The thorough characterization of the monohydrated cocrystal between PXL and salicylic acid is also discussed, together with its resolution by PC.

The conclusions and the perspectives close this manuscript.

CHAPTER 1: LITERATURE REVIEW & PRESENTATION OF THE STRATEGICAL APPROACHES

1.1 Chirality

Chirality is the property of handedness, and it is a phenomenon of great importance in biology and chemistry. If you attempt to superimpose your right hand on top of your left, the two do not match up (Figure 1.1). Any object can have this property, including molecules. In other words, an object that is chiral is an object that is not superimposable to its mirror image. If the object is superimposable to its mirror image, it is achiral.

Figure 1.1 A pair of chiral objects (hands): enantiomers.

The chiral object and its mirror image are called enantiomers, the word enantiomer being derived from the Greek word "εναντιοζ" (enantios) meaning "opposite". Chirality often comes from the presence of an asymmetric atom, which is called the chiral center or the stereogenic center.[13] Both enantiomers of a molecule are designated according to Cahn-Ingold-Prelog convention which assigns the letters *R* or *S* (from the Latin *rectus* = right and *sinister* = left) to the chiral center.[14] One of the two enantiomers rotates the plane of polarized light clockwise, therefore it is assigned to the optical descriptor (+) or D (dextrorotatory), while the other is described as (-) or L (levorotatory), which corresponds to the anticlockwise rotation (Figure 1.2). Two enantiomers have identical physical and chemical properties but may behave differently in chiral media, giving rise to different biological properties.[15]

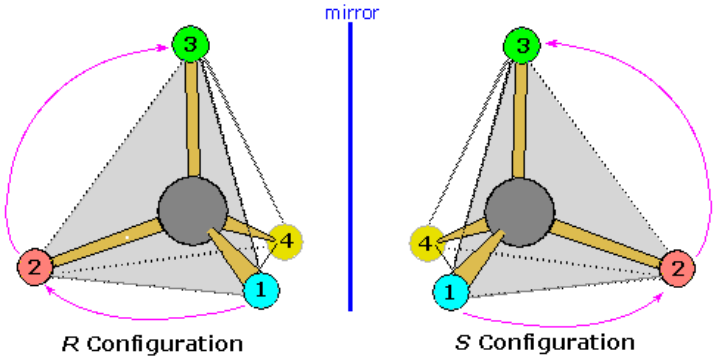

Figure 1.2 Enantiomers classified based on their opposite specific rotation used to distinguish between the (*R*) and (*S*) enantiomers.

Measurement of enantiomeric purity of a mixture of enantiomers is often evaluated by the enantiomeric excess (ee). It describes the excess of one enantiomer of the other. For example, the ee of a 1:1 substance is 0%, and is called racemic, while an ee of 100% refers to an enantiopure sample. *ee* is calculated using the following equation:

$$\text{Enantiomeric excess (ee) (\%)} = \frac{|[R]-[S]|}{[R]+[S]} \times 100 \qquad (1)$$

With [*R*] and [*S*], the amounts of enantiomer (*R*) and (*S*) respectively.

1.2 Application of chirality in pharmaceutical industry

In the pharmaceutical industry, 56% of the drugs currently in use are chiral and 88% of these molecules are marketed as racemic compounds (consisting of an equimolar mixture of two enantiomers).[16] Also, most agrochemicals (insecticides, herbicides…), fragrances, flavors and food are chiral molecules.[17] On the other hand, almost all-natural compounds found in nature are under pure enantiomeric form. For example, sugar like deoxyribose and ribose in DNA and RNA are right-handed, and all proteins are made exclusively from L α-amino acids. Actually, without such a uniform chirality, current life could not exist.

Manufacturers became interested in marketing chiral solids under their pure enantiomeric form. This is called 'chiral switching'[18] and it has been claimed that it will bring clinical benefits in terms of improved efficacy, more predictable pharmacokinetics or reduced toxicity.[19] Many examples exist in literature describing toxicity of many chiral drugs like ketamine (anesthetic), penicillamine[20] (chelating agent), ethambutol[21] (antitubercular agent) exclusively because of their distomer. For example, only *R*-(-)-ketamine (distomer) is responsible for agitation, hallucination, restlessness, in contrast to *S*-(+)-ketamine (i.e., the eutomer).[22]

The quest to enantiopurity is now at the center of academic and industrial concerns due to Food and Drug Administration and other agencies regulations,[23] which requires the development of new chiral drugs as single enantiomers.

1.3 Solid state of chiral molecules

1.3.1 Solid state and solid-liquid phase equilibrium

Different methods are used to identify the crystallization behavior of a chiral racemic mixture. Binary or ternary phase diagrams are widely used to establish the solid-liquid phase behavior of a mixture of two enantiomers. In 1981, Collet et al.[24] described the three fundamental racemic systems: racemic conglomerate, racemic compound and solid solution. These systems and their distinctive solid packing and binary phase diagrams are schematically described in Figure 1.3.

A racemic conglomerate is a racemic physical mixture of the two enantiomers,[25] with only a single enantiomer in each crystal (Figure 1.3 - a). Powder diffractogram of a racemic conglomerate is superimposable to that of the pure enantiomer.

Racemic compound forming systems represent the main category of racemic mixtures with 90-95% of cases. It is a 1:1 stoichiometric compound with a centrosymmetric arrangement of the enantiomers. The phase diagram is characterized by two eutectic points that are symmetric with reference to the racemic composition. X-ray diffraction patterns of the racemic compound is different from those of a pure enantiomer (Figure 1.3 - b).

The third type of chiral systems are solid solutions. It occurs when no chiral discrimination between (+) and (-) enantiomers occurs in the packing: they coexist in a completely random distribution in the crystal lattice.[24] Three types can exist in such a system (type I, II and III) depending on the melting point of the pure enantiomers versus that of the racemic solid (Figure 1.3 - c).

In addition to these different solid-state behaviors, one can also add the possible occurrence of polymorphs which further complicate the phase diagrams. From a pharmaceutical development perspective, the solid-state landscape can also be extended to solvates, cocrystals, salts or even amorphous form. The complexity of all possible situation is summarized in Figure 1.4. Polymorphs, solvates/hydrates and cocrystals will be described in the next section.

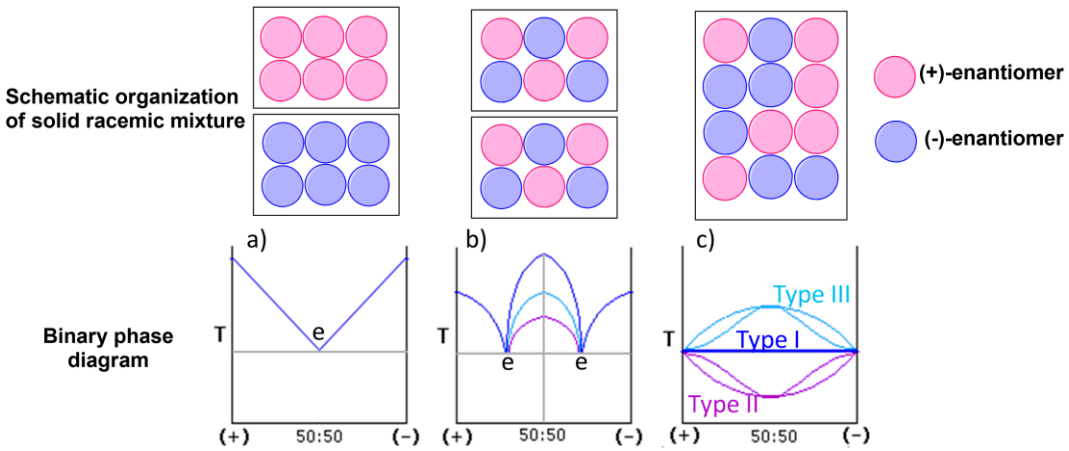

Figure 1.3 Schematic presentation of a) conglomerate, b) racemic crystal forms and c) solid solution.

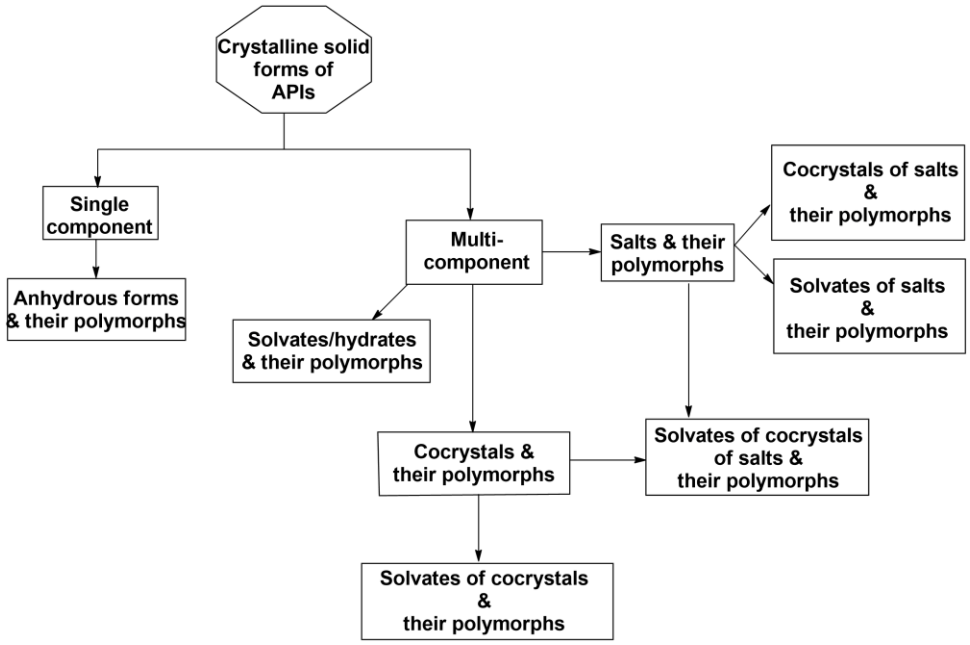

Figure 1.4 Diversity of solid forms of crystalline APIs.

1.3.2 Polymorphism

If a compound can exist in more than one crystalline solid form, those different forms are referred to as polymorphs and the phenomenon is known as polymorphism (Figure 1.5).[26] Different polymorphs may be formed as function of the crystallization conditions or of temperature, pressure, relative humidity, etc....[27,28] Different polymorphs of the same compound exhibit different properties

(solubility, melting point, density, crystal shape and arrangement, optical and electrical property, etc.).[29]

Changing the crystal form of a pharmaceutical ingredient will modify the physicochemical properties (*e.g.* solubility, stability, dissolution rate, etc.) for that drug.[30–32] Thus it is important to understand the behavior of polymorphs and their thermodynamic stability.

Two types of polymorphism exist: (i) conformational polymorphism[33] and (ii) packing polymorphism.[34,35] The first one occurs when relatively flexible molecules adopt different conformations in different crystal structures.[36] If polymorphism occurs only because of packing differences, the polymorphism is called packing polymorphism.[37]

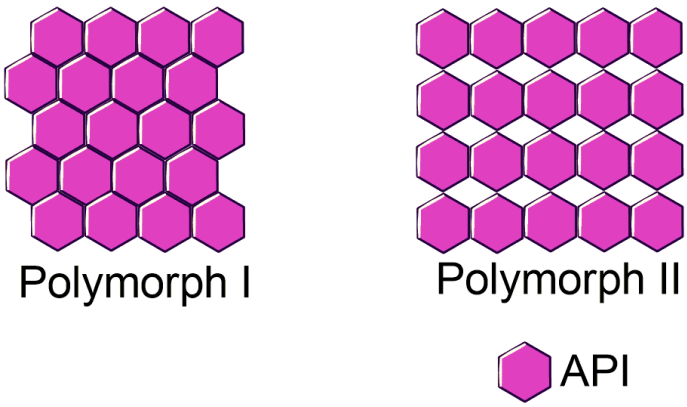

Figure 1.5 Packing polymorphism: different crystalline forms of the same substance.

Two polymorphs can be enantiotropically or monotropically related as a function of the thermodynamic behavior as represented in Figure 1.6.[38–40]

If the two polymorphs A and B are enantiotropically related to each other (Figure 1.6 - a), polymorph A is stable below the transition temperature T_t, it has less free energy G_A than the polymorph B. Polymorph B is more stable above this temperature T_t because its free energy G_B becomes less than G_A. Transition from one polymorph to the other occurs at T_t, the free energy curves of A and B cross at this point before the melting point is reached.[41,42] Each polymorph has its stability domain.

The two polymorphs A and B are monotropically related (Figure 1.6 - b) [43,44] if only one polymorph A is more stable at all temperature below the melting point, since its free energy (G_A) is less than the other polymorph B (G_B). The other polymorph B is unstable since it has the highest free energy. Given that the free energy curves of A and B do not cross, there is no reversible transition below the melting point.[35] Form B can still be attained *via* metastable equilibria.

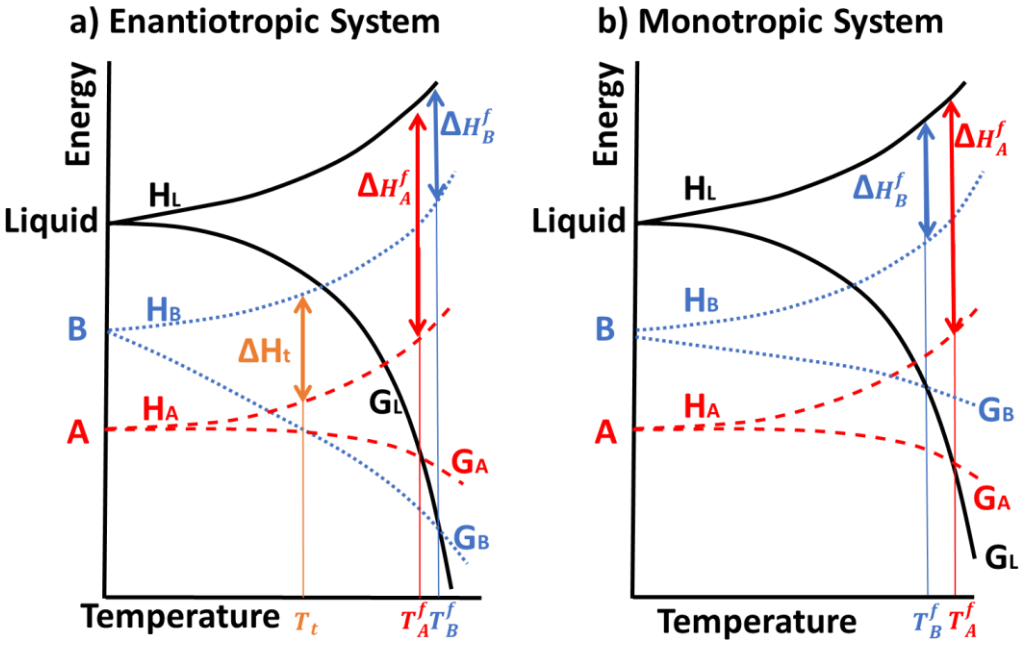

Figure 1.6 a) Enantiotropic system and b) Monotropic system. A and B: two polymorphs, L: liquid, H_i : enthalpy, ΔH_i^f: enthalpy of fusion, T_i^f: melting temperature, ΔH_t: enthalpy of transformation between two polymorphs, T_t: transition temperature between two polymorphs, G_i: Gibbs energy.

Several methods exist to characterize polymorphs and their transitions,[45,46] such as observing the morphology changes of the crystals by microscopic methods,[47–49] or by studying the phase transition by thermal analysis[50–53] and Differential Scanning Calorimetry (DSC).[54,55] Other methods are also employed to characterize polymorphs, like vibrational spectroscopy[56–58] (Infrared and Raman spectroscopy) or solid-state NMR[59–61]. Crystallographic methods are also very common, in particular X-ray diffraction (single crystal and/or powder diffraction).[62–64]

1.3.3 Solvates and Hydrates

Solvates are crystals that result from the co crystallization of the compound with a solvent molecule. These compounds are called hydrates if the solvent is water (Figure 1.7). On a survey of the Cambridge Structural Database, about 50% of the entries for solvates are hydrates.[65] The structure is scaffolded by means of weak interactions, usually hydrogen bond in case of hydrates. Formation of a solvate most often results in a different crystal structure with reference to that of the anhydrous.

As a result, the solvate of a pharmaceutical compound displays different physical, chemical and mechanical properties than those of the anhydrous form(s), *e.g.* stability, solubility, dissolution rate, particle size distribution and bioavailability.[66,67] Several drugs such as cephalexin,[68] ampicillin,[69] cromolyn sodium (disodium cromoglycate),[70] and others are being developed or are currently marketed as hydrates. The discussion about solvate formation in this thesis will focus primarily on crystal hydrates and their dehydration mechanism.

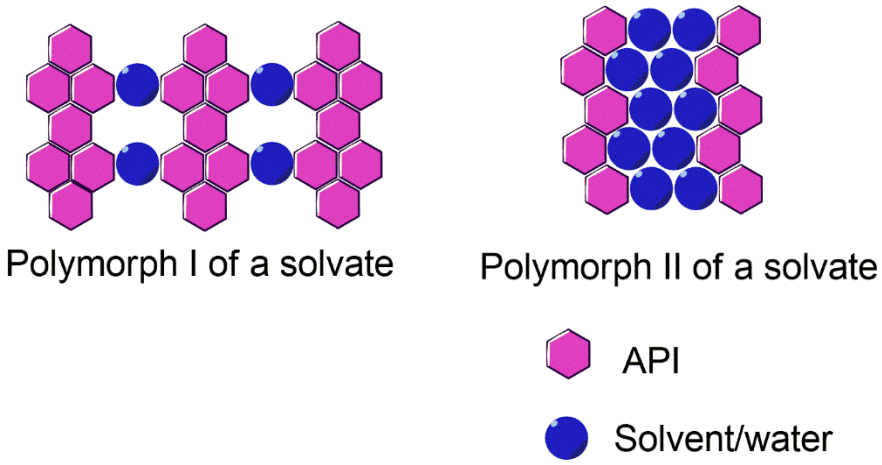

Figure 1.7 Solvate solid forms and their polymorphs.

In 1999 Morris classified hydrates into three categories depending on the structural aspects and on the interaction between the water molecule and the different entities in the crystal lattice.[71]

Class I of hydrates represents systems with isolated hydrate site(s), *i.e.* water molecules have not connected with each other by direct hydrogen bonding. Instead, the water molecules form bonds only with the drug molecules.[72]

Hydrates classified as Class II are referred to as channel hydrates. The water molecule in this class interacts with an adjacent water molecule while also forming noncovalent bonds with the APIs.[73] It results in the occurrence of channel of water molecules throughout the structure.

Crystals characterized as Class III hydrates are also known as ion-coordinated site hydrates. In this case, the water molecules form ion-water bonds that are stronger than hydrogen bonds.[74]

Complementary to Morris classification, Petit et al.[75] proposed a classification concerning dehydration/desolvation mechanism. The mechanisms are related to the possible filiation of structural information and are divided in two categories: Class I, associated with the absence and class II mechanisms correspond to the presence of structural filiation. Each class is divided into several subclasses according to the process of release of water molecules (cooperative or destructive)

and to the eventual process of reorganization (cooperative or through a nucleation and growth process). This classification will be used in this thesis and will be stated as Rouen96 model.

1.3.4 Cocrystals and properties modification

The United States Food and Drug Administration (FDA) describes cocrystals as 'solids that are crystalline single-phase materials composed of two or more different molecular and/or ionic compounds generally in a stoichiometric ratio which are neither solvates nor simple salts'[76] (Figure 1.8). It is worth noting that cocrystals can also be polymorphic and many examples can be found in literature.[77–79]

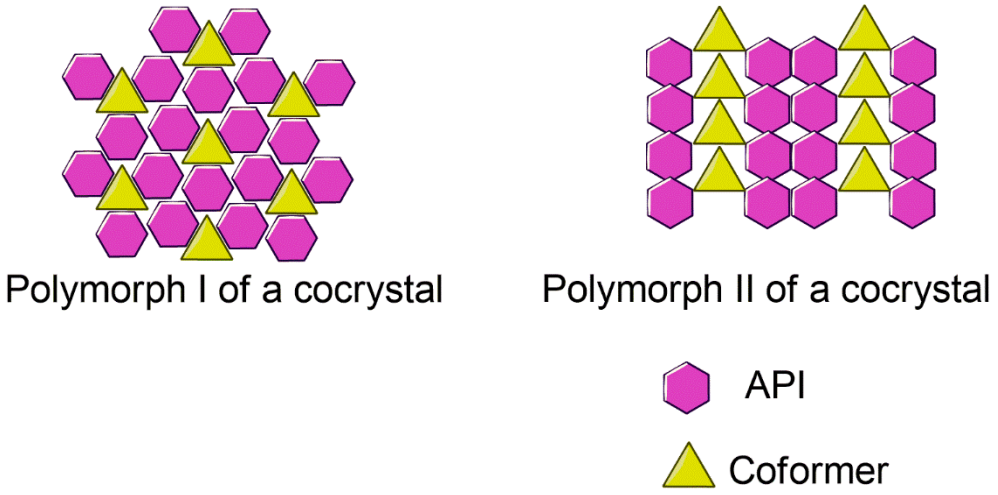

Figure 1.8 Two different polymorphs of a cocrystal between an API and a coformer.

Cocrystals gained interest due to large potential applications in agrochemicals,[80] photonic application,[81] semiconductors,[82] explosive materials[83,84] and especially in the pharmaceutical field.[85–87] Indeed, cocrystallization can improve the physical and chemical properties of an API (solubility, dissolution rate, stability, compressibility, etc.[88–91]) without changing its molecular structure nor its pharmacological behavior. It gives the opportunity to generate intellectual properties (each new co-crystal of an API is potentially patentable).

It is worth to mention that cocrystals can also incorporate solvent from the solution into their crystal lattice to form cocrystal solvates/hydrates. In some cases, solvent molecules can stabilize crystal structures when there is an imbalance in the number of acceptors and donors.[92] Characterization of cocrystals involves both structural (studied by infrared spectroscopy, single crystal X-ray crystallography

and powder X-ray diffraction) and physical properties (studied by differential scanning calorimetry, thermogravimetric analysis, etc.).

1.4 Methods of Enantiomeric Separation: Description and Constraints

1.4.1 Overview

Several techniques are used to obtain enantiopure compounds for chiral APIs:

- Asymmetric synthesis[93]
- Kinetic resolution[94]/Dynamic kinetic resolution[95]
- Diastereomeric crystallization[96]
- Chiral chromatography[97]
- Viedma Ripening[10]
- Preferential crystallization[98]

The first option is the conversion of a prochiral substrate by asymmetric synthesis. It can be performed either by using a catalysis,[99] an enzyme,[100] or by chiral auxiliary,[101] *e.g.* chiral additive. The reactions are often complex which limits their industrial applications. While this technique is effective and capable of producing high ee in some situations, application is limited due to extensive development times, availability and price of chiral additive materials (catalysts or enzymes).[102]

Kinetic resolution (KR) is based on the different reaction rates between a chiral substance and two enantiomers of a racemic mixture: one enantiomer will react faster allowing the easy separation of the formed chiral substance from the unreacted remaining enantiomer. Dynamic Kinetic Resolution (DKR) makes use of chiral catalyst to overcome the limitation of maximum 50% yield in a classic KR.[103]

The third method, diastereomeric resolution by crystallization also known as Pasteurian Resolution[96] is the most common method due to its simplicity and is widely used in the production of pharmaceutical APIs. However, this method suffers from low theoretical yield and large amount of waste produced if no recycling is implemented. Also, an additional step is needed to recover the API at the end of the process, this step is also needed in case of resolution of a cocrystal.

Chromatographic methods gained considerable interest due to an ever increasing range of stationary phases allowing the separation of racemic mixtures.[104] The limitation of this technique resides in the high costs of stationary phases, equipments and the use of large quantities of solvent.

Viedma ripening enables access to enantiopure products in a reliable way, simply through grinding a suspension of racemic conglomerate crystals in

combination with racemization in solution, resulting in complete deracemization of the solid phase. The scope of Viedma ripening has so far remained limited due to the lack of suitable racemization strategies.[10]

1.4.2 Preferential Crystallization (PC)

Preferential crystallization[105] (PC) is one of the most straightforward and efficient separation and purification process. It has many advantages, involving low costs and permits access to highly pure product. However, it is now commonly stated that to perform a PC process, the mixture of enantiomer should crystallize as a conglomerate.[106] In the very common case that the racemic mixture is a racemic compound (90-95% of cases), a screening of solid phase is usually performed up to the formation of a stable conglomerate. Yet, PC on metastable conglomerates remains achievable.[12] Hereafter, we will discuss this type of chiral resolution process.

1.4.2.1 Forewords about Nucleation and Metastable Zone Width

As in every crystallization process, PC is governed by the fundamental mechanisms of crystallization: nucleation, growth, aggregation, etc.

In a supersaturated clear solution, nucleus can be formed spontaneously by primary nucleation only if the upper limit of the metastable zone is reached.[107] But if foreign particles are present in the solution, it is possible for the nuclei to form on those surfaces, this process is called heterogeneous nucleation. On the other hand, nucleation is secondary if the crystals of the same material act as attrition agents or secondary nuclei, in this case nuclei form even at low supersaturation. Let us consider a solution supersaturated with a single compound. The solution necessarily exhibits a metastable zone, which is the range of supersaturation attainable without spontaneous nucleation of the system.[108] The diagram shown in Figure 1.9 exemplifies a cooling crystallization procedure and illustrates this concept. At point A the solution is homogeneous, the temperature is higher than the equilibrium temperature (the solution is undersaturated). Cooling down to point B gives rise to a saturated solution. The solution remains clear until the point C although the solution is then supersaturated: this is the metastable zone. Below this temperature (i.e. the metastable limit), nucleation occurs spontaneously. In the metastable zone, nucleation is unlikely but can be triggered by seeding. Indeed, the width of the zone is influenced by many factors such as the cooling rate,[109] the agitation,[110] presence of foreign particles (dust, impurity, additives…) acting as nuclei,[111,112] viscosity,[113] type of solvent, etc.[114]

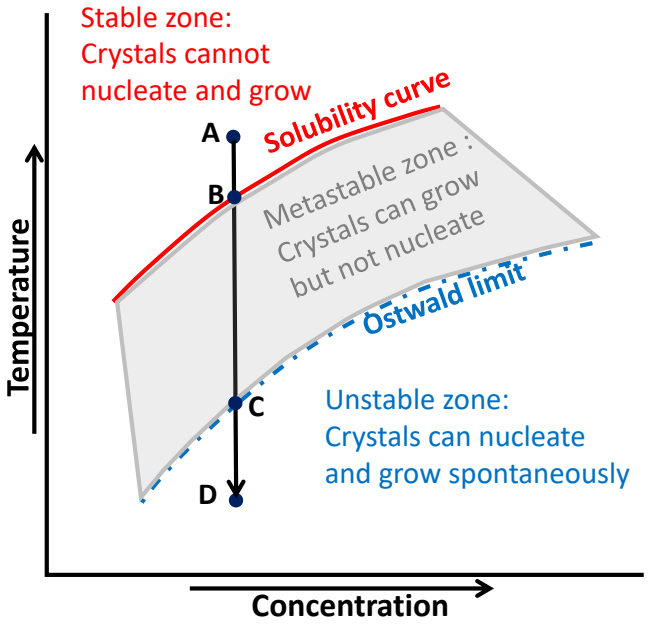

Figure 1.9 General solubility curve showing A: undersaturated solution, B: saturated solution, C: metastable limit and D: zone of spontaneous nucleation.

The success of PC relies on the out-of-equilibrium crystallization of a single enantiomer from the racemic or quasi racemic solution while the other enantiomer remains in solution without nucleating. Measuring the Induction Time (t_i) and Metastable Zone Width (MSZW) associated to the crystallization of pure enantiomers from their solution provides valuable data for the design of a robust PC process and help the selection of solvents and experimental conditions such as supersaturation, temperature, cooling profile, etc.

1.4.2.2 PC process

Conducting PC consists in managing the crystallization kinetics of each enantiomer from their racemic (or quasi racemic solution) supersaturated solution: the crystallization of one enantiomer is triggered while the nucleation of the counter-enantiomer is delayed. This is therefore an out-of-equilibrium process which must be carefully designed and controlled to prevent the spontaneous nucleation of the undesired enantiomer. For a good efficiency of this process, it is well known that enantiomers must crystallize as a conglomerate and no solid solution should occur between the enantiomers.

Different variation of PC process are described in the literature: seeded isothermal preferential crystallization (SIPC), seeded polythermic programmed preferential crystallization (S3PC), auto-seeded polythermic programmed preferential crystallization (AS3PC).[98,115]

The concept of SIPC is best represented schematically as visualized in Figure 1.10. At first, we consider a supersaturated clear solution below the solubility lines at the crystallization temperature T_c represented by point A. At this point the system is artificially enriched with one of the two enantiomers (*R*). The solution is seeded with a known amount of crystals of the pure enantiomer present in excess in the solution (*R*). As a result, (*R*) starts to crystallize due to secondary nucleation and crystal growth and its concentration decreases in the solution that follows the route from A to B.

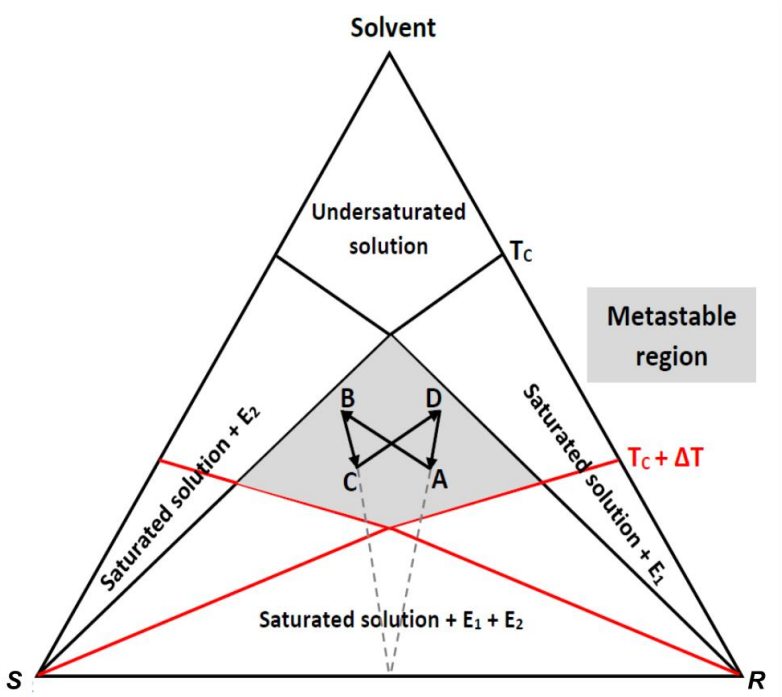

Figure 1.10 Schematic representation of the SIPC process via two isotherms of the ternary system between two enantiomers (*R* and *S*) and a solvent.

Thus, the crystallized enantiomer should be collected before the crystallization of the counter enantiomer occurs. After filtration, a mass of racemic mixture corresponding to the mass of pure enantiomer crystallized is added to the solution to compensate, the temperature is increased to obtain a clear solution and then decreased to T_c (B → C), seed crystals of (*S*) are added at this point, the entrainment of (*S*) starts and the solution becomes enriched with (*R*) (C → D). After filtration, the process can be repeated after compensation of the solution with the suitable amount of racemic mixture (D → A).

It is worth to mention that the process is controlled by the fact that it performs in the MSZW, graphically illustrated in grey in Figure 1.10. As stated above, this zone should be evaluated in order to assess the duration of entrainment without spontaneous nucleation of the counter enantiomer.

Practically, this is best performed by conducting test runs during which the enantiomeric excess of the solution is monitored. While crystallization of the seeded enantiomer (*e.g.* the (+) enantiomer) occurs, the enantiomeric excess of the solution gets progressively enriched in (-). Upon spontaneous nucleation of the counter enantiomer, the evolution of the enantiomeric excess of the liquor re-increases up to 0 % ee. The “filtration windows” is set before that event.

The Seeded Polythermic Programmed PC procedure (S3PC) is a variant of the SIPC process. The difference lies in the fact that entrainment occurs during a programmed cooling of the solution. In this process, the system is at the thermodynamic equilibrium at the beginning: the racemic solution is saturated. After seeding, the driving force of the crystallization is kept under control by using an adequate cooling profile.

Figure 1.11 - b shows an isoplethal section showing the experimental principle of S3PC: the initial composition of the solution is given by point A (Figure 1.11- a), the medium is cooled down to T_{homo}. At this temperature the solution becomes saturated and remains clear. Seeds (*R* enantiomer) are introduced in the medium and a controlled cooling profile is applied to initiate the crystal growth. The liquid phase composition follows the solubility curve HL and the equilibrium is maintained between the temperatures T_A to T_L. Between T_L and T_F, the counter enantiomer can crystallize at any moment. The temperature program should therefore be adjusted on a case by case basis to promote soft crystal growth and secondary nucleation of the crystallized enantiomer.[115] The liquid phase will contain an excess of the *S*-enantiomer and therefore *S*-enantiomer is non-equilibrated, and *R*-enantiomer is in metastable equilibrium. As in SIPC mode, the medium will be filtered and an amount of racemic mixture equal to the amount of crystallized solid is added and the process is then repeated.

AS3PC is an improvement of S3PC: seeds are indeed needed for each experiment in the cyclic operation of SIPC and S3PC. AS3PC can be described as a two-step process: first *in situ* crystallization of the enantiomer present in excess is performed by cooling the system at T_B in the domain “*R*+*saturated solution*”, the starting composition in this case is given by point E_B in Figure 1.11- b. At this point *R*-enantiomer crystallizes naturally and the resulting slurry is in equilibrium with its saturated solution: these crystals will act as seeds for the PC process. A controlled cooling ramp from T_B to T_L is applied and the system remains close to equilibrium moving along the metastable solubility curve BL and down to F (similarly to S3PC). After filtration, the liquid phase contains an excess of the counter enantiomer and the system is compensated with racemic mixture and a new operation can be started again.

In all PC modes, the recycling of the mother liquor between each run prove that this technique is at least economical, and it is theoretically possible to resolve any amount of racemic mixture due to the successive recycling.

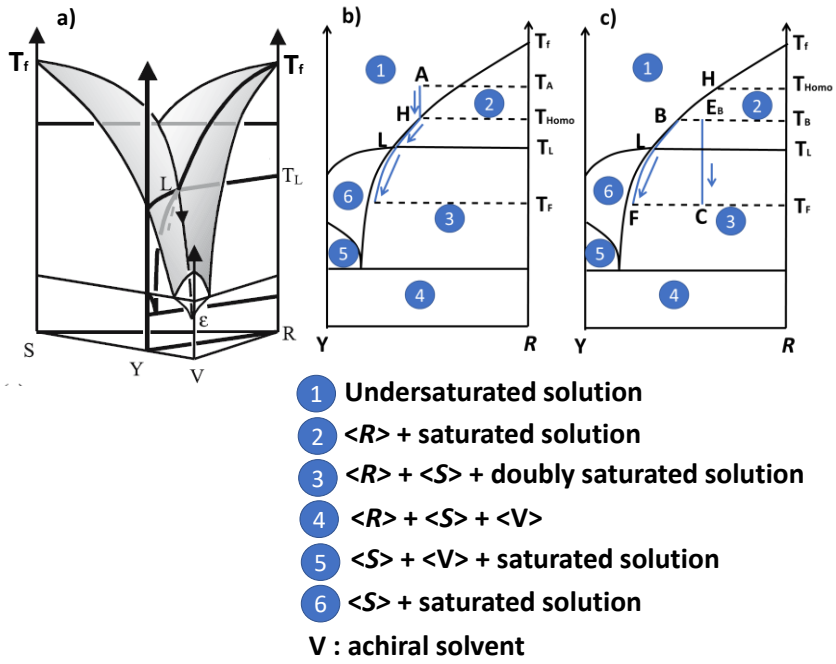

Figure 1.11 a) T-R-Y isoplethal section from a ternary phase diagram showing the principle of b) Seeded Programmed Polythermic Preferential Crystallization (S3PC) and c) Auto-Seeded Programmed Polythermic Preferential Crystallization (AS3PC). [115]

1.4.2.3 Preferential crystallization of hydrates in a ternary system

Fundamentally, no difference is found between the entrainment of a solvate/hydrate or a non-solvated crystal form. However, experimental conditions (solvent nature, temperature, pressure, humidity, etc.) may affect the chemical characteristics and the behavior of the hydrate. For example, it might be necessary to store the seeds under specific conditions to avoid dehydration or decomposition of the solid phase that will be used for the stereoselective nucleation and crystal growth in the system.

1.5 PC in the case of racemic compound forming systems: the case of Diprophylline

One of the starting point of this thesis work is based on the work of Brandel *et al.*.[12] They have reported that the chiral compound Diprophylline (Figure 1.12, DPL hereafter)[12] exhibits a rich solid state landscape with four crystal forms: a stable racemic compound, two metastable solid solutions and a metastable conglomerate. In that study, it was found that a solution of racemic DPL in polar solvents such as water, DMSO and DMF can remain highly supersaturated for

several hours before any spontaneous nucleation. This large MSZW hindered the nucleation of the stable racemic compound (and any other form) which allowed the crystallization of the pure enantiomer when the solution was seeded with homochiral seeds in DMF. It was also stated that this behavior is due to the conformational diversity of DPL in the solvated state which is related to the conformational flexibility of the molecule. The conformation(s) adopted by the molecule at the solvated state was proposed as the reason why primary nucleation was so difficult.[116]

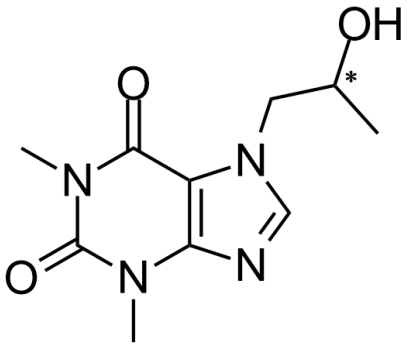

Figure 1.12 Chemical structure of (*RS*)-DPL.

This study suggested that the key parameter for the successful implementation of PC is not necessarily associated to the presence of a stable conglomerate and could be also the use of a solvent which delays spontaneous nucleation of racemic compounds. This assumption enlarges the use of PC in some cases of racemic compounds forming system. Indeed, a large MSZW allows the use of the metastable equilibria of the conglomerate, whereas the stable equilibria of the racemic compound can be overpassed. In such a situation, the solubility of the conglomerate is larger than that of the racemic compound. Therefore, the concentration of the solution should be high enough to reach a sufficient supersaturation value with respect to the conglomerate (PC should not be held in the grey zone but should take place in the green zone of Figure 1.13).

Assuming that a solvent fulfilling the above criteria is identified, PC might be applied for any chiral molecule crystallizing as a stable racemic compound. This would considerably expand the scope of chiral resolution by PC. Therefore, the strategy presented by Brandel *et al.* should involve a screening procedure (adopted in this work) based on the measurement of induction times.[116] This aims to identify a solvent in which a large MSZW can be reached.

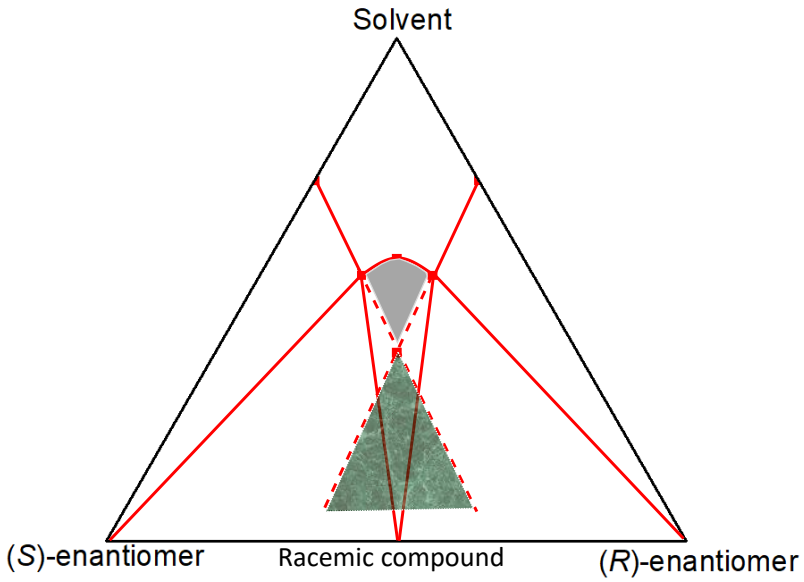

Figure 1.13 Isothermal section of a ternary phase diagram representing a stable racemic system (red lines) and its metastable conglomerate (dashed lines).

1.6 Methodology to implement preferential crystallization in unfavorable cases

The starting assumption of the present work was that PC can be performed despite the presence of a stable racemic compound between the enantiomers. In the work of Brandel et al., implementation of PC was made possible by the selection of a suitable solvent (*i.e.* dimethylformamide) and did not required the addition of any external impurities.[12] Seeding the supersaturated solution with the pure enantiomer enabled the stereoselective crystallization *via* secondary nucleation and crystal growth. A careful analysis of the system revealed that the nucleation inhibition of the racemic compound is most likely due to conformation blockage at the solvated state which hamper its primary nucleation from that solvent.[116]

During this work, two systematic experimental plans were designed aiming to develop a more general approach to be applied for different racemic compound forming system (Figure 1.14).

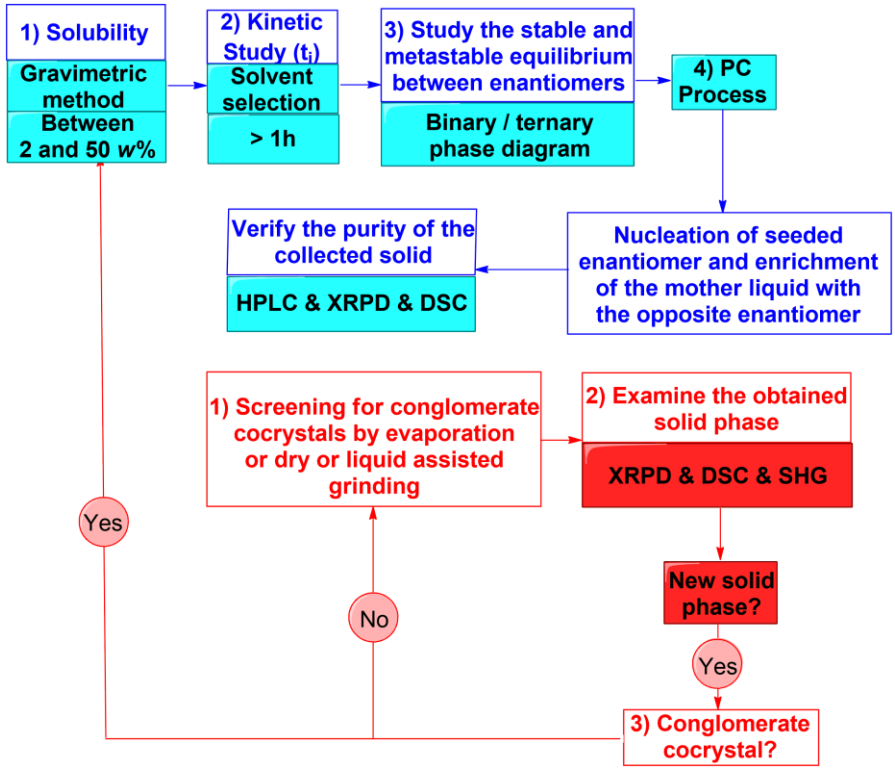

Figure 1.14 Schematic structure of the experimental plan.

The first work plan (in blue in Figure 1.14) was derived with the aim of identifying more candidates for that type of unconventional PC processes. Experimentally, this implies: (i) measurement of the solubility and the nucleation properties (induction time (t_i)) of different racemic compounds in different solvents. (ii) Those showing large t_i were further investigated and the polymorphic landscape was established using phase diagrams and (iii) these data have been used to design PC.

The second plan shown in red in Figure 1.14 explores the possibility to perform PC from conglomerate obtained by cocrystallization of the candidate. Experimentally, this implies: (i) a screening of co-crystal, (ii) if a new conglomerate solid phase is detected, (iii) a suitable solvent for PC is identified before (iv) applying the resolution process under the right conditions.

These two ways for chiral resolution were particularly explored in this work. The choice of model molecule to implement this procedure was based on criteria deducted from the successful case of DPL.[12]

1.6.1 Criteria for Compound Selection for the First Work Plan

Concerning the first work plan, the following criteria for compound selection were identified:

- The mixture of enantiomer must obviously exist as a stable racemic compound. The knowledge about the presence of any metastable conglomerate was not mandatory. However, we favored systems for which the melting point of the racemic compound was lower compared to that of the pure enantiomer. By consequence, the melting temperatures of the conglomerate and the racemic compound are in the same range. (Figure 1.15).
- As for DPL molecule, the selected molecule must have a flexible conformation since this feature might favor the occurrence of nucleation blockage.[12]

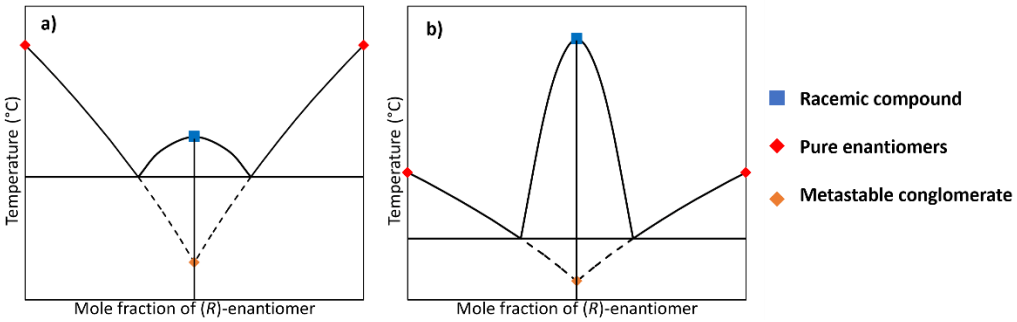

Figure 1.15 Schematic representation of a) the melting temperature of the racemic compound and the conglomerate are in the same range and b) the melting temperature of the conglomerate and the racemic compound are not in the same range.

The solubility of twenty chiral racemic compounds and their nucleation behavior in twenty-two different solvents was explored (the list of the used racemic compounds and solvents can be found in the Annex A section). Two compounds were selected, i) proxyphylline (PXL hereafter, Figure 1.16 - a) which belongs to a series of theophylline derivatives, same as DPL and ii) 3-(2-propylphenoxy)-propane-1,2-diol (P3D hereafter, Figure 1.16 - b). They were chosen for further investigations because they fulfill the aforementioned criteria especially the flexibility of their moiety substituent.

As mentioned before, the preliminary step for the design of PC was to carefully establish the solid-state landscape of the selected molecules. Trials to apply PC on P3D molecule failed and thus this molecule was directly discarded. Nevertheless, the solid-state study of P3D was done and can be found in the Annex B section.

By consequence, PXL will be the main studied molecule in this thesis. The next chapters will discuss the solid-state diversity of PXL and its resolution through the two experimental plans (Figure 1.14) respectively.

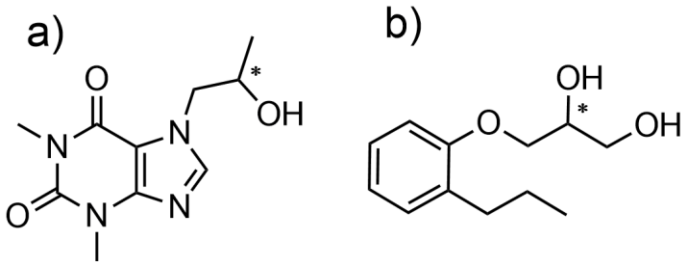

Figure 1.16 Chemical structure of a) PXL and b) P3D. The star indicates the chiral center.

CHAPTER 2: CHARACTERIZATION OF THE SOLID-STATE LANDSCAPE OF 7-(2-HYDROXYPROPYL) THEOPHYLLINE (PXL)

All the details of experimental set-up and procedures used during this work are gathered in Annex A.

2.1. Study of the binary phase diagram between PXL enantiomers

2.1.1 Introduction and state of art of the compound

Proxyphylline (PXL hereafter, Figure 2.1) is a xanthine derivative that acts as a cardiac stimulant, vasodilator and bronchodilator. It's used for relief of acute bronchial asthma and for reversible bronchospasm associated with chronic bronchitis and emphysema.[117]

Some information about the solid state of racemic PXL were available from the literature. In 1974, Kuhnert Brandstatter et al.[118] suggested the existence of two "modifications" (*i.e.*, Polymorphs) of PXL: Mod I with a melting points of 134-136 °C and Mod II at 115-117 °C. In 1977, Eckert and Muller[119] suspected the existence of at least five forms based on DSC and hot stage microscopy (HSM) investigations with the following melting points: 132.5-134.5 °C for Mod I, 117-121 °C for Mod II and III, and 112-114 °C for Mod IV and V. Griesser et al.[120] (2000) reported, mainly from HSM and DSC, that Mod I melts between 133 and 136 °C, Mod II can be obtained by annealing the supercooled melt (SCM) of racemic PXL between 75 and 95 °C, the melting point of Mod II was observed between 113 and 116 °C. A third modification, Mod III, was obtained by annealing the SCM of racemic PXL between 55 and 65 °C. Mod III has a melting around 82-85 °C. These data are summarized in Table 2.1. No studies were conducted on the polymorphism of the pure enantiomer of PXL.

In this chapter, solid-state characteristics of PXL will be investigated by a combination of suitable experimental techniques (thermochemical study, single crystal and powder X-ray diffraction). The crystal forms are named with roman numerals in order of their melting point.

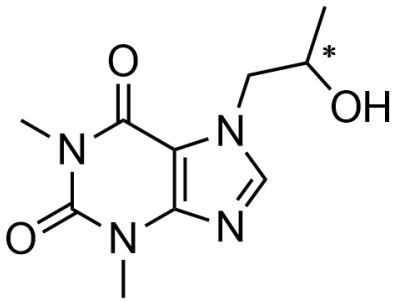

Figure 2.1 Chemical structure of PXL. The star indicates the chiral center.

Table 2.1 Solid forms of (*RS*)-PXL described in the literature.

	Preparation technique	Melting temperature
Mod I	Commercial	134-136 °C[118]
		132.5-134.5 °C[119]
		133-136 °C[120]
Mod II	/	115-117 °C[118]
	DSC and hot stage microscopy	117-121 °C[119]
	annealing the SCM of (*RS*)-PXL between 75 and 95 °C	113-116 °C[120]
Mod III	DSC and hot stage microscopy	117-121 °C[119]
	annealing the SCM of (*RS*)-PXL between 55 and 65 °C	82-85 °C[120]
Mod IV and Mod V	DSC and hot stage microscopy	112-114 °C[119]

2.1.2 Identification and characterization of the different forms in the binary system

The binary system between PXL enantiomers were re-investigated during this work. The stable racemic form of PXL (Mod I) was purchased from TCI EUROPE. The stable enantiopure form (PE I) was synthesized according to a published procedure as detailed in Annex A.[121]

Three metastable racemic forms of PXL were obtained:

- Mod II is a physical racemic mixture manually prepared by manual grinding between (*R*) and (*S*)-PXL.
- Mod III was obtained by crystallization experiments from different solvents (chloroform, toluene, water, cyclohexane, heptane) and could be also prepared

by annealing the supercooled melt (SCM) of racemic PXL ((*RS*)-PXL) for 30 minutes at 80 °C

- Mod IV was prepared by annealing the SCM of (*RS*)-PXL at 80 °C for 10 minutes.

Solvent crystallization of the enantiopure form of PXL (PE-PXL) always lead to the formation of the stable form PE I, whatever the used solvent or conditions. A metastable enantiomeric form PE II was detected by means of DSC after heating the SCM of the pure enantiomer at 10 °C/min from 25 to 200 °C. A third form, PE III was prepared by annealing the SCM of the pure enantiomer at 80 °C for 30 minutes.

2.1.2.1 Characterization by X-ray powder diffraction

All the accessible phases were characterized by XRPD. The patterns of the stable and metastable racemic and enantiopure forms of PXL are presented in Figure 2.2.

Mod III and Mod IV were prepared directly on the XRD sample plate holder by annealing the SCM of (*RS*)-PXL at 80 °C for 30 minutes and 10 minutes, respectively.

The pattern of the metastable form PE III was obtained by melting the stable form PE I on an XRD sample plate holder and annealing its melt for 30 minutes at 80 °C. Due to the metastability of PE II, it was impossible to detect its X-ray pattern since it transforms directly to the stable form PE I.

For these analyses, it can be stated that PE I and Mod II share the same pattern (Figure 2.2 - b and Figure 2.2 – e) : Mod II could be identified as a metastable conglomerate. On the other hand, PE III and Mod IV have the same XRPD. Thus, Mod IV could be a conglomerate, or it represents the racemic composition of a total solid solution of PE III (Figure 2.2 - d and Figure 2.2 - f).

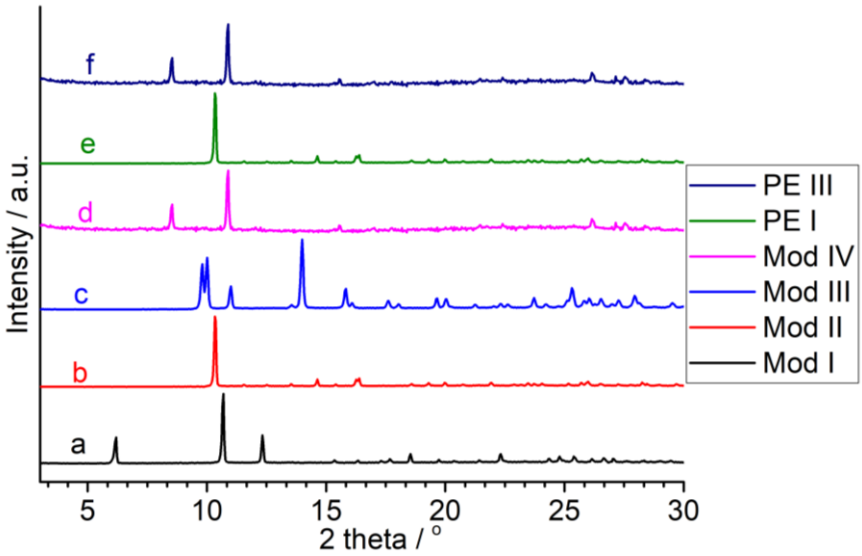

Figure 2.2 Experimental XRPD patterns of stable and metastable racemic and enantiopure forms of PXL, a) Mod I, b) Mod II, c) Mod III, d) Mod IV, e) PE I and f) PE III.

2.1.2.2 Crystal structure

Trials to grow single crystals were carried out in order to access the crystal structure of the various forms and to understand the relationships between the different forms of PXL at the molecular scale. All attempts to grow single crystal of racemic PXL with good quality suitable to be studied by Single crystal X-Ray diffraction failed.

Only single crystals of PE I could be obtained by slow evaporation at room temperature of a solution of pure enantiomer in ethanol/isobutyl alcohol (1:1). The crystallographic data of PE I is represented in Table 2.2. Diffraction analysis of PE I at room temperature shows the structure to be orthorhombic $P2_12_12_1$.

The asymmetric unit is composed of two molecules of PXL (Figure 2.3). Along *a*, the continuous sequence of the intermolecular hydrogen bonds (HB) binds the alcohol group of one molecule with the amino group of a second molecule, and the alcohol group of the second molecule to the carboxyl group of the first one. This arrangement leads to the formation of periodic bond chain (Table 2.3 and Figure 2.4). These chains are packed along *b* and *c* through weak interactions (vdW) as seen in Figure 2.5.

Table 2.2 Crystallographic data and refinement parameters of PE I.

	PE I
Chemical Formula	$C_{10}H_{14}N_4O_3$
Molecular Weight / g.mol^{-1}	238.25
Crystal System	Orthorhombic
Space Group	$P2_12_12_1$
Z , Z' (asymmetric units per unit cell)	8, 2
a / Å	7.7763(1)
b / Å	17.133(3)
c / Å	17.171(3)
α / °	90
β / °	90
γ / °	90
V / Å3	2287.7(6)
d_{calc} / g.cm^{-3}	1.383

Table 2.3 Hydrogen bond table. Distance in Å. And angle in °.

D-H...A	d(D-H)	d(H...A)	d(D...A)	<(DHA)
O(1)-H(1)...N(2A)#1	0.82	2.03	2.841(5)	169.9
O(1A)-H(1A4)...O(3)#2	0.82	1.94	2.756(5)	170.4

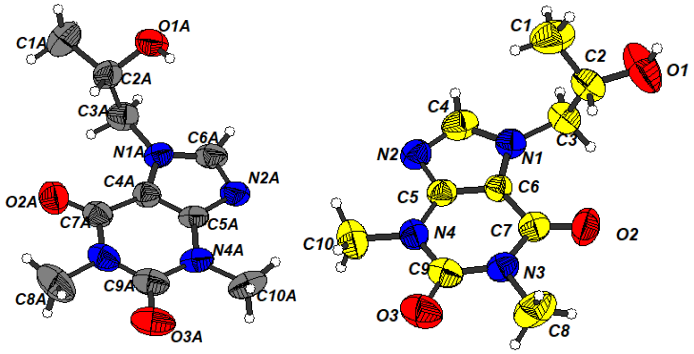

Figure 2.3 Asymmetric unit in thermal ellipsoidal representation of the orthorhombic structure of PE I, with atom labels.

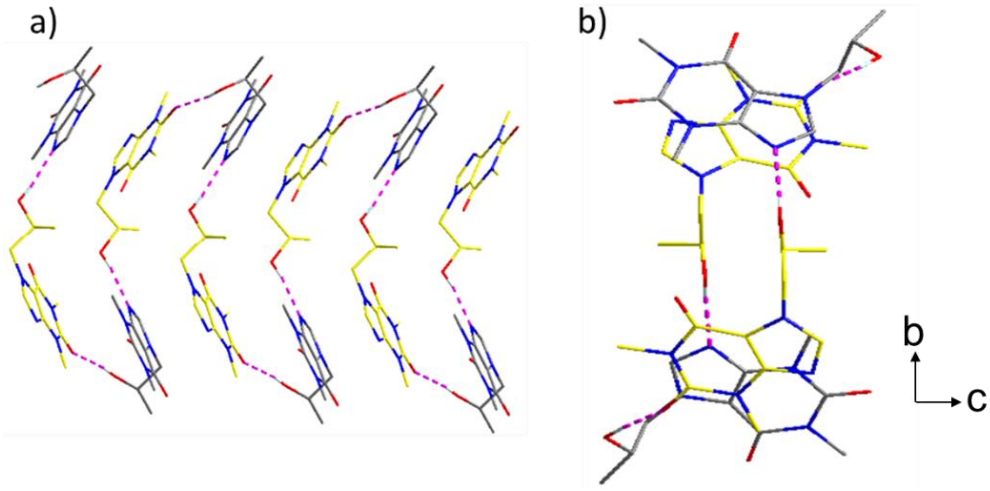

Figure 2.4 a) Molecular bond chains formed by the hydrogen bonds and b) Projection along *a* of one periodic bond chain.

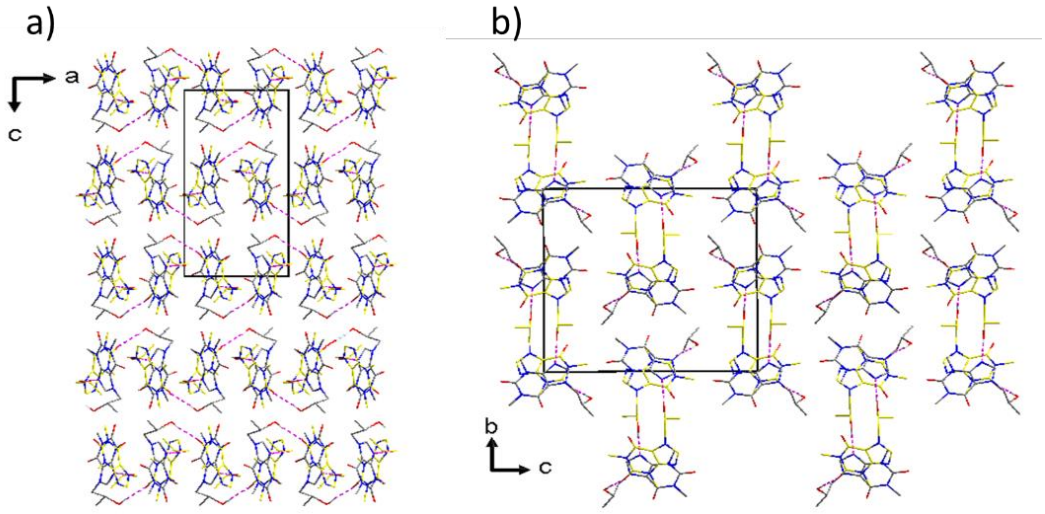

Figure 2.5 a) Projection along *b* and b) projection along *a*.

2.1.2.3 Thermal analyses

Thermogram of the pure stable racemic form Mod I (Figure 2.6 - a) (heating rate of 5 K/min) shows only one endothermic event ($\Delta_{fus}H$ = 26.0 KJ/mol), corresponding to the melting of this form at T_{onset}=134.9 °C. The DSC curve confirms that the substance is stable and do not decompose under these experimental conditions. Thermogram of Mod II represented in Figure 2.6 - b shows one endothermic event at 116.2 °C ($\Delta_{fus}H$ = 25.1 KJ/mol). Since Mod II is a physical mixture of both enantiomers, it can already be suggested that this

temperature correspond to the eutectic melting of the metastable conglomerate between PE I enantiomers.

Mod III and Mod IV present an endothermic peak (corresponding to their melting) at 112.0 °C and 89.5 °C respectively, followed by an exothermic event (corresponding to recrystallization). The recrystallized form was Mod I since the melting of that form was detected upon further hearing. (Figure 2.6 - c and Figure 2.6 - d). We can note that we never obtained a fifth solid form (Mod V) during this study.

According to the thermal behavior, Mod I is the only thermodynamic stable form for the racemic section: Mod II, III and IV are monotropically related to Mod I.

The thermogram of the pure stable enantiomeric form PE I shows a single melting endotherm at 149.5 °C with an enthalpy of fusion of 29.1 $kJ.mol^{-1}$ (Figure 2.7 - a). While heating the SCM of PE-PXL at 10 K/min, and after an exothermic peak due to recrystallization event, a small melting endotherm at 114.8 °C was detected (although markedly compensated by the exothermic recrystallization of PE I). It was associated to the melt of the metastable enantiopure form PE II (Figure 2.7 - b). Similarly, while heating the SCM of PE-PXL at 5K/min, an exothermic peak due to recrystallization was detected and followed by the melt of another form, PE III at 98.4 °C (Figure 2.7 - c). Again, this melting was calorimetrically compensated by the concomitant recrystallization of PE I. Due to the high metastability of PE II and PE III it was not possible to reliably measure any heat of fusion. Only one enantiopure solid form is thermodynamically stable (PEI). PE II and PE III are monotropically related to PE I.

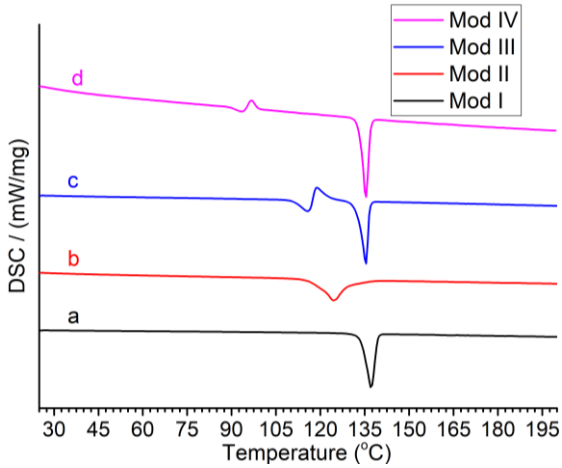

Figure 2.6 Differential scanning calorimetry (DSC) study at a heating rate of 5 K/min of racemic PXL: a) Mod I, (b) Mod II, (c) Mod III and d) Mod IV.

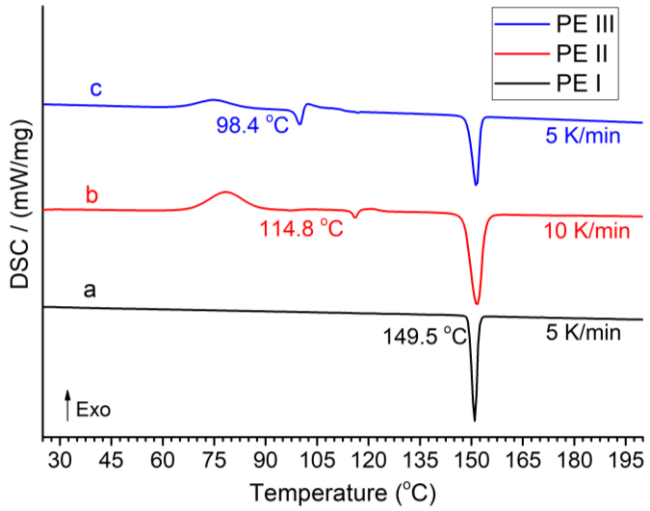

Figure 2.7 Differential scanning calorimetry (DSC) study at a heating rate 5 K/min of the pure enantiomer of PXL: a) PE I (synthesized) at 5 K/min, (b) PE II (SCM) at 10 K/min and c) PE III (SCM annealed at 80 °C for 30 min) at 5 K/min.

2.1.2.4 Binary phase diagram between PXL enantiomers

As a preliminary step, the theoretical binary phase diagram between PXL enantiomers was constructed using the Schröder-Van Laar (to establish the liquidus of PE I) and Prigogine–Defay (to establish the liquidus of Mod I) equations.[24] The results are presented by black lines (for the stable equilibrium) and black dashed lines (for the metastable equilibrium) in Figure 2.8. By these calculations two invariants can be predicted: one at 129 °C (stable equilibrium) and one at 116.2 °C (metastable equilibrium). The phase equilibrium between PE II, PE III, Mod III and Mod IV cannot be experimentally investigated due to their metastability. As previously reported during XRPD analyses, a conglomerate may be present between Mod IV and PE III (they show the same XRPD, Figure 2.2). It is worth to note that the eventual presence of a solid solution is not forgotten but this situation is not presented on the phase diagram for clarity.

Since the starting stable solid phases could be isolated, six different composition mixtures between Mod I and PE I were prepared and analyzed by DSC (Figure 2.9). PE I and Mod I presents a melting peak at 149.5 °C and 134.9 °C respectively. For mixture containing 67%, 80% and 90% of PE I, the thermal behavior is the same: one endothermic peak at 130 °C associated to eutectic transformation presented by grey rhombus in Figure 2.8) and a variable liquidus peak depending on the composition (T_{peak} was taken in this case). For the sample with 60% of PE I the behavior is different: the first endothermic peak seems associated to a metastable equilibrium and the second one to the stable liquidus.

All these experimental points are in good agreement with the theoretical calculation.

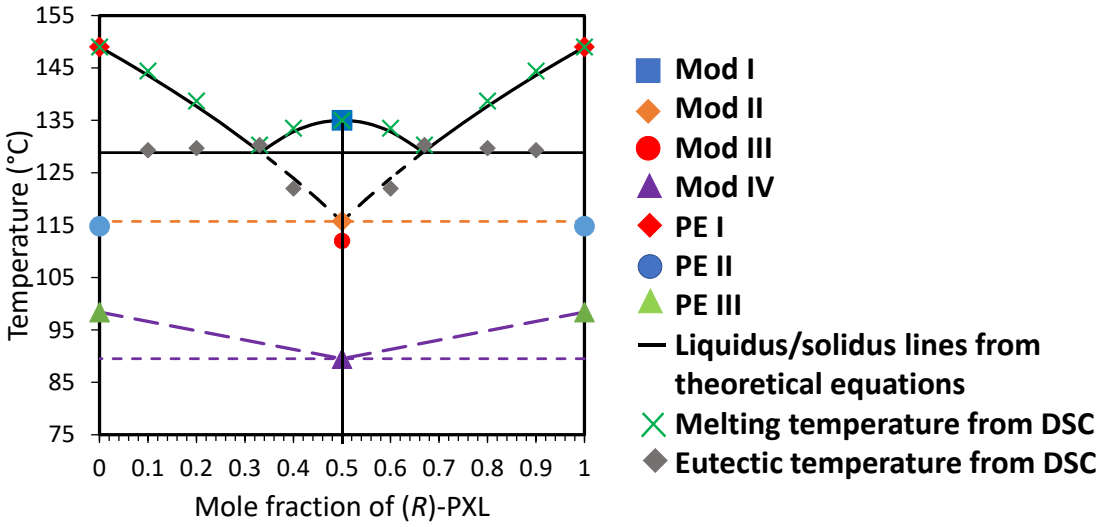

Figure 2.8 Binary phase diagram for the stable and metastable equilibrium between the pure enantiomers of PXL.

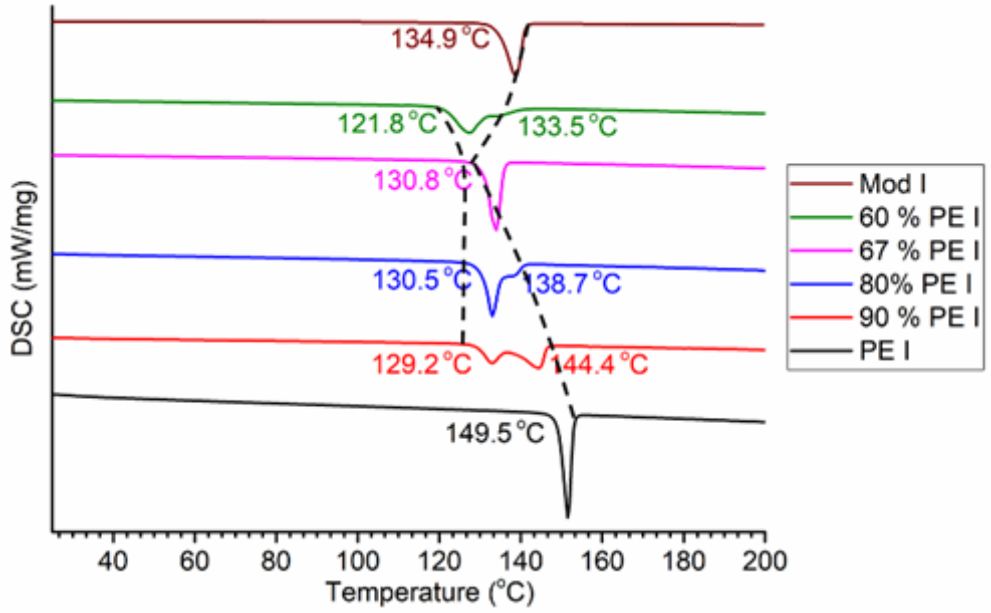

Figure 2.9 DSC curves obtained at a heating rate of 5 K/min of Mod I and PE I mixtures. The compositions are indicated in the thermogram.

2.2. Discussion

The determination of the binary phase diagram between PXL enantiomers has demonstrated the existence of a double polymorphism (i.e., polymorphism of both racemic mixture and of the pure enantiomer). PXL enantiomers can crystallize either as a stable racemic compound, a metastable racemic compound and two metastable conglomerates and/or solid solution. This system exhibits a rich crystallization behavior, similar to the DPL molecule. Even if we could not get any data about the molecular organizations in the solid state, this behavior certainly results from the flexibility of these molecules as for DPL.

The existence of two conglomerates (even metastable) in this system, implies that the self-stereorecognition of PXL enantiomers is efficient and is a favorable criterion for the design of PC process.

Such preliminary work and assessment of the solid-state behavior is of fundamental importance as it establishes a clear understanding of the thermodynamic stability of each form and provides a solid basis for the work presented in the next chapter.

CHAPTER 3: DIRECT PREFERENTIAL CRYSTALLIZATION APPLIED TO PXL

The main results of this work were already published: Harfouche, L. C.; Brandel, C.; Cartigny, Y.; ter Horst, J. H.; Coquerel, G.; Petit, S. Enabling Direct Preferential Crystallization in a Stable Racemic Compound System. *Mol. Pharm.* **2019**, *16* (11), 4670–4676.

3.1 Introduction

This chapter reports on the application of direct PC in the binary system of PXL enantiomer despite the existence of a stable racemic compound. This work based on the strategy presented in 1.6 describes a basic process design including a solvent selection procedure as well as an approach to identify optimal process conditions. Resolution is enabled through the careful selection of a solvent in which all possible phases have low nucleation rates. From solvents, Mod III, Mod IV, PE II and PEIII are not accessible and will not be considered further in this section, “reducing” the solid-state landscape of PXL to the stable racemic compound (Mod I) and to the metastable conglomerate (Mod II).

3.2 Solvent selection: solubility study and isotherms

The starting assumption of this work is that the key parameter for the successful implementation of PC for a stable racemic compound-forming system such as the one between PXL enantiomers, is the selection of a solvent in which the spontaneous nucleation of the stable crystal form as well as the metastable conglomerate are kinetically inhibited.

If a highly supersaturated solution can be maintained for a sufficiently long period of time in this solvent, seeding with a single enantiomer would mainly promote its growth whereas the stable racemic compound or the counter enantiomer would not nucleate. Obviously, in the case of a racemic forming system, PC can only be envisaged if the solution is also supersaturated with reference to the metastable conglomerate.

In a preliminary step, a large collection of solvents was tested for suitable solubility (s^*). Those solvents for which the PXL solubility at 20 °C lies between 2 and 50 w% were further investigated by determining induction time t_i at 1 mL scale using the Crystal 16 apparatus (see Annex C).

For samples showing large t_i values at 1 mL scale, tests were made at larger scale (10 or 20 mL), at a supersaturation ratio $1.5 \leq \beta \leq 2.5$ in respect to the stable racemic

compound (Mod I hereafter) (Table 3.1). Spontaneous nucleation of Mod I occurred much more rapidly at larger scale and this type of dependency of the nucleation has been discussed elsewhere.[122]

Table 3.1 Solubility (*s) data and induction time values of Mod I in different solvents at 20 °C at [a]20 mL scale or [b]10 mL scale.**

Solvents	T_c (°C)	*s** (w%)	β[c]	t_i (minutes)
Acetone	20	4.4	2	10[a]
Chloroform	20	21.8	2	25[b]
1,4-dioxane	20	6.6	1.5	15[a]
Propan-1-ol	20	3.2	2	100[b]
n-butyl acetate	20	1.2	1.5	/
Dimethyl sulfoxide	20	21.4	2	5[a]
N,N-dimethylformamide	20	29.4	/	20[b]
THF	20	5.6	1.5	5[b]
Methyl tert-butyl ether	20	non-soluble	/	/
Methanol	20	11.7	1.5	20[b]
Acetonitrile	20	6.0	2	15[a]
Toluene	20	non-soluble	/	/
Ethyl acetate	20	1.8	1.7	2[b]
Ethanol	20	5.5	1.5	20[a]
Water	20	47.7	2.5	180[b]
DCM	20	12.2		
Butan-2-ol	20	4.6	2.3	20[a]
Cyclohexane	20	non-soluble	/	/
n-heptane	20	non-soluble	/	/
Methyl isobutyl ketone	20	3.3	1.5	5[b]
Isopropyl alcohol	20	2.7	2.3	15[b]
Isobutyl alcohol	10	2.1	2.3	60[a]
Isobutyl alcohol	20	2.9	2.3	60[a]

[a]20 mL scale, [b] 10 mL scale, [c] maximum supersaturation ratio tested.

Despite t_i values larger than 180 and 100 minutes found in water and 1-propanol respectively, preliminary PC attempts were unsuccessful due to the primary heterogeneous nucleation and crystallization of the stable racemic compound immediately after seeding with crystals of pure enantiomer. This spontaneous crystallization was detected by means of X-ray powder diffraction (XRPD) of the solid phase sampled during the experiment.

These solvents were therefore discarded. This shows that a large metastable zone width is necessary but not sufficient to ensure the success of PC under these particular circumstances. Based on the promising t_i results, it was chosen to further investigate the resolution process in isobutyl alcohol (IBA).

3.3 Solubility measurements and ternary isotherms

Knowledge of the ternary phase diagram between PXL enantiomers and the solvent is needed in order to rationalize any resolution procedure by PC. In presence of a solvent, PXL crystallizes either as a stable racemic compound (Mod I) or as a metastable conglomerate (Mod II) between pure enantiomer PE I. The solubility values of the three crystal forms (Mod I, Mod II and PE I) in the solvent IBA are shown in Table 3.2 and Figure 3.1. To evaluate the error of the solubility data obtained with the isothermal method, repeated measurements were made and the standard deviation (s.d.) was calculated. Results are shown in Table 3.2.

As expected, the *s** of the metastable conglomerate Mod II in IBA is higher than that of the racemic compound Mod I and the solubility difference substantially increases with temperature. For instance, at 10°C *s** of Mod II is 1.3 times higher than that of Mod I and roughly twice that of PE I. At 40 °C the *s** of Mod II becomes twice higher than that of Mod I and trice that of PE I.

Table 3.2 Average and standard deviation (s.d.) of solubility data of the pure enantiomer PE I, racemic compound Mod I and metastable conglomerate Mod II in IBA. (n: number of experiments, μ: mean value).

T_s (°C)	PE I(w%)	s.d.[a](PE I)	Mod I(w%)	s.d.[a](Mod I)	Mod II (w%)	s.d.[a](Mon II)
5	1.4	0.22	1.8	0.13	/	/
10	1.5	0.40	2.1	0.05	2.7	1.62
25	2.2	0.29	3.5	0.34	5	1.11
30	/	/	/	/	6.8	0.05
35	4.0	0.65	5.0	0.12	/	/
40	5.3	0.28	7.3	0.43	15.4	0.08
50	/	/	15.4	0.09	/	/
60	10.2	0.53	/	/	/	/

[a]s.d. = $\sqrt{\frac{1}{n-1}\,(\sum_{i=1}^{n}(X_i-\mu)^2}$

$\mu = \frac{\sum X_i}{n}$

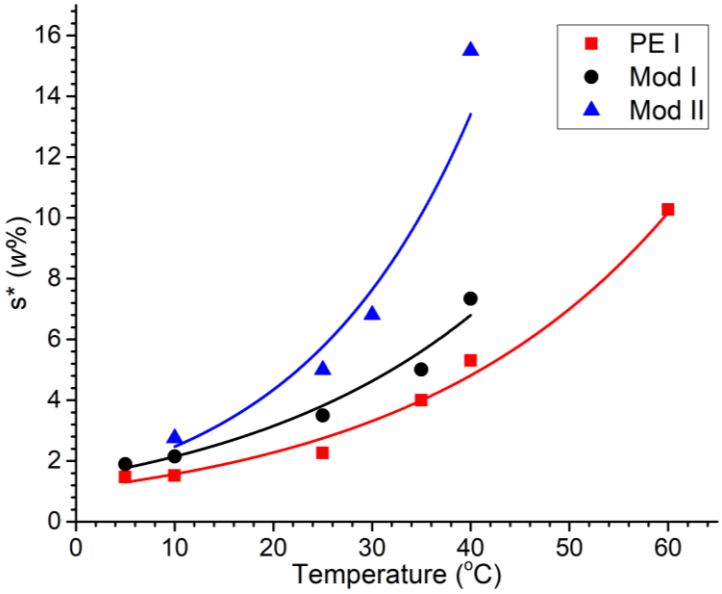

Figure 3.1 Solubility curves of the three crystal forms of PXL in IBA as function of temperature. PE I: pure enantiomer of PXL, Mod I: stable racemic compound, Mod II: metastable conglomerate.

These solubility data were used for the construction of the ternary isothermal sections at 10 and 25 °C (Figure 3.2) (temperature used for PC processes) and to plot the metastable solubility lines representing the virtual crystallization limits (experimental detain can be found in Annex A, A.2.14). The slope of the solubility curves of the enantiomers can be described using the molar solubility ratio α_{mol}, defined as the solubility of the racemic conglomerate divided by the solubility of the pure enantiomer. As discussed by Jacques et al.,[24] the PC process is less efficient when α_{mol} is higher than 2. In the present case, α_{mol} ratio drops from 2.8 at 40°C to 1.8 at 10°C which indicates that PC of Mod I in IBA is more favorable at lower temperature.

Based on the ternary isothermal sections, two processes of PC have been used to resolve PXL in IBA: Seeded Isothermal Preferential Crystallization (SIPC) and Seeded Programmed Polythermic Preferential Crystallization (S3PC).[98] In Figure 3.2 the initial concentration of Mod I in IBA (C_o) used in this work is represented with black and red triangles respectively for SIPC and S3PC modes. Under these conditions, the solution is supersaturated at the crystallization temperature (10 or 20°C) regarding both Mod I and Mod II.

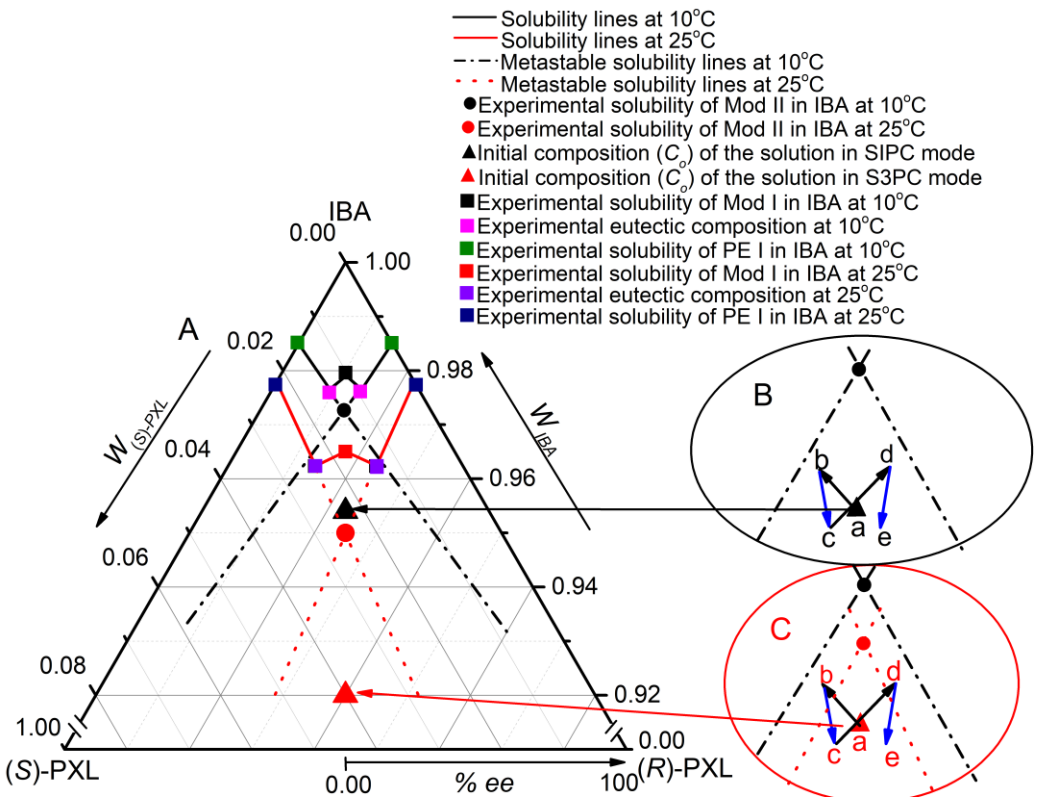

Figure 3.2 A: Ternary solubility phase diagram including the metastable solubility lines (dashed lines) for PE I (*R*) and (*S*) in IBA at 10 and 25 °C used as T_c for SIPC and S3PC respectively (*W* is for weight fraction). B: Performance of PC process for enantioseparation in SIPC mode, C: Performance of PC process in S3PC mode. Signification of (a,b,c,d and e) is described in the text.

3.4 Preferential Crystallization of PXL by SIPC

As evidenced in Table 3.1, a supersaturated solution of racemic PXL in IBA with a supersaturation ratio of β = 2.3 at 20 mL scale and at 10 °C takes at least 1h to crystallize spontaneously as Mod I which prompted us to perform a resolution procedure using the SIPC mode.

Four SIPC experiments were monitored as function of time with various seed mass using the conditions in Table 3.3. The principle of SIPC, is presented in Figure 3.2 - B which depicts the envisaged evolution of the composition of the mother liquor during the process (it is exemplified by the SIPC experiment using 150 mg of seeds).

The starting solution saturated with Mod I at T_s=35 °C (s^*=5 *w*%) is indicated as a black triangle in Figure 3.2. After rapid cooling to T_c=10 °C (s^*=2.1 *w*%, β = 2.3 with reference to Mod I and 1.8 with reference to Mod II), the supersaturated solution is seeded with 150 mg of fine particles of the pure *R* enantiomer. This

induces the stereoselective crystallization of this enantiomer while the enantiomeric excess of the mother liquor evolves from ee_a = 0 % (point a in Figure 3.2 – B) to ee_b = (-) 5.10 % (point b in Figure 3.2 – B) within 20 minutes.

At (b), the system is filtered resulting in, 212.2 mg of crystals with an enantiomeric purity of 91.3%. The liquor is then compensated with 47.73 mg of Mod I and with solvent, thus moving from point b to point c (ee_c = (-) 3.80 %).

After homogenization of the system at 35 °C, the liquor, enriched in PE I (*S*) enantiomer is cooled to 10 °C and seeded with 150 mg of PE I (*S*) to complete the cycle and move from (-) 3.15 % ee_c to (-) 0.15 % ee_d (point d in Figure 3.2 - B) within 30 minutes, 201.0 mg of solid was collected with an *ee* of (+) 89.7 %.

To move from point d to point e (Figure 3.2 - B), the liquor is again compensated with 30.29 mg of Mod I and solvent, homogenized at 35 °C then cooled down to 10 °C to start a new cycle. The process can thus be continuously cyclized.

Table 3.3 Starting Experimental Conditions for SIPC. m_{IBA}: mass of isobutyl alcohol, $m_{Mod\ I}$: initial mass of Mod I dissolved in solvent, C_o: initial total concentration of the solution, T_s: initial saturation temperature, T_c: constant crystallization temperature, $s^*_{Mod\ I_{10°C}}$: solubility of Mod I at 10°C in IBA, $s^*_{Mod\ II_{10°C}}$: solubility of Mod II at 10°C in IBA.

Conditions	SIPC
m_{IBA} (g)	17
$m_{Mod\ I}$ (mg)	894
C_o (w%)	5.0
T_s (°C)	35
T_c (°C)	10
$s^*_{Mod\ I_{10°C}}$	2.1
$s^*_{Mod\ II_{10°C}}$	2.7
Y_{theo} [a] (%)	20

[a] Y_{theo}: theoretical yield defined as $\frac{C_o - C_{Mod\ II_{10°C}}}{2\ C_o}$(x100).

In order to determine the suitable balance between seed mass and duration before filtration, the impact of the seed amount on the entrainment effect was assessed by using various amounts of seeds ranging from 50 to 150 mg. The enantiomeric excess values in the solution as a function of time are shown in Figure 3.3 - a. After seeding with (*S*) enantiomer seed crystals, the solution is progressively enriched in the counter (*R*) enantiomer. This is a clear indication that an out-of-equilibrium stereoselective crystallization of PE I (*S*) is occurring despite the existence of the stable racemic compound.

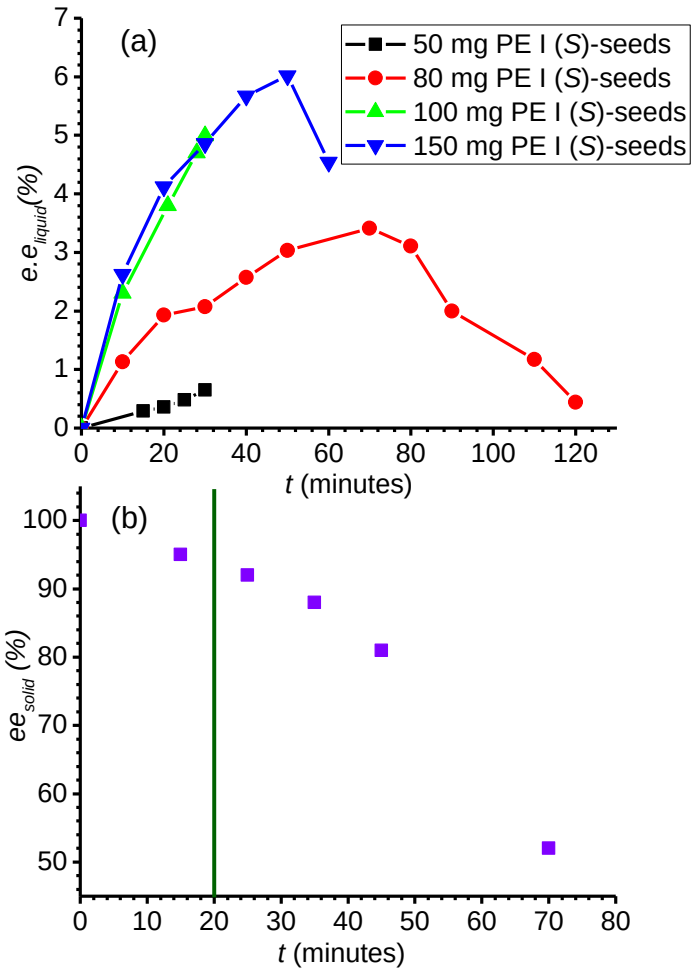

Figure 3.3 Evolution of enantiomeric excess of preferential crystallization in SIPC mode starting from racemic conditions monitoring (a): the liquid phase enriched with PE I (*S*) after seeding with 50 mg, 80 mg, 100 mg and 150 mg of PE I (*S*) and (b) the solid phase with 80 mg of PE I (*S*)-seeds. The vertical green line crossing the point t = 20 minutes taken as filtration window shows the time required to produce PE I (*S*) with good purity while steadily increasing the excess of PE I (*R*) in the liquid phase.

One can also see that the higher the seed mass, the higher and the faster the liquor gets enriched in the opposite enantiomer until the seed mass reaches 100 mg. This can be either because PE I (*S*) enantiomer crystallize faster from solution due to larger seed crystal surface area, or because less Mod I is formed when more seeds are added, so that less PE I (*R*) is removed from solution.

In the profile given in Figure 3.3 - a (red curve), one can see that the entrainment starts after seeding with 80 mg of PE I (*S*)-seeds, yet after 60-70 minutes the *ee* of the liquid phase decreases. This probably results from the heterogeneous nucleation of Mod I, and possibly of the counter enantiomer. Therefore, one could

expect that the filtration window of the process could be as high as 60 to 80 minutes since the enantiomeric excess of the liquor is then maximized.[123] However, the optical purity in the solid phase in Figure 3.3 - b indicates a gradual decrease of the crystal enantiomeric purity with process time.

XRPD analyses of the crystals filtered at 15- and 30-minutes reveals that this is due to the spontaneous crystallization of the racemic compound Mod I after approximately 20 minutes (Figure 3.4) This shows that the introduction of PE I facilitates the formation of Mod I crystals, probably through a heterogeneous nucleation mechanism. Consequently, the filtration window was set at 20 or 30 minutes rather than 60-80 min to compromise between the purity and the mass of the collected solid.

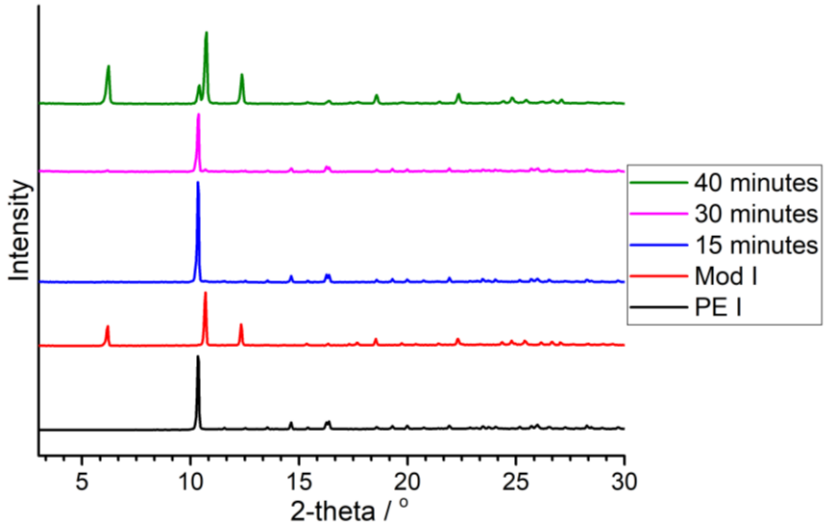

Figure 3.4 X-ray Diffraction analyses of the crystals filtered before and after the filtration window.

The experimental results for 4 consecutive SIPC cycles are given in Table 3.4 and shows that PC of PXL is successful in these conditions since high enantiomeric purity crops can be produced. These results indicate that the increase in seed mass increases the deposition rate of the pure enantiomer, which is the amount of crystalline material in units of gram/second that is deposited, due to the higher surface area offered by the larger amount of seeds and also to the slow nucleation kinetics of Mod I during the 20 first minutes.

This significantly increases the enantiomeric excess of the liquid phase, thus accelerating the resolution process. Herein, it can be concluded that the seed mass affects the resolution rate and the yield of the produced solid in a SIPC mode. It can also be deduced from these data that the crystallization behavior of PXL during the SIPC process is mainly driven by the crystal growth of the seeds rather than secondary nucleation of PE I. This prompted us to perform the resolution by

implementing a controlled cooling profile with the aim of improving the efficiency of the process.

Table 3.4 Experimental results of the SIPC cycles in IBA at 10 °C. ee_o (%): initial enantiomer excess in the liquid phase, W_{seeds}: mass of seeds, t_{end}: duration time in minutes, $W_{c.s}$ and $e.e._{c.s}$: weight and enantiomeric excess of the collected solid with seeds included, $W_{P.E.}$: weight of produced pure enantiomer, Y_{exp}: experimental yield, ee_f (%): enantiomeric excess of the liquid phase at the end of the process.

Nb	ee_o (%)	W_{seeds} (mg)	t_{end} (min)	$W_{c.s.}$ (mg)	$e.e._{c.s.}$ (%)	$W_{P.E.}$ (mg)	Y_{exp} (%)	ee_f (%)
1	0.00	(*R*) 50	20	65.5	(*R*) 89.3	8.49	4.74	(*S*) 1.30
2	(*S*) 1.00	(*S*) 50	30	57.6	(*S*) 90.7	2.60	1.45	(*R*) 0.30
3	0.00	(*R*) 80	20	108.0	(*R*) 92.9	19.86	11.10	(*S*) 2.25
4	(*S*) 1.70	(*S*) 80	30	110.5	(*S*) 90.2	18.87	10.55	(*R*) 0.11
5	0.00	(*R*) 100	20	145.3	(*R*) 91.7	32.84	18.36	(*S*) 4.29
6	(*S*) 3.64	(*S*) 100	30	140.6	(*S*) 91.6	28.38	15.87	(*R*) 0.20
7	0.00	(*R*) 150	20	212.2	(*R*) 91.3	43.73	24.45	(*S*) 5.10
8	(*S*) 3.80	(*S*) 150	30	201.0	(*S*) 89.7	30.29	16.94	(*R*) 0.15

3.5 Preferential crystallization by S3PC

Compared to SIPC, the S3PC process is assumed to provide advanced control over the supersaturation profile and therefore to favor a gentler crystallization behavior, reducing the likelihood of spontaneous nucleation. Figure 3.2 - C depicts a cyclic operation of the PC process in S3PC mode to produce both enantiomers for the first two runs. A supersaturated solution was prepared at 25 °C (C_o = 8 w%), resulting in a supersaturation ratio of β = 2.3 at 25°C for the racemic compound Mod I which is identical to that applied for SIPC. Therefore, the supersaturation with reference to Mod II is 1.6, slightly lower than that employed for SIPC (β_{SIPC}=1.8) which creates a moderate variation of ca. 10 % compared to SIPC. Starting at a lower supersaturation for Mod II constitutes an advantage for S3PC and thus the driving force of the crystallization is controlled by the cooling profile.

The data of two successive S3PC cycles carried out by recycling the mother liquor are reported in Table 3.5. Based on our SIPC results we have chosen seed masses in the range of 80-100 mg. In the first cycle and starting from a racemic composition (point (a) in Figure 3.2 - C) the solution is seeded with 100 mg PE I (PE I (*R*)) and linearly cooled down to 10 °C. A cooling rate of 0.75 °C/min was applied. The solution moves from ee_a = 0% (point a in Figure 3.2 - C) to ee_b = 3.3% (point b in Figure 3.2 - C) and is then filtered to collect 160.0 mg of crude crops with optical purity of 92.0%. After compensation with 47.0 mg of Mod I and with solvent, a new run can be per-formed (points c, d and e in Figure 3.2 - C) with a

cooling profile of 0.375 °C/min. A slower cooling profile was adapted in this case because we found that at least 40 minutes of cooling are required in order to get a solution enriched with the opposite enantiomer (i.e. the required starting condition for the next run). Such a slow cooling profile, however, systematically resulted in the concomitant spontaneous nucleation of Mod I. Compared to SIPC for which the nucleation of Mod I was sufficiently delayed at 10 °C, the higher nucleation rate of this phase in S3PC might be related to the higher concentration in solution (8 w% for S3PC vs 5 w% for SIPC as C_o).

Table 3.5 Two successive S3PC cycles of PXL in IBA. ee_o (%): initial enantiomer excess in the liquid phase, W_{seeds}: mass of seeds, t_{end}: duration time in minutes, $W_{c.s.}$ and $e.e._{c.s.}$: weight and enantiomeric excess of the collected solid with seeds included, $W_{P.E.}$: weight of produced pure enantiomer, Y_{exp}: experimental yield calculated compared to the theoretical yield of 33.125%, ee_f (%): enantiomeric excess of the liquid phase at the end of the process.

Nb	ee_o (%)	W_{seed} (mg)	t_{end} (min)	$W_{c.s.}$ (mg)	$e.e._{c.s.}$ (%)	$W_{P.E.}$ (mg)	Y_{exp} (%)	ee_f (%)
1	0.00	100 (*R*)	20	160.0	(*R*) 92.0	47.20	9.96	(*S*) 3.30
2	(*S*) 2.30	100 (*S*)	40	210.2	(*S*) 81.1	70.47	14.97	(*R*) 1.53
3	(*R*) 1.40	80 (*R*)	40	134.2	(*R*) 81.2	28.57	6.02	(*S*) 0.40
4	(*S*) 0.20	100 (*S*)	40	156.0	(*S*) 82.6	28.85	6.08	(*R*) 1.85

This shows that the used conditions are not suited for S3PC. Additional experiments should be designed to implement this process under smoother conditions in order to assess the enantiomeric selectivity of S3PC and to reach an advanced control over the primary heterogeneous nucleation of Mod I.

3.6 Discussion

This chapter showed the results obtained using our first work plan described in Figure 1.14 and demonstrated that, as in the case of DPL, the major limitation of PC (i.e. the requirement of a stable conglomerate) can be overcome using this strategy. Even though scale-up was not performed and various experimental parameters might still be optimized, this study provides a second proof of concept for implementation of PC in a system that crystallizes as a stable racemic compound. During the implementation of the PC process using both isothermal and polythermal modes, several critical factors were identified: (i) large MSZW that should exceed the ratio of solubility of conglomerate and racemic compound, and thus the absence of spontaneous nucleation of the racemic compound after seeding (ii) fast growth rate of enantiopure compound, (iii) optimal mass and quality of seeds.

Our study showed that a large MSZW is necessary but is not the only factor enabling PC in this type of system since seeding with pure enantiomer can also trigger the primary heterogeneous nucleation of the racemic compound. Therefore, process optimization is mandatory for successful implementation of the method proposed here, and further studies are required to optimize process parameters such as stirring mode, supersaturation, temperature, cooling profile, mixture of solvents, and also seed quality. The present work therefore open doors for new perspectives toward a possible enlargement of the application field of PC but also suggests that the SIPC method should be preferred when using that strategy owing to the results obtained for S3PC.

In the next chapter the second complementary approach for chiral resolution of PXL via a conglomerate cocrystal will be presented and the work strategy will be detailed.

CHAPTER 4: RESOLUTION OF PXL VIA THE FORMATION OF CHIRAL COCRYSTALS

This part is based on two publications:

1. Harfouche L., Cartigny Y., Brandel C., Petit S., Coquerel G. (2020). Discovering of New Proxyphylline Chiral Cocrystals: Solid State and Dehydration Mechanism. Submitted to Crystal Growth and Design (under review, January 2020). SMS laboratory, University of Rouen, Mont saint Aignan, France.
2. Harfouche L., Cartigny Y., Brandel C., Petit S., Coquerel G. (2020). Resolution by Preferential Crystallization of Proxyphylline by using its Salicylic Monohydrate Co-crystal. Chem. Eng. Technol. Accepted manuscript. SMS laboratory, University of Rouen, Mont saint Aignan, France.

4.1 Introduction

In this chapter we conduct a study aiming at converting racemic PXL into a conglomerate by cocrystallization procedure. This phase could be an intermediate for preferential crystallization (for experimental plan see Figure 1.14). To the best of our knowledge, no cocrystal of PXL has ever been reported in the literature. In this study, we describe the discovery of 10 solid forms with a 1:1 stoichiometry between PXL and the cocrystal formers and the study of the solid-state landscape of four cocrystals between PXL and salicylic acid (SA). One of these phases crystallize as a conglomerate, the PC of this chiral cocrystal was then envisaged.

4.2 Cocrystal screening

Cocrystals were prepared by grinding or by dissolution/evaporation. All experiments were carried out with a 1:1 stoichiometric ratio of PXL and coformer. Grinding (in dry conditions or by liquid assisted grinding (LAG) was performed at room temperature using a Retsch Mixer Mill model MM400 with 10 mL zirconium oxide grinding jars containing one 12 mm zircon grinding ball at a rate of 20 Hz for 20 min. LAG experiments were performed by adding ca. 10-20 µl of a selected solvent to the solid mixture prior to grinding.

Water, acetone, ethanol, methanol, isopropanol (IPA), n-hexane, dichloromethane (DCM), and chloroform ($CHCl_3$) were used for the LAG experiments. For the same stoichiometric mixture, a dry grinding was also performed. Cocrystals were also prepared by complete evaporation of solvent after dissolution of a 1:1 stoichiometric mixture of PXL and a chosen coformer in a minimum amount of solvent (approximately 5-10 mL) followed by slow evaporation of the solvent at room temperature.

The seven coformers presented in Figure 4.1 induced the crystallization of new solid phases with PXL. Nuclear magnetic resonance (^{1}H NMR) analyses confirmed the 1:1 stoichiometry and showed that no mechanochemistry occurred (Annex C). The preparation method of the first six new cocrystals are introduced in Table 4.1, their XRPD and DSC data can be found in Annex C. The produced cocrystals from PXL and salicylic acid (SA) are further studied below.

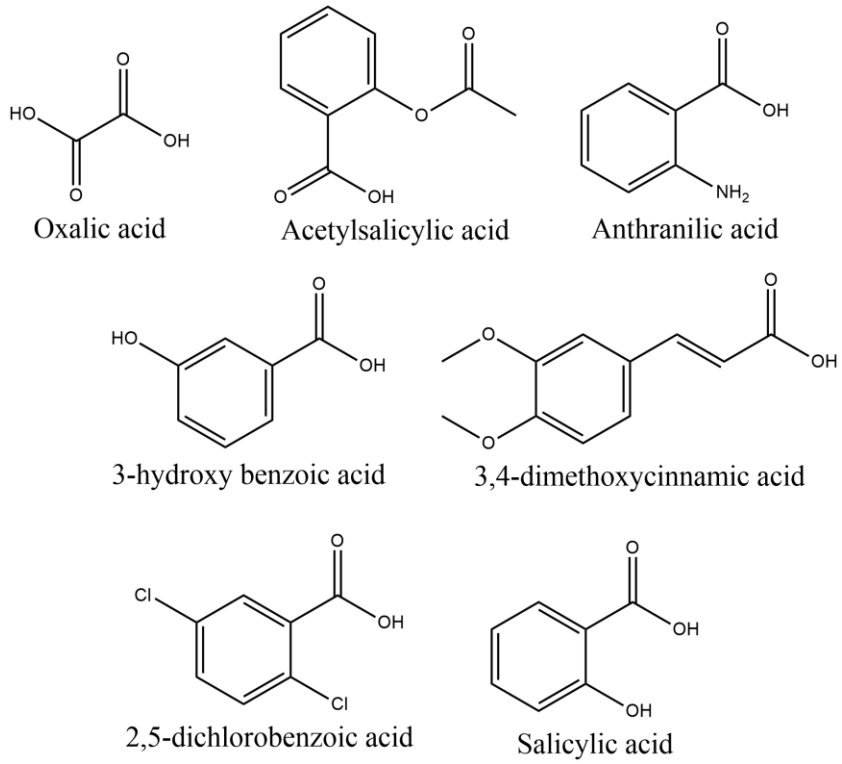

Figure 4.1 Molecular formula of the seven coformers that produced new solid phases with PXL.

Table 4.1 Preparation methods to obtain new cocrystal forms of PXL with six different coformers.

Coformer	Neat Grinding	LAG	Evaporation
Oxalic acid (OA)	+	Acetone, IPA, DCM, $CHCl_3$	/
Acetylsalicylic acid (AA)	+	Acetone, heptane, DCM, MeOH, EtOH	MeOH
Anthranilic acid (Ant)	+	Acetone, EtOH, MeOH, DCM	/
3-hydroxybenzoic acid (HBA)	/	MeOH	/
3,4-dimethoxycinnamic acid (DMCA)	+	/	/
2,5-dichlorobenzoic acid (DClBA)	+	/	Heptane

+ : cocrystal formation / : no new solid phase was identified

4.3 Preparation and identification of PXL:SA phases

Crystallization of racemic PXL and SA in 1:1 ratio resulted in different cocrystal forms. (i) The first form was obtained by slow complete evaporation from methanol/water (3:7 *v*:*v*) solution or by liquid assisted grinding (LAG, 10 µl of methanol/water). (ii) The second form was prepared by wet milling (20 µl of heptane/EtOH (1:1)) and (iii) the third form was obtained by annealing the second form at *ca.* 98 °C for 15 min or directly from LAG (10 µl EtOH). These cocrystals are kinetically stable when placed in an open environment at room temperature.

Using gravimetric measurements (annealing at 70 °C for 10-15 minutes), it was deduced that the first form is a monohydrate labeled (*R*)/(*S*)-H hereafter, whereas the two other forms are anhydrous ((*R*)/(*S*)-A1 and (*RS*)-A2 respectively). The product obtained after the dehydration of (*R*)/(*S*)-H by annealing procedure was found to be a third anhydrous form (*R*)/(*S*)-A3. Figure 4.2 shows the X-Ray powder diffraction (XRPD) patterns of the different racemic cocrystals obtained between PXL and SA.

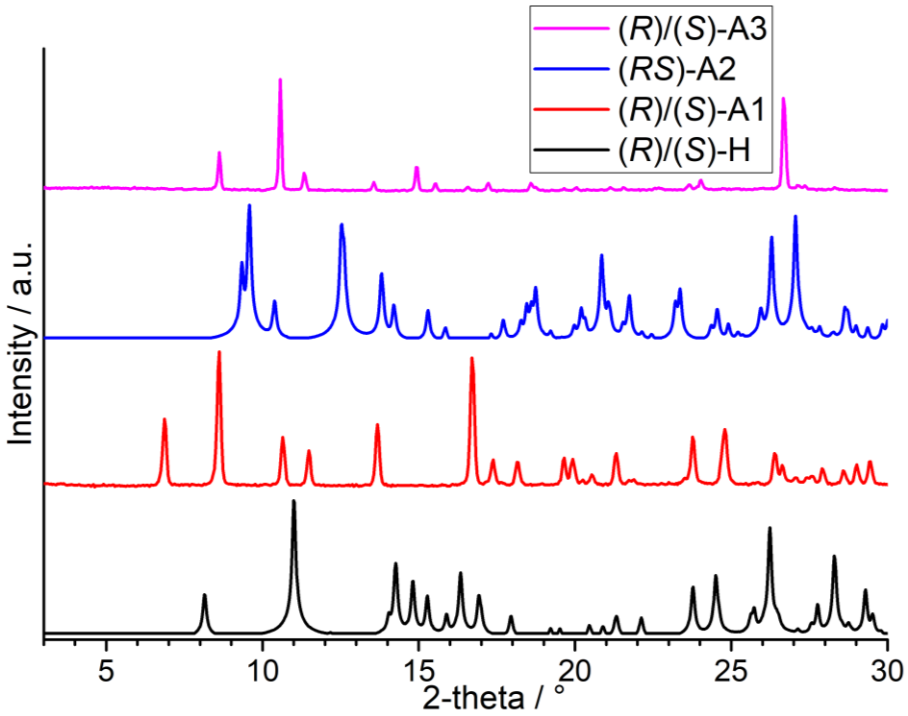

Figure 4.2 Comparison of PXRD patterns of the cocrystal samples obtained with 1:1 PXL and SA.

Table 4.2 summarizes the SHG results of the four racemic cocrystals. The signal identified for (*R*)/(*S*)-H, A1 and A3 indicates that they are non-centrosymmetric crystals while (*RS*)-A2 is a centrosymmetric solid phase. One can reasonably suppose that (*R*)/(*S*)-H, (*R*)/(*S*)-A1 and (*R*)/(*S*)-A3 are conglomerates.

Table 4.2 SHG activity for the solid form obtained after 1:1 molar ratio mixture of Mod I and SA.

Coformer	SHG signal	SHG intensity	Suspected nature of the racemic solid
(*R*)/(*S*)-H	+	35000	Non-centrosymmetric
(*R*)/(*S*)-A1	+	36000	Non-centrosymmetric
(*RS*)-A2	-	-	Racemic compound
(*R*)/(*S*)-A3	+	38000	Non-centrosymmetric

In order to confirm the suspected nature of the studied solids, trials to grow single crystals were carried out. Up to now all attempts to grow single crystal of (*R*)/(*S*)-A1 and (*R*)/(*S*)-A3 with sufficient quality for Single crystal X-Ray diffraction (SC-XRD) analysis failed. Only single crystals of (*R*)/(*S*)-H and (*RS*)-A2 were obtained, the crystal structure of each form was studied to verify the chiral nature of these solid forms, the molecular conformations and their packings.

4.4 Single crystal X-ray diffraction studies

Crystallographic data for (*R*)/(*S*)-H and (*RS*)-A2 are summarized in Table 4.3.

Table 4.3 Crystallographic data for (*R*)/(*S*)-H and (*RS*)-A2.

Chemical Formula	$[C_{10}H_{14}O_3N_4]$ $[C_7H_6O_3],H_2O$	$[C_{10}H_{14}O_3N_4]$ $[C_7H_6O_3]$
	(*R*)/(*S*)-H	*RS*-A2
Crystal System	Monoclinic	Triclinic
Space Group	$P2_1$	$P\bar{1}$
Z, Z' (asymmetric units per unit cell)	2,1	2,1
a / Å	7.289(1)	9.652(2)
b / Å	11.952(2)	10.216(2)
c / Å	10.886(1)	10.435(2)
α / °	90	65.538(4)
β / °	95.175(3)	81.132(5)
γ / °	90	79.862(4)
V / Å3	944.6(2)	918.3(3)
R indices on I >σ2I	R1=0.0742 wR2=0.1791	R1=0.0564 wR2=0.1104
Independent reflexions / with I> I >σ2I	3668/2061	3584/1606

Single crystal X-ray analysis of (*R*)/(*S*)-H obtained by evaporation from aqueous solution shows that the solid is a monohydrate cocrystal crystallizing in the $P2_1$ space group and forming a conglomerate. The asymmetric unit is composed of one molecule of PXL, one molecule of SA and one water molecule (Figure 4.3). No hydrogen atom is exchanged between the salicylic acid and the proxyphylline molecule.

The different entities establish strong interactions through intermolecular hydrogen bonding. The water molecule establishes a hydrogen bond network with three PXL molecules that hold this structure altogether.

Along *c*, the water molecule is intercalated between two molecules of PXL establishing hydrogen bonds. These two molecules generate a periodic bond chains spreading along *c*. SA molecules are connected to these periodic bond chains (PBC) by a third H-bond (Figure 4.4, Table 4.4). A hydrogen bond is also depicted between adjacent PBC along the *b* direction that leads to molecular layers in *bc*. The overall crystal packing also features $\pi\pi$ stacking interactions ensuring the cohesion of the packing (distance ~3.6/3.7Å from the centroid of the aromatic ring of SA and the center of the C1-C6 bond in PXL) (Figure 4.5).

The description of this structure clearly demonstrates the importance of water molecules in the crystal structure cohesion. The possibility of creating isomorphic

desolvated form (*i.e.* made of about the same packing of the PXL and SA molecules as in the solvate) seems to be not accessible. To confirm this hypothesis, the preparation and the study of single crystals of the desolvated form is required.

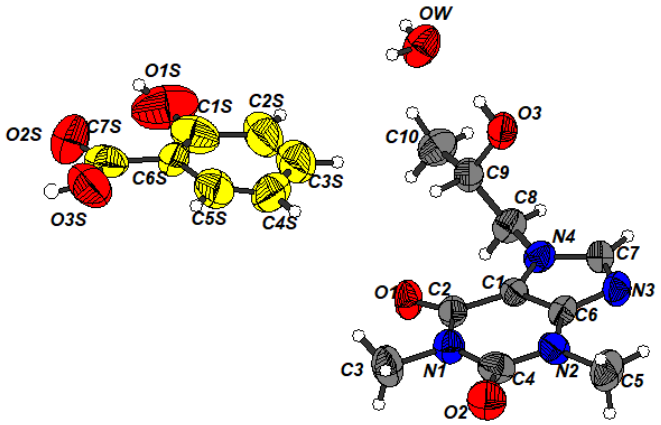

Figure 4.3 Asymmetric unit of (*R*)/(*S*)-H in ellipsoidal representation with atoms labelled. (Carbon atoms are displayed in grey for PXL and in yellow for SA)

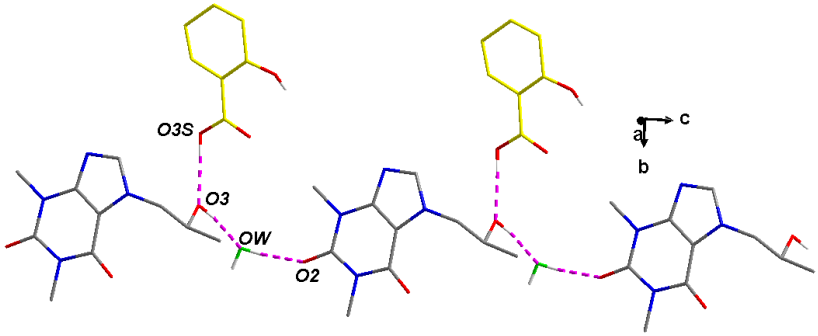

Figure 4.4 Periodic bond chain spreading along the *c* axis. The water molecule (in green) is intercalated between two consecutive PXL along *c*, the SA molecules are connected to this molecular chain. The intra-chain H-bonds are displayed as pink dashed lines.

Table 4.4 Hydrogen bond table in (*R*)/(*S*)-H.

D-H...A	d(H...A)
Intra chain H-bond –pink lines	
OW-H(2O)...O(2)	1.92(6)
O(3)-H(3)...OW	1.90(6)
O(3S)-H(3S1)...O(3)	1.81(7)
Inter chain H-bond- blue lines	
OW-H(1O)...N(3)	2.12(7)

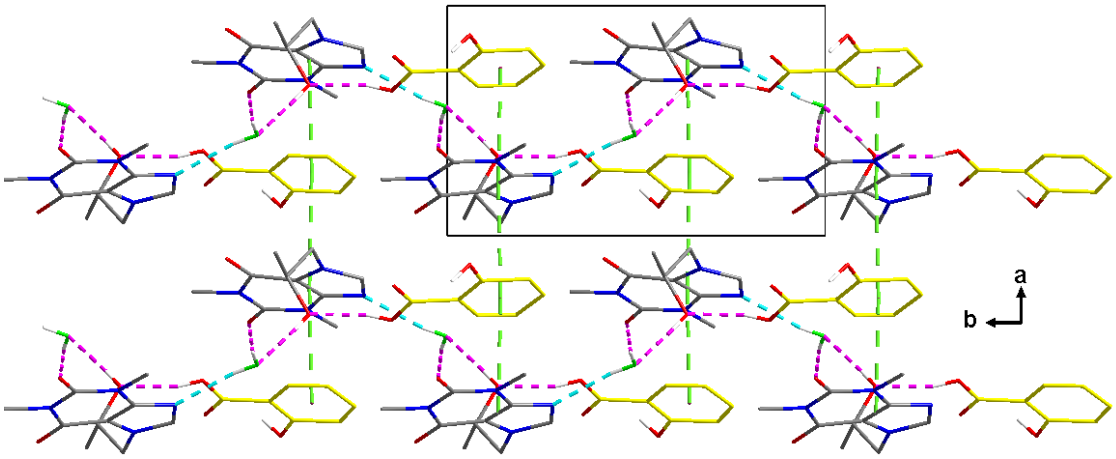

Figure 4.5 Two molecular layers stacked along *a*, the $\pi\pi$ interactions are featured in dashed green lines. (The H-bonds are displayed in dashed pink lines when intra PBC and dashed blue lines when inter PBC).

For (*RS*)-A2, a single crystal was obtained by leaving a supersaturated solution of the (*R*)/(*S*)-H in ethanol at 10 °C. The crystal data confirm that it is a racemic compound with a $P\bar{1}$ space group. The asymmetric unit is composed of one PXL molecule and one SA molecule (Figure 4.6 - a). Interestingly, the conformations of PXL and SA from the asymmetric unit of (*R*)/(*S*)-H and (*RS*)-A2 are similar (Figure 4.6 - b) but the structural features of the two crystal lattices do not indicate any structural filiation.

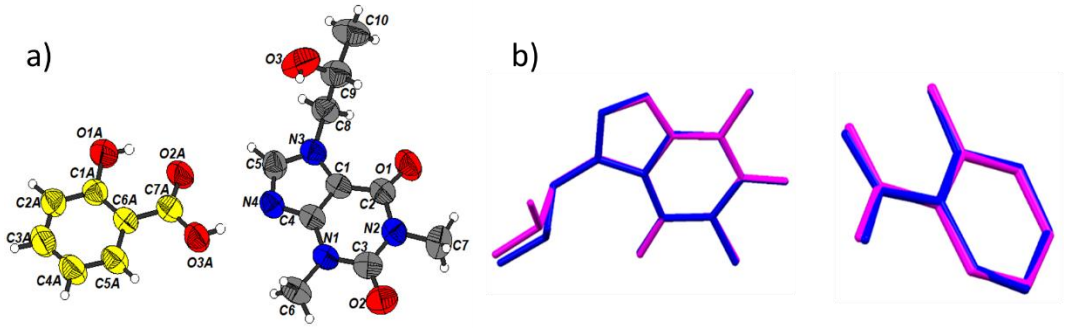

Figure 4.6 a) Asymmetric unit of (*RS*)-A2 in ellipsoid representation with atom labels. (Carbon atoms are displayed in grey for PXL and in yellow for SA) and b) Conformational similarity between the PXL molecules from the asymmetric unit of Form-H (Blue) and Form-A2 (Pink).

The molecular entities establish strong hydrogen bonds (Table 4.5). These interactions lead to a centrosymmetric dimer (PXL-SA) (Figure 4.7). The cohesion is ensured by $\pi\pi$ interactions along c axis (Figure 4.8). The combination of H-bonds and this first type of $\pi\pi$ interactions (d~3.5 Å) give rise to dimers and generate PBC in the $[10\bar{1}]$ direction (Figure 4.9). Adjacent PBC establish a second type of $\pi\pi$ interactions (d~3.6Å) that give rise to molecular layers in ac (Figure 4.9). The cohesion between the layers is ensured by van der Waals interactions.

Table 4.5 Hydrogen bond in (*RS*)-A2.

D-H...A	d(H...A)
O(3)-H(3)...O(2)	2.02(3)
O(3A)-H(3A1)...N(4)	1.87(3)
O(1A)-H(1A)...O(2A)	1.84(3)

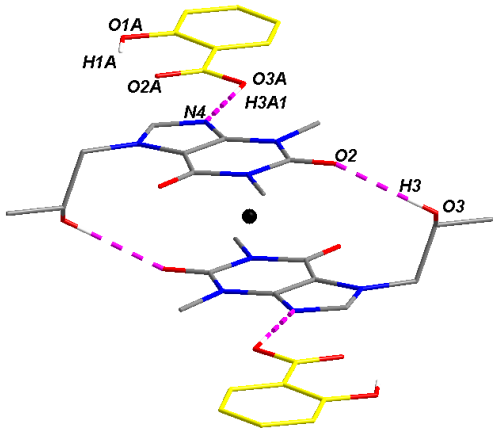

Figure 4.7 Molecular block built from hydrogen bond interactions (dashed pink lines). (The black dot represents an inversion center).

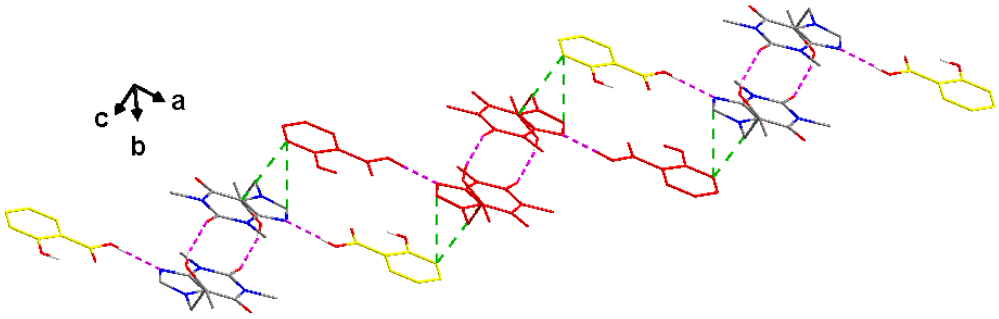

Figure 4.8 Periodic bond chain formed through $\pi\pi$ interactions (C2A to C1, d~3.5Å and C2A to N4, d~3.6Å) in dashed green line.

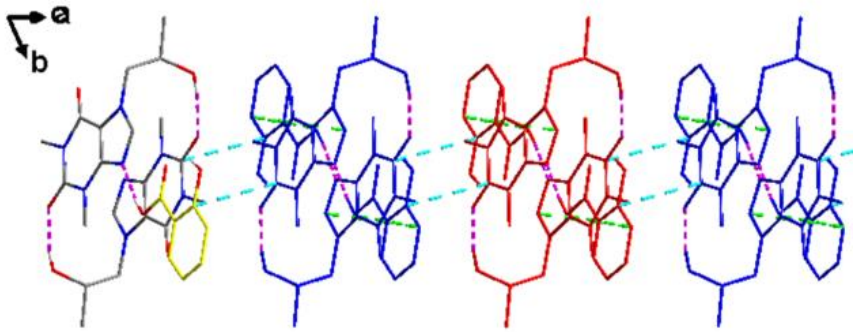

Figure 4.9 Projection along [$10\bar{1}$] of several periodic bond chains (represented in blue, red or standard) interacting though a second type of $\pi\pi$ interactions in dashed blue lines. (C1A to C3, d~3.6Å).

4.5 Study of the dehydration behavior of the monohydrate cocrystal

Using DSC/TGA, X-Ray Diffraction and DVS we examined the dehydration behavior of the monohydrate cocrystal under its racemic ((*R*)/(*S*)-H) and enantiomeric pure form (PE-H). It should be mentioned that (PE-H) was obtained from the same procedure as that used to prepare (*R*)/(*S*)-H by using the pure enantiomer of PXL instead of the racemic mixture.

4.5.1 Nonisothermal Dehydration Analysis

Figure 4.10 shows the DSC and TGA profiles of (a) (*R*)/(*S*)-H and (b) PE-H obtained with a heating rate of 10 K/min. The thermograms show a broad endotherm (black curves in Figure 4.10 - a and b, with a peak at ca. 80 °C attributed to the dehydration. The associated weight loss of 4.3% corresponds to one molecule of water per molecule of cocrystal (theoretical value = 4.7%). After the dehydration process, a sharp endotherm is observed at 90.4 °C in both cases, followed by another broad endotherm ending at *ca.* 112 °C. The shape of these two endothermic peaks is consistent with the occurrence of an invariant phenomenon and a liquidus line respectively. The thermogravimetric profile shows a second weight loss that begins at about 125 °C and which can be explained by the loss of SA by evaporation. This was further confirmed by XRPD experiments performed separately at different temperatures.

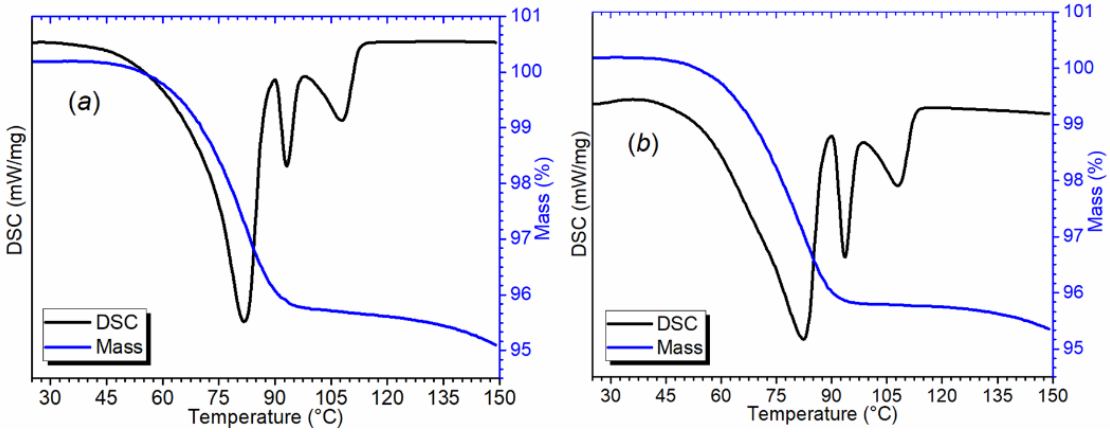

Figure 4.10 DSC and TGA curves of the monohydrate cocrystal (a) (*R*)/(*S*)-H and (b) PE-H.

To get a better understanding of the dehydration process, samples of (*R*)/(*S*)-H and PE-H were analyzed by XRPD at room temperature after annealing the solid for 10 minutes at different temperatures ranging from 60 to 130 °C. The XRPD patterns of the dehydration products are compared in Figure 4.11 highlighting the

impact of the annealing temperature on the final product. It should be mentioned that the experiments conducted on samples of (*R*)/(*S*)-H and PE-H give rise to the same patterns during heating until melting (Figure 4.11 - e to Figure 4.11 - h) and to different solid phases after annealing the melt at high temperature (Figure 4.11 - i and j).

The dehydration product at 60 °C (Figure 4.11 - e) consists of the coexistence of the hydrate and the anhydrous form A3. At 85 °C (Figure 4.11 - f) the dehydration is complete and A3 is the only obtained form, whatever the starting phase ((*R*)/(*S*)-H and PE-H). This confirms the result obtained by SHG (Table 4.2) indicating that (*R*)/(*S*)-A3 is a racemic conglomerate. In both cases, the XRPD pattern collected at 90 °C (Figure 4.11 - g) shows the existence of A3 and the pure enantiomer of PXL (PE I), indicating a partial decomposition of the cocrystal due to sublimation of a small fraction of SA (collected on the cover lid).

This behavior confirms the decomposition of the cocrystal at this temperature due to a peritectic transition (*i.e.* E-A3$_{(s)}$ ⇆ PE I$_{(s)}$ + Liquid). No pattern is seen at 115 °C due to melting of the solid material (small peaks can still be detected due to the presence of small amounts of PE I in equilibrium with the melt). Leaving the obtained melt for 24h at 130 °C leads to the total evaporation of SA and the recrystallization of PXL under its racemic or enantiopure form depending on the nature of the starting material (Figure 4.11 - i and j respectively).

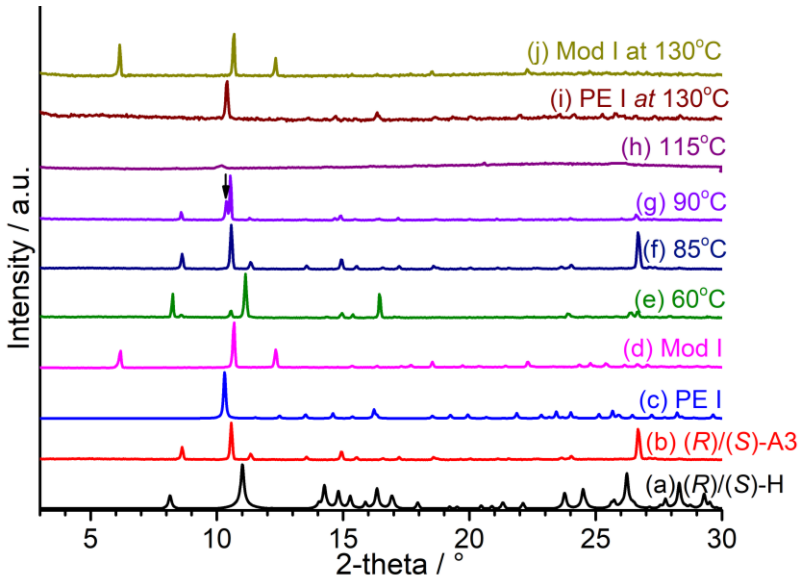

Figure 4.11 XRPD reference patterns of (a) (*R*)/(*S*)-H or (E-H), (b) (*R*)/(*S*)-A3 or E-A3, (c) PE I, (d) Mod I and XRPD patterns of (*R*)/(*S*)-H and E-H dehydrated by 10 minutes annealing at (e) 60 °C, (f) 85 °C, (g) 90 °C, (h)115 °C, 130 °C for (i) E-H and (j) (*R*)/(*S*)-H. All patterns were collected at room temperature.

4.5.2 Gravimetric Vapor Sorption Analysis

Dynamic moisture sorption-desorption isotherms (T = 25 °C) were performed on both (*R*)/(*S*)-H and PE-H. Interpretation of the curves will only be given for (*R*)/(*S*)-H solid, because the same results were obtained for E-H (Figure 4.12). Before the first sorption step, the solid was exposed to a dry atmosphere (0% RH) leading to the total dehydration of the solid. During the first sorption up to 95%RH, the mass uptake increased to a maximal value of 3%wt, which is inferior to the theoretical expected value for a monohydrate stoichiometry (4.7 *w*%).

The desorption 1 highlights the stability of the hydrate if RH>10%. Under dry conditions, a mass loss of *ca.* 8.0 % indicates that the departure of water in these conditions is accompanied by another departure of matter. During the subsequent sorption/desorption 2 a similar behavior is recorded: the cocrystal (under RH > 75 %) undergoes an incomplete rehydration (2.6 *wt*% mass uptake) and an excessive mass loss is recorded during the drying step.

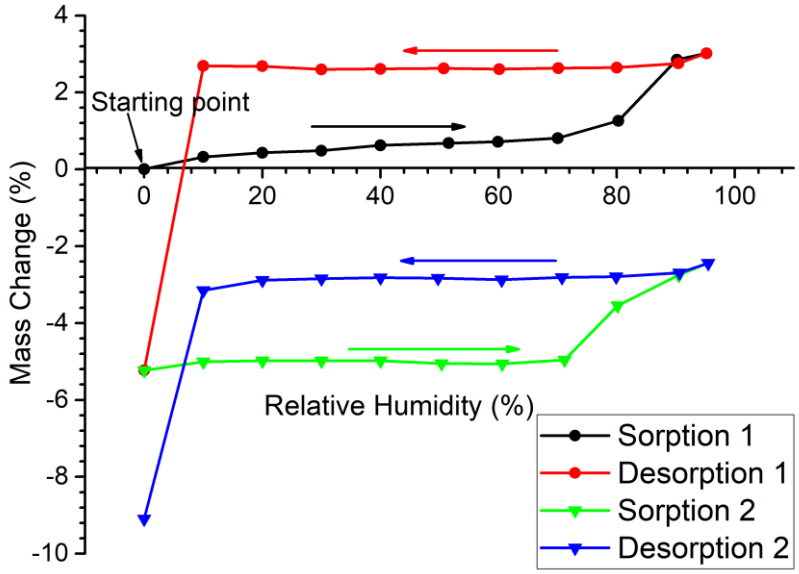

Figure 4.12 Mass change versus relative humidity (%) recorded at 25 °C for (*R*)/(*S*)-H.

The difference in the uptake/loss mass during the successive sorption/desorption cycles is consistent with a concomitant dehydration/decomposition of the cocrystal. This was confirmed by two experimental complementary information: (i) XRPD analyses (under ambient RH) of (*R*)/(*S*)-H samples after DVS experiments indicates that the resulting solid is a mixture of (*R*)/(*S*)-A3, (*R*)/(*S*)-H and Mod I with no trace of SA (Figure 4.13) and (ii) DVS experiments made on solid SA lead to a continuous mass loss under dry

conditions related to a sublimation phenomenon. (Figure 4.14). Besides, PXL samples (racemic or enantiopure forms) are stable under variable humidity (no hydration, no degradation, data not shown).

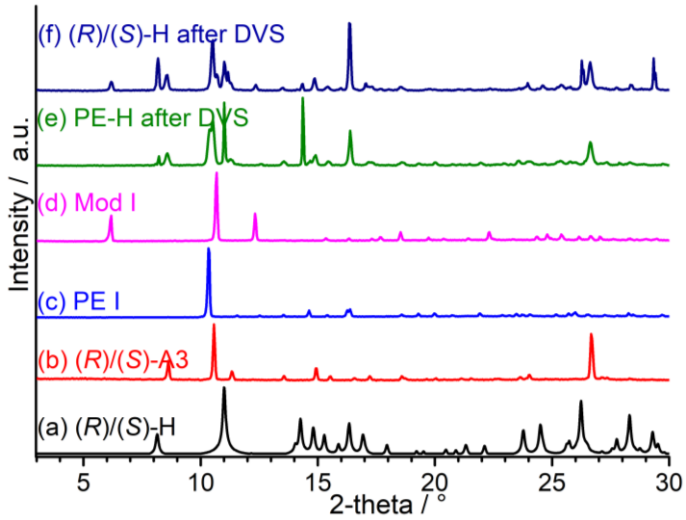

Figure 4.13 XRPD patterns of a) (*R*)/(*S*)-H, b) (*R*)/(*S*)-A3, c) PE I, d) Mod I, e) PE-H after two sorption-desorption cycles in the DVS and f) (*R*)/(*S*)-H after two sorption-desorption cycles in the DVS.

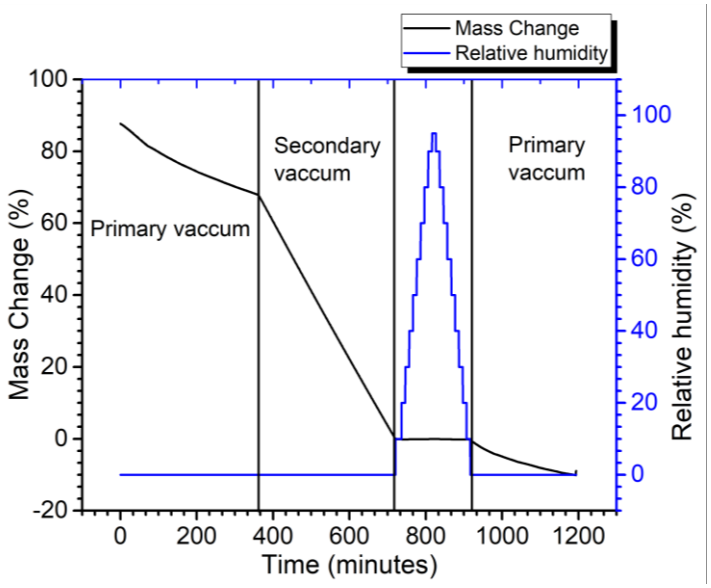

Figure 4.14 Sorption-desorption cycle performed at 25 °C for SA with DVS vacuum. Mass change (%) is referred to the mass at the end of the first drying step.

From this experiment, it can be deduced that during the gravimetric vapor sorption experiments, the departure of water molecules during dehydration (leading to the (*R*)/(*S*)-A3 phase) is irreversibly associated to SA sublimation. Nevertheless, due to kinetic reasons, the total decomposition of (*R*)/(*S*)-A3 (into PE I) is not reached and the rehydration of the remaining solid is made possible by increasing relative humidity.

4.5.3 Hot stage microscopy observations

Microscopy observation carried out on a single crystal of the monohydrated cocrystal under a heating rate of 1 °C/min are presented in Figure 4.15. The opacity of the crystal increases during the dehydration step starting at 45 °C without losing its external morphology. At around 70 °C, the water starts to be evacuated from the crystal, through what seem to be canals (photos at 77 and 82 °C). The shape of the single crystal is altered and becomes rough up to 96-111 °C. Upon further heating, melting occurs concomitantly with the crystallization of a solid from the inner part of the initial crystal. This new solid form (photo at 131 °C) appears to be the pure enantiomer of PXL (PE I), because its melting point was seen to be between 151-153 °C.

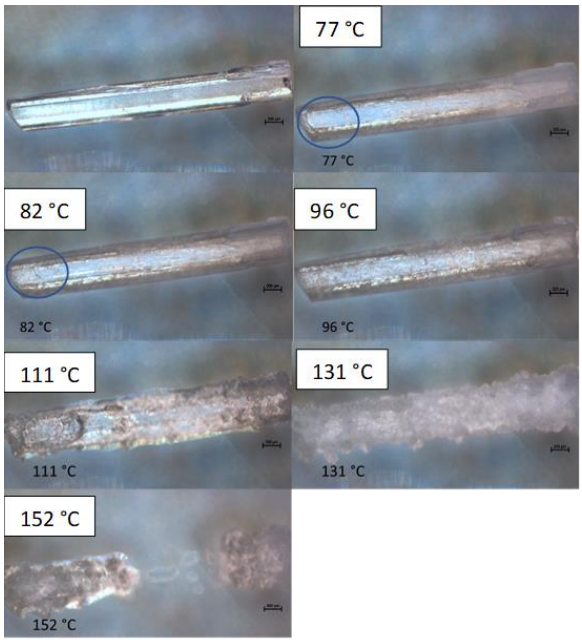

Figure 4.15 Hot stage microscopy observation of a monohydrate single crystal at 1 °C/min at different temperature.

4.6 Study of the binary system between (*R*) and (*S*)-anhydrous cocrystal

In order to study the binary system, the pure enantiomer of the anhydrous forms was prepared between PE I (*R*) or (*S*) and SA according to the different described methods suitable for the preparation of the racemic anhydrous cocrystals. A single anhydrous pure enantiomer form (PE-A1) was obtained and identified by XRPD showing the same pattern as (*R*)/(*S*)-A1 indicating that this phase is a racemic conglomerate (confirming the hypothesis surmised after SHG measurements, Table 4.2). Figure 4.16 displays the DSC curve for the racemic conglomerate (*R*)/(*S*)-A1, the racemic compound (*RS*)-A2 and the pure enantiomer PE-A1 obtained at a heating rate of 5 K/min in the temperature range of 20 to 200 °C. The DSC curve of (*R*)/(*S*)-A1 shows one melting event at 84 °C (Figure 4.16 - a) and a recrystallization (exothermic peak happening directly after melting) followed by the endothermic melting at 103 °C. This melting temperature corresponds to that of (*RS*)-A2 with $\Delta_{fus}H$ = 41.3 kJ/mol (Figure 4.16 - b). The recrystallization of (*R*)/(*S*)-A1 into (*RS*)-A2 after melting was confirmed by XRPD at room temperature (RT) after annealing the melt for 10 minutes at 95°C (Figure 4.17). Therefore, one can deduce that the racemic conglomerate (*R*)/(*S*)-A1 is metastable referred to the racemic compound (*RS*)-A2. For the PE-A1 solid form, only one endotherm is detected at 101.4 °C with $\Delta_{fus}H$ = 43.3 kJ/mol. (Figure 4.16 - c).

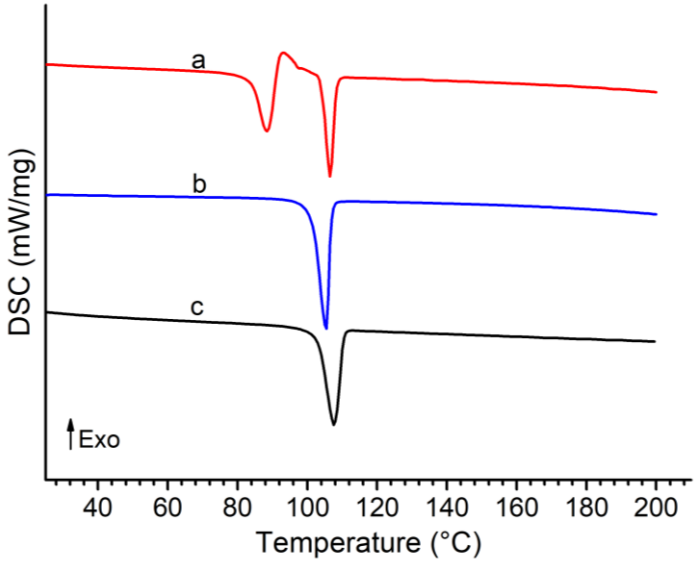

Figure 4.16 Thermograms of the anhydrous forms a) (*R*)/(*S*)-A1 (red profile), b) (*RS*)-A2(blue profile) and c) PE-A1 (black profile).

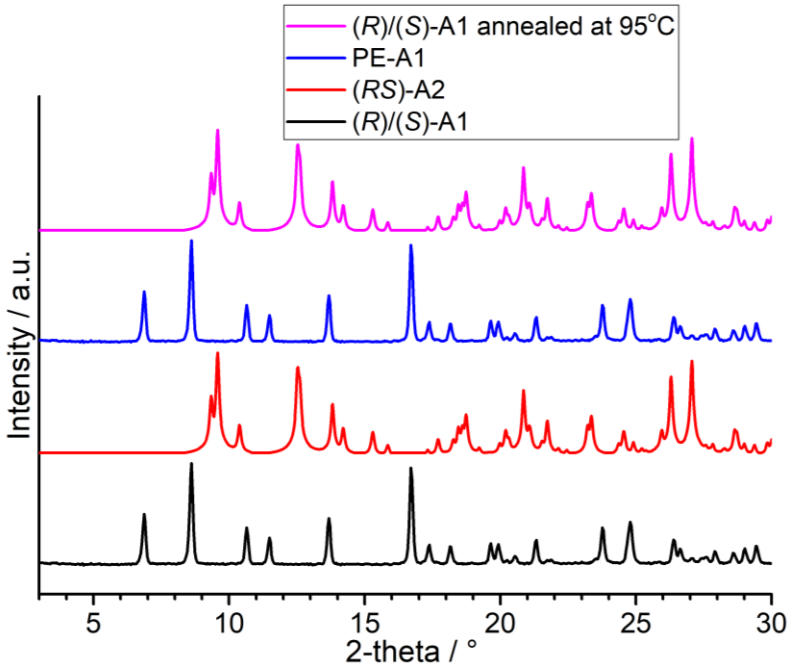

Figure 4.17 XRPD patterns of (*R*)/(*S*)-A1, (*RS*)-A2, PE-A1 and the obtained solid after annealing (*R*)/(*S*)-A1 at 95 ºC.

By using the data collected from DSC measurements, the binary system displayed on Figure 4.18 could be proposed. The liquidus of the binary phase diagram was calculated by using Schröder-Van Laar[24] and Prigogine–Defay equations[24]. In order to propose a full description of the solid-state landscape, one can add to Figure 4.18, the existence of the phases (*R*)/(*S*)-A3 and PE-A3. Contrary to the other phases of the system, the indicated temperature on this figure does not correspond to a melting point but to a decomposition point (peritectic transition) since the anhydrous cocrystal A3 is associated to the presence of PXL above this temperature.

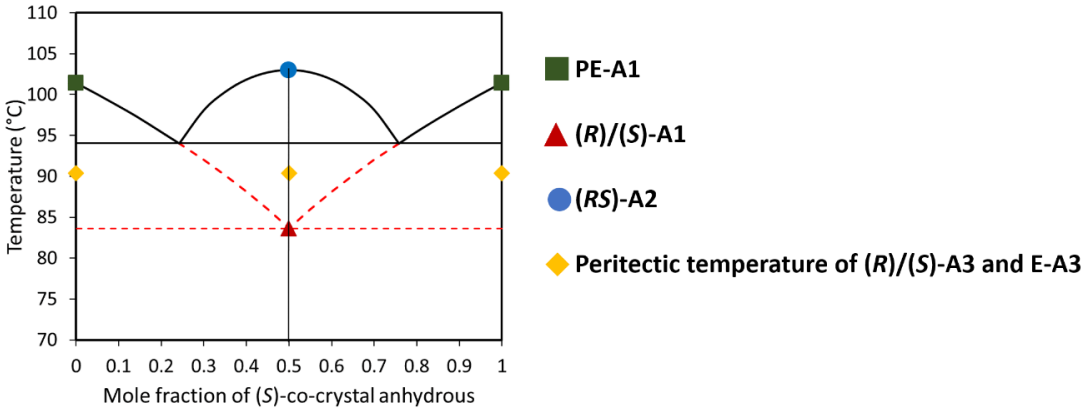

Figure 4.18 Binary phase diagram between the anhydrous cocrystal enantiomers. Stable equilibria are shown by solid lines whereas the metastable equilibria are indicated by dashed lines.

4.7 Discussion on cocrystal forms

The preparation routes of the different solid forms of cocrystals formed between proxyphylline (PXL) and salicylic acid (SA) are summarized in Figure 4.19.

Among the various solid phases of PXL-SA cocrystals characterized during this study, it can be claimed that a stable conglomerate could be stabilized via the crystallization of a monohydrated form. Figure 4.20 - a aims at representing the quaternary phase diagram under isobaric and isothermal conditions of the system: PE I (*R*)/PE I (*S*)/SA/Water. In this system, the ternary isoplethal section Cocrystal (PE I (*R*)/SA) / Cocrystal (PE I (*S*)/SA) / Water (in grey in Figure 4.20 - a and b) shows the stable conglomerate forming system. This situation paves the way for PXL resolution by using preferential crystallization which will be considered as the next step.

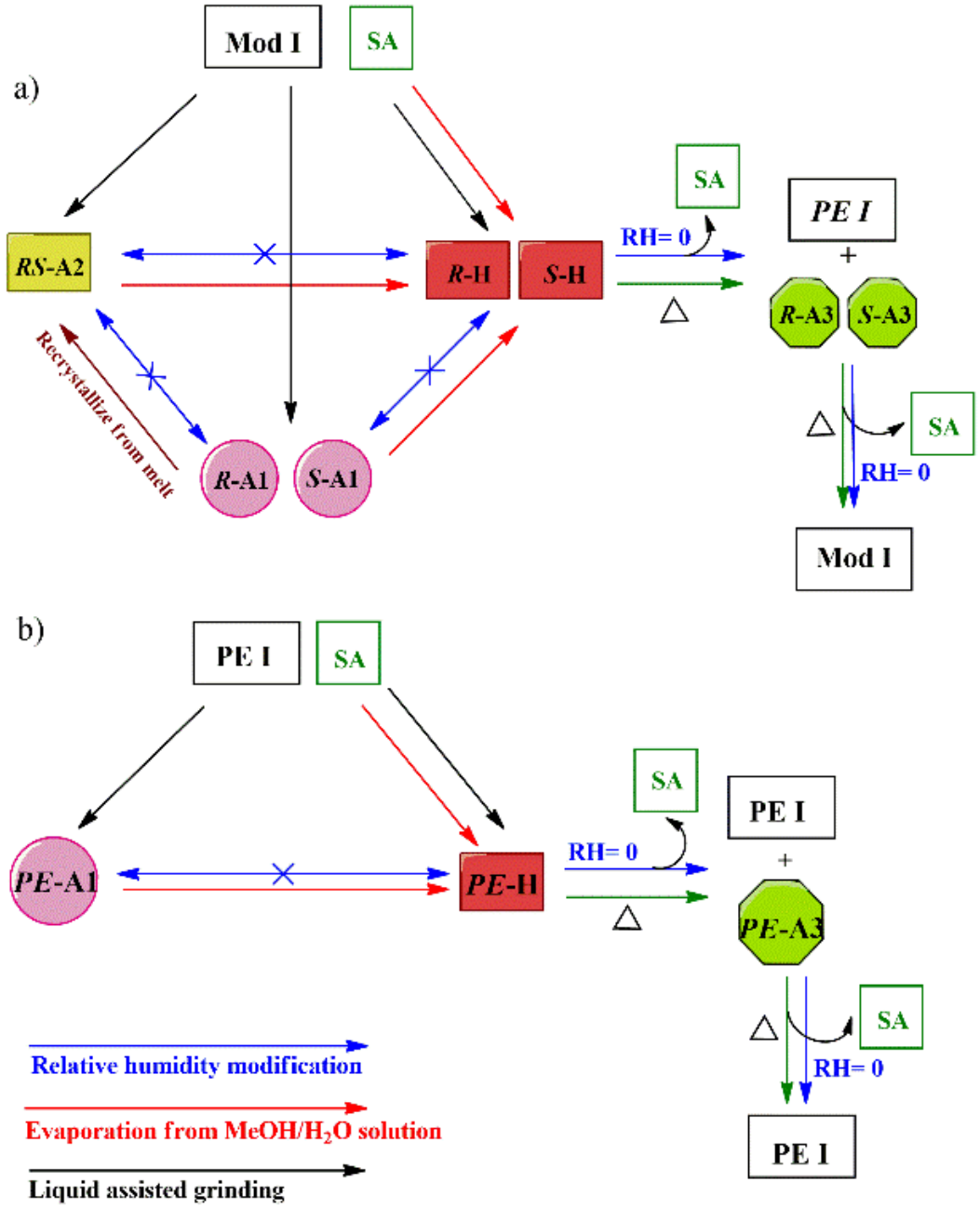

Figure 4.19 Summary of experimental conditions required to crystallize: the monohydrate in a) racemic form ((*R*)/(*S*)-H) and b) enantiopure form (*R*-H) and the anhydrous forms a) racemic compound (*RS*-A2) and the conglomerate compound ((*R*)/(*S*)-A1) and b) the enantiopure form (*R*-A1) of the cocrystal between PXL and SA.

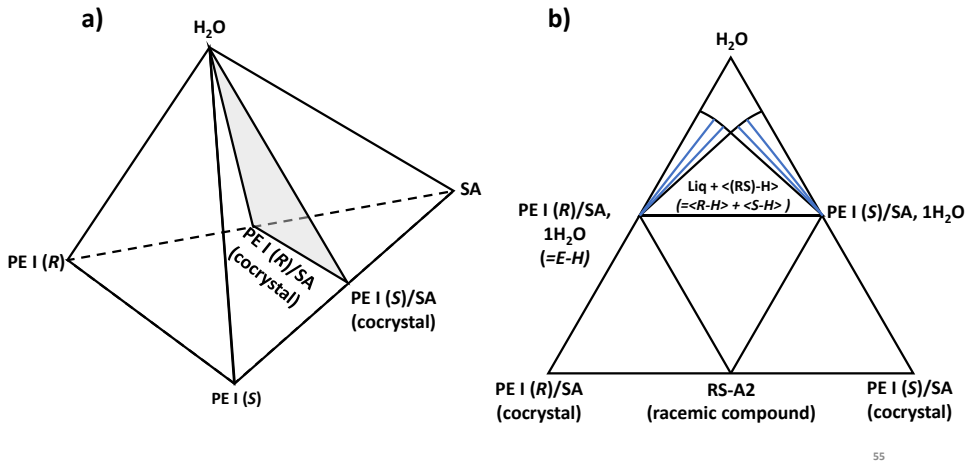

Figure 4.20 a) representation of an isobaric and isothermal section of the quaternary phase diagram between water, the enantiomers of PXL and SA, b) isoplethal section representing the ternary section between water and the enantiomers of the cocrystal between PXL and SA.

The dehydration mechanism of (*R*)/(*S*)-H phase is quite peculiar since the departure of water molecule leads to a metastable cocrystal phase ((*R*)/(*S*)-A3) which can decompose by increasing temperature or under drying conditions (0%RH or reduced pressure). All these observations prove that the dehydration process is irreversibly associated to a decomposition of the cocrystal (due to departure of SA), and the anhydrous form A3 is thermodynamically metastable. However, experimental investigations proposed in this study by working in kinetic conditions (short time to avoid complete departure of SA), show that the dehydration/rehydration mechanism of PXL-SA monohydrated cocrystals can be classified as destructive/reconstructive-class I process according to Rouen96 model[75] as already observed in the ciclopirox-olamine system published by Renou et al.[124] During the dehydration, the disruption of H-bonds due to the departure of water molecules likely induce a collapse of the crystal lattice. This may cause an easier departure of SA molecules.

One can note that the (*R*)/(*S*)-A3 phase was never observed by classical crystallization routes (solution or grinding) : this phase seems to be only accessible *via* the initial formation of the monohydrated form as in the Rimonabant case.[125] These assumptions could be confirmed by a thorough description of the relationship between crystallographic features of (*R*)/(*S*)-H and (*R*)/(*S*)-A3. Unfortunately attempts to obtain (*R*)/(*S*)-A3 single crystals were unsuccessful up to now.

From a chiral discrimination point of view, this study shows the existence of three conglomerate forming systems between PXL and SA: two metastable anhydrous forms (A1 and A3) and one stable hydrated form (H) in water at RT.

The chiral resolution of PXL via PC of the monohydrated form will be discussed in the next section.

4.8 Solubility study of the monohydrate cocrystal

As explained and exemplified in the previous chapters, the selection of a suitable solvent (or mixture of solvents) for an effective preferential crystallization (PC) operation is crucial in order to achieve a successful resolution. In the scope of our first strategy (Figure 1.14 and chapter 3), solvent selection was based on their capacity to inhibit the nucleation of a stable racemic compound. In the scope of the second strategy (which is considered in the present chapter), the selected solvent should also be able to inhibit nucleation in order to retain the undesired enantiomer in solution for as long as possible. It was found that a solution of (*R*)/(*S*)-H in a mixture of ethanol and water in a 7:3 volume ratio with a concentration of 50.0 *w* % remains supersaturated for at least 8 h if cooled down to 10 °C (*s** = 30.0 *w* %, β = 1.67). Moreover, at the investigated scale of 10 mL, this persistent metastable equilibrium is highly reproducible. This mixture of solvents, labeled V hereafter, was therefore selected for the resolution of (*R*)/(*S*)-H.

Table 4.6 presents the solubility data of the pure enantiomer of the cocrystal, (+)-H, and of the racemic mixture, (*R*)/(*S*)-H, in V at different temperatures. The molar solubility ratio α_{mol}, calculated from the ratio of the solubility of the racemic mixture over that of the pure enantiomer (both expressed in mole fraction)[126, 127] are between 1.5 and 1.8 for the studied isotherms. It is usually stated that the efficiency of PC is favored for systems where α_{mol} is lower than 2.

Table 4.6 Solubility "*s" and standard deviation (s.d.) of (+)-H and (*R*)/(*S*)-H in V at different temperatures.**

T_s (°C)	(+)-H *s** (*w* %)	s.d.[a]$_{((+)\text{-H})}$	(*R*)/(*S*)-H *s** (*w* %)	s.d.[a]$_{((R)/(S))\text{-H})}$
5	15.1	0.01	27.0	0.02
10	19.8	0.01	30.0	0.02
20	27.9	0.01	45.3	0.01
25	32.0	0.01	53.8	0.004

[a] s.d. = $\sqrt{\frac{1}{n-1}\left(\sum_{i=1}^{n}(X_i-\mu)^2\right)}$

$\mu = \frac{\sum X_i}{n}$

4.9 Resolution by preferential crystallization

The process of PC and the different operating modes have been thoroughly described in a number of publications.[98,123] SIPC and S3PC were described in Chapter 3, AS3PC will be described hereafter. The enantio-enriched solution in AS3PC mode is first heated to $T_B < T_{homo}$ (Figure 1.11) where a single enantiomer is in thermodynamic equilibrium with its saturated solution. The system is then auto seeded and progressively cooled down to T_F. At the end of the process, the suspension is filtered before the spontaneous nucleation of the counter enantiomer. Then, the solution is compensated by the same mass of racemic mixture as the mass of the crude crops and by solvent, and re-heated so that a new run can start to afford crops of the opposite enantiomer.

4.9.1 Seeded Isothermal Preferential Crystallization (SIPC)

A racemic solution of (*R*)/(*S*)-H (7.57 g) in V (C_0 = 47 *w* %) was first heated up to 50 °C to ensure that even the smallest crystals are dissolved before cooling down to T_F=10 °C (where *s** = 30.0 *w* %, β=1.6). Once T_F is reached, both enantiomers are supersaturated and are within their metastable zone. This supersaturated solution is then seeded by introducing manually 120 mg of ground dry crystals of (+)-H in the solution.

Figure 4.21 presents the evolution of the enantiomeric excess of the liquor (black squares) and of the solid in suspension (red circles) during an optimization PC run. After seeding the racemic (*R*)/(*S*)-H supersaturated solution with pure (+)-H, the enantiomeric excess of the liquor decreases progressively as the solution gets enriched in (-)-H while the out-of-equilibrium stereoselective crystallization of (+)-H occurs. After 4h of entrainment the ee of the solution tends to zero towards the racemic composition and the monitoring of the ee of the solid phase also presents a marked drop after this threshold. This is due to the spontaneous crystallization of (-)-H which gets more and more supersaturated as PC proceeds. In order to collect (+)-H with maximum yield and optimal enantiomeric purity, it is therefore necessary to filter the suspension before reaching the critical solution concentration after which (-)-H crystallizes.

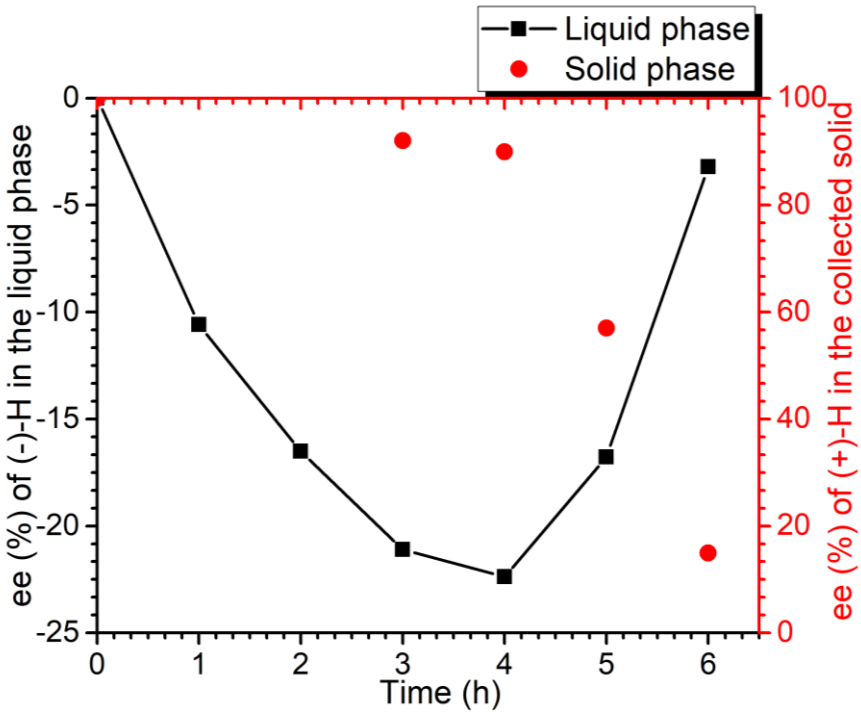

Figure 4.21 Monitoring of the SIPC process starting from racemic mixture and seeding with (+)-H.

Based on this monitoring, three successive PC runs have been performed. The first run started with a racemic solution (ee = 0 %). The solution was filtered after 180 minutes of entrainment and the crystals were washed with pure cold water. After drying, 1.5 g of solid were isolated with an optical purity of 91.0 % and the productivity of this run was 41.5 $g.h^{-1}.L.^{-1}$. The enantiomeric excess in the filtered liquor was (-) 20.7 %. The medium was compensated with 1.3 g of racemic mixture, warmed at 50 °C, and cooled back to 10 °C, thus affording a solution with an ee = -16.3 %. The solution was then seeded with (-)-H to trigger a new stereoselective crystallization. The results obtained during the next runs are gathered in Table 4.7. When starting from enriched solutions, the filtration window could be increased to 210 min since monitoring (data not shown) indicated that nucleation of the counter enantiomer was further delayed under these conditions. Table 4.7 shows that the productivity is also enhanced to ca. 57.7 $g.h^{-1}.L.^{-1}$ when the process starts from an enriched liquid phase. Table 4.7 highlights that the liquid phase achieves unusually high ee (a literature overview indicates that the average value attained in the mother liquor is of ca. 7 – 12 % ee) and that the final crystals are obtained with high optical purity.

Table 4.7 Results of the SIPC mode. ee_o [%]: initial enantiomer excess in the liquid phase, t_{end}: duration time in minutes, $W_{c.s.}$ and $e.e._{c.s}$: weight and enantiomeric excess of the collected solid including seeds, $W_{P.E.}$: weight of produced pure enantiomer, ee_f (%): enantiomeric excess of the liquid phase at the end of the process, *Pr :* calculated productivity in $g.h^{-1}L^{-1}$. *Mass* of seeds is 120 mg.

Run Num.	ee (%)	t_{end} (min)	$W_{c.s.}$ (g)	$e.e._{c.s.}$ (%)	$W_{P.E.}$ (g)	ee_f (%)	Pr ($g.h^{-1}.L^{-1}$)
1	0.0	180	1.5	(+) 91.0	1.3	(-) 20.7	41.5
2	(-) 16.3	210	2.2	(-) 91.6	1.9	(+) 14.2	54.1
3	(+) 10.8	210	2.4	(+) 89.2	2.1	(-) 23.3	57.7

4.9.2 Seeded Polythermic Preferential Crystallization (S3PC)

S3PC provides more control on supersaturation upon cooling from T_{homo} to T_F. For this reason, the process can be operated at higher initial concentrations compared to SIPC and can therefore afford a higher mass of pure enantiomer. The yield and the productivity of PC are thus improved. A racemic solution with a concentration of C_o = 52 *w* % (9.24 g of (*R*)/(*S*)-H in V) was used: after heating to T = 50 °C (*i.e.* well above the saturation temperature), the clear racemic solution was rapidly cooled down to 20 °C (*i.e.* slightly below the saturation temperature where β=1.14), seeded with 120 mg of enantiopure crystals and then cooled down to 5°C (where *s** = 27.0 *w* %) with a cooling rate of 0.15 °C/min.

The evolution of the compositions in the liquid and solid phases after seeding the racemic solution alongside the selected temperature profile are shown in Figure 4.22. The evolution of the composition of the solid phase is similar to the case of the SIPC process. However, the composition of the mother liquor shows a more damped evolution which highlights a gentler control on the driving force during the entrainment. For the first run, the ee of the solid and liquid phases when T_F was reached were of 88.7 and (-) 14.5 % respectively. Similar to SIPC, two other runs were performed by recycling the liquors after filtration and the results are summarized in Table 4.8. Compared to SIPC, the productivity is enhanced to 67.3 $g.h^{-1}.L^{-1}$ during the first run, although the enantiomeric excess of the liquid phase at the end of the process is lower (14.5 % in S3PC compared to 20.7% in SIPC). For the second and third run, one can see that the polythermal mode delivers slightly higher amounts of crude crops but a lower productivity due to much longer process time.

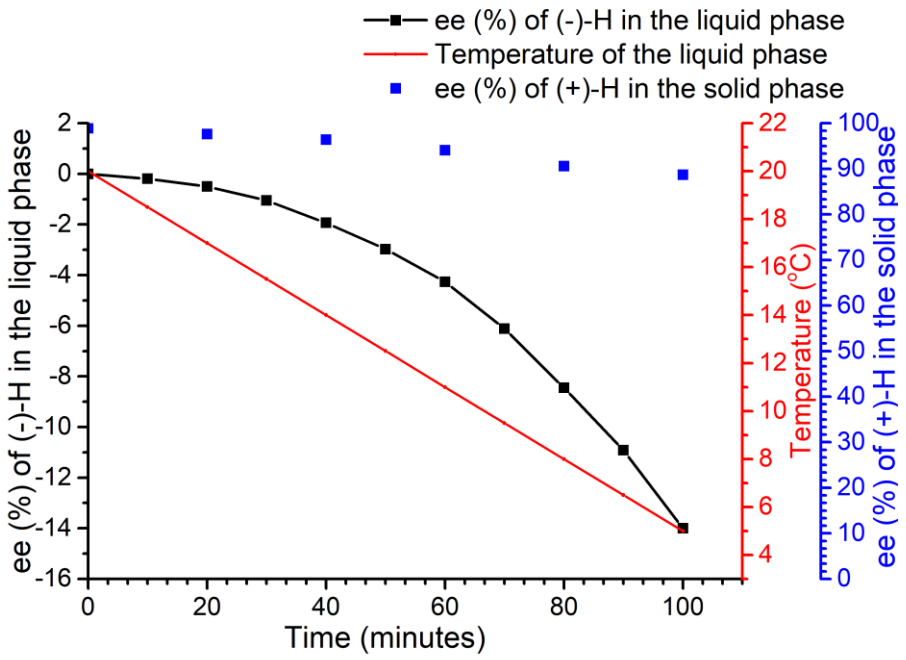

Figure 4.22 Evolution of the ee (%) in the liquid phase (black curve), in the solid phase (blue squares) and temperature profile (red line) for S3PC process after seeding with (+)-H crystal.

Table 4.8 Results of the S3PC mode. ee_o [%]: initial enantiomer excess in the liquid phase, t_{end}: duration time in minutes, $W_{c.s.}$ and $e.e._{c.s.}$: weight and enantiomeric excess of the collected solid including seeds, $W_{P.E.}$: weight of produced pure enantiomer, ee_f (%): enantiomeric excess of the liquid phase at the end of the process, *Pr :* calculated productivity in g.h^{-1}.L^{-1}. *Mass* of seeds is 120 mg.

Run Num.	ee (%)	t_{end} (min)	$W_{c.s.}$ (g)	$e.e._{c.s.}$ (%)	$W_{P.E.}$ (g)	ee_f (%)	Pr (g.h^{-1}.L^{-1})
1	0.0	100	1.4	(+) 88.7	1.2	(-) 14.5	67.3
2	(-) 11.6	250	2.4	(-) 90.1	2.2	(+) 12.2	49.0
3	(+) 8.8	250	2.8	(+) 87.6	2.5	(-) 21.8	55.9

4.9.3 Auto Seeded Polythermic Preferential Crystallization (AS3PC)

The benefit of using AS3PC compared to the two previous methods is that the system does not require manual seeding and because it gives a better control on the crystallization, its scale up is much easier. Indeed, it starts from a domain in the (*R*)-H/(*S*)-H/V ternary phase diagram where a single enantiomer is already in equilibrium with its saturated solution whereas, the other enantiomer is undersaturated at this temperature (*i.e.*, T_B). To the starting racemic mixture of

9.24 g (*R*)/(*S*)-H in V (C_o = 52 *w* %), 120 mg of pure (+)-H were added. The system was equilibrated at T_B=24.1 °C affording a suspension of 99 mg (+)-H in equilibrium with a (+) 0.23 % ee solution. Then, the temperature was progressively decreased to 5 °C with a 0.191 °C/min cooling rate in order to induce PC of the (+)-H crystals. For this run, Figure 4.23 shows the evolution of the enantiomeric compositions in the liquid and solid phases upon cooling and it can be seen that the counter enantiomer remains in solution (*i.e.*, no decrease of the enantiomeric excess in the solid phase was detected before filtration). 1.3 g of crystals were collected with an optical purity of 98.1 % ee. The filtered liquor, now enriched in (-) enantiomer, was compensated with 1.3 g of racemic mixture and was equilibrated for 90 minutes at T_B. From there, a new experiment was launched by decreasing the temperature to 5 °C with a cooling rate of 0.0764 °C/min.

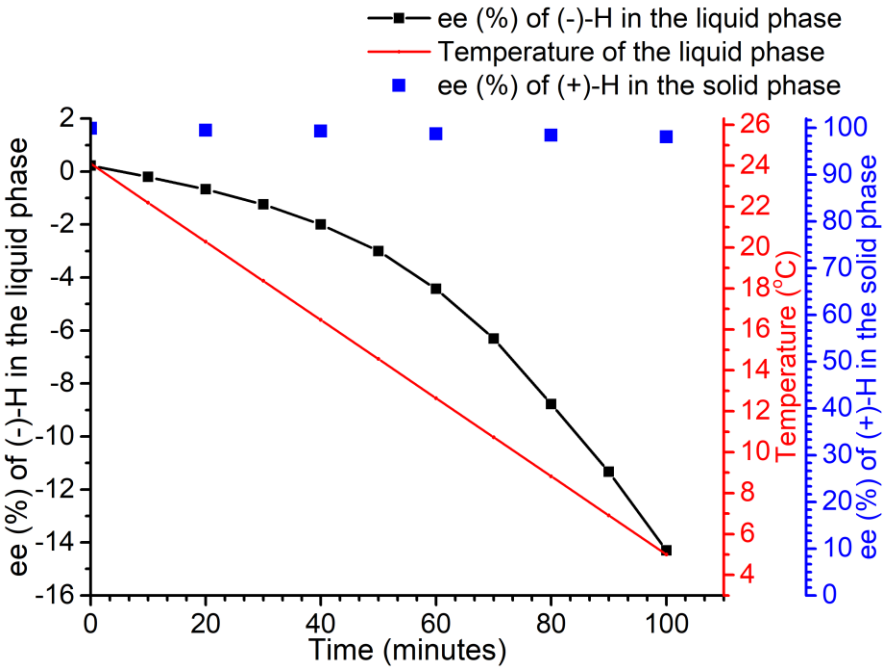

Figure 4.23 Evolution of the ee (%) in the liquid phase (black curve), in the solid phase (blue squares) and temperature profile (red line) for AS3PC process after seeding with (+)-H crystal.

The main data are summarized in Table 4.9. The marked influence of the cooling rate is revealed by comparison between the two first runs. Using AS3PC, a mean optical purity of *ca.* 94 % for the crude product is obtained, this value is higher than that obtained with S3PC (88.8 %) and SIPC (90.6 %) modes.

Table 4.9 Results of the AS3PC mode. ee_o (%): initial enantiomer excess in the liquid phase, t_{end}: duration time in minutes, $W_{c.s.}$ and $e.e._{c.s}$: weight and enantiomeric excess of the collected solid including seeds, $W_{P.E.}$: weight of produced pure enantiomer, ee_f (%): enantiomeric excess of the liquid phase at the end of the process, *Pr :* calculated productivity in $g.h^{-1}.L^{-1}$.

Run Num.	ee (%)	t_{end} (min)	$W_{c.s.}$ (g)	$e.e._{c.s.}$ (%)	$W_{P.E.}$ (g)	ee_f (%)	Pr ($g.h^{-1}.L^{-1}$)
1	(+) 0.23	100	1.3	(+) 98.1	1.2	(-) 14.3	76.5
2	(-) 11.0	250	2.3	(-) 92.1	2.2	(+) 12.1	50.8
3	(+) 9.4	250	2.6	(+) 93.4	2.5	(-) 18.4	58.3

4.9.4 Recovery of PXL pure enantiomer

It should be noted that the X-ray diffraction patterns of the crude crops at the end of each run in all modes showed characteristic peaks of the monohydrate cocrystal (Figure 4.24) which indicates the robustness of the process. In addition, a single recrystallization of the solid collected from any PC experiment (example: 2.8 g, ee_{solid} = 87.6 %) in a mixture of methanol and water (1:1) led to almost enantiopure solid with a yield of up to 92 % (2.3 g, ee_{solid} = 99.2 %). Upon annealing of the monohydrate cocrystal at 130 °C, dehydration occurs, followed by melting of the anhydrous form concomitantly with the evaporation of salicylic acid. This led to the isolation of pure PXL: 2.5 g of (+)-H, ee = 99.8 %) were left for 75 h at 130 °C, and, as expected, almost 1 g of (+)-PXL have been obtained with the same chemical purity as the starting material.

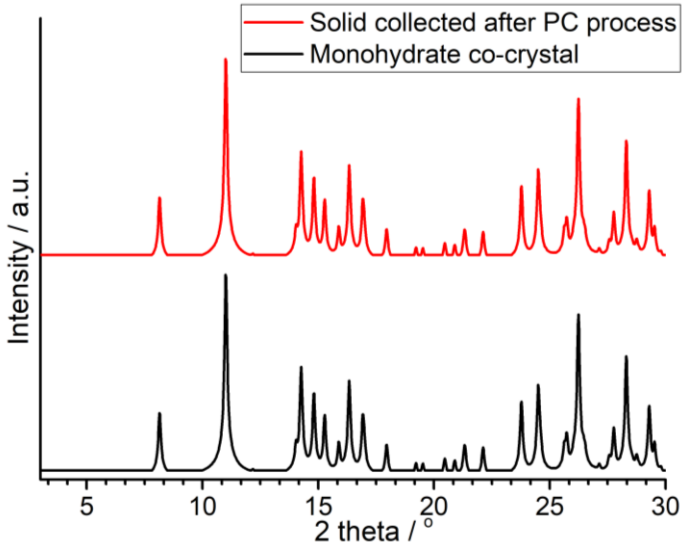

Figure 4.24 Experimental XRPD patterns of the monohydrate cocrystal (black pattern) and of the solid collected at the end of PC processes (red pattern). During all PC experiments the collected solid at the end of the process shows the same XRPD pattern.

4.10 Discussion about applying PC on a conglomerate cocrystal

The results obtained during the implementation of PC to the monohydrate cocrystal conglomerate are presented using isothermal (SIPC) and polythermal (S3PC and AS3PC) modes. Even if these non-optimized tests have been run at an unfavorable small scale (notably by using a magnetic bar as a stirrer) the interesting feature of these results is the unusually high enantiomeric excess attained in the solution at the end of every PC mode. This phenomenon can reasonably be associated to the long induction times required for spontaneous nucleation in the selected mixture of solvents. Although further experimental analyses are required to investigate on the molecular origin of such inhibitions, it can be suggested that the establishment of the molecular interactions required to nucleate the opposite enantiomer (and by extension, any other phase) is hindered, possibly due to the cocrystal nature of the system. Moreover, the recovery of the pure enantiomer of PXL obtained after preferential crystallization might be simply achieved by dehydration followed by sublimation of SA molecules.

These preliminary experimental results highlight the promising potential of using cocrystal conglomerates for the development of PC processes. Indeed, this example could be linked to another conglomerate which has a double salt-cocrystal character and for which the enantiomeric excess in the liquid phase at the end of the entrainment was reported above 20 %.[128]

CONCLUSIONS AND PERSPECTIVES

1. Conclusions

The objective of this work was to develop new strategies based on new “out of the box” ideas, to extend the use of preferential crystallization (PC) to racemic forming systems. This aim was systematically achieved through two novel approaches (as shown in Figure 1.14):

I. Chiral resolution *via* a metastable conglomerate.
II. Chiral resolution *via* a conglomerate cocrystal.

To enable PC on a racemic system, it was necessary to identify a suitable model compound which could meet the requirements of the process. Some specific criteria were proposed in this work, based on previous research conducted on diprophylline:[12]

i. The compound should crystallize as a stable racemic system.
ii. The molecule should have a conformational flexibility: this may lead to new bonding, and thus to different conformations in the solvated state. Some of these can make the spontaneous nucleation more difficult. Conformationally flexible molecules and the ability to form hydrogen bonds are essential in cocrystal formation.
iii. The melting point of the racemic compound should be lower than that of the pure enantiomer. Thus, the accessibility of a metastable conglomerate would be facilitated.

Nineteen racemic compounds were screened (Table A.1). Only proxyphylline (PXL) was selected for the study.

Solid phase characterization of PXL showed diversity in the crystallization behavior of this system. In this work, the binary phase diagram was constructed between the enantiomers. It revealed that PXL can crystallize as a stable racemic compound, a metastable racemic compound and two metastable conglomerates. Such a versatile behavior may result from the conformational flexibility of this molecule. The occurrence of a metastable conglomerate implied that PC may be performed on the racemic PXL.

PC of PXL was first attempted *via* a metastable conglomerate (the first proposed approach). Based on the induction time (t_i) measurements of PXL in different solvents, enantioseparation by PC was achieved by working in isobutyl alcohol (IBA), and despite the existence of a stable racemic compound. Enantioseparation was achieved by inhibiting the nucleation of the undesired forms and by seeding the supersaturated solution in the metastable zone with the pure enantiomer.

These results show the potential of using PC on stable racemic systems, under certain conditions. Even though this approach is not currently attractive for the pharmaceutical industry, it opens new perspectives for the application of PC.

The second approach was performed in two steps. Firstly, a cocrystal was screened using dry or solvent assisted grinding and evaporation methods. This step yielded 10 new cocrystal forms between PXL and different coformers (Table A.1), including three anhydrous cocrystals and one monohydrated conglomerate forming system with salicylic acid (SA). The dehydration mechanism of the hydrate was investigated. The results suggested the presence of a destructive mechanism, due to the concomitant loss of water and SA. Secondly, the PC was applied on the conglomerate monohydrate cocrystal between PXL and SA. It was successfully resolved by crystallization from a water/ethanol mixture. Thanks to the fundamental work done for the cocrystal, PXL was collected at the end of the process as a pure enantiomer, by a simple annealing experiment.

The process proposed in the second approach is robust and reproducible, with a high yield and high process productivity. This proposed approach, possibly attractive to the pharmaceutical industry, can be used to widen the applicability of PC to cocrystal systems. A disadvantage may be the supplementary step required to access the pure active pharmaceutical ingredient (API) at the end of the process.

Two basic investigations were used in both proposed approaches (Scheme 1):

i. The thermodynamic study of the compound including the solid-state landscape evaluation (polymorphism formation, phase diagram study).
ii. The kinetic aspects represented by the induction time measurements.

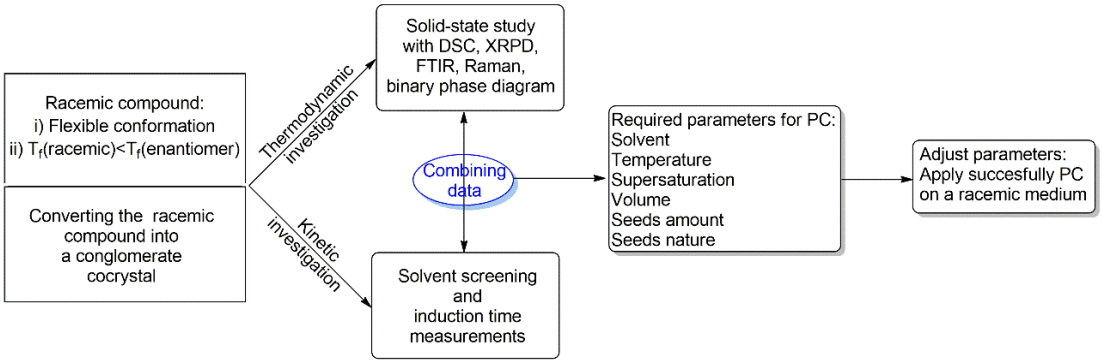

Scheme 1 General procedure to separate enantiomers of a racemic compound, based on the control of thermodynamic and kinetic parameters.

2. Perspectives

The yield obtained through the first approach was relatively low. The chosen necessary criteria should be re-evaluated as follows:

(i) The long t_i is a necessary condition, but not a sufficient one. PC applied on racemic PXL was unsuccessful in water and 1-propanol, even though a long t_i was detected in both solvents. This indicates that seeding with a pure enantiomer can also trigger the primary heterogeneous nucleation of the racemic compound. The

reason may be the low growth rate due to slow surface integration on seed crystals in the work conditions.

- It would be interesting to improve the crystal growth kinetics, by changing the parameters of the growth environment (such as temperature, supersaturation, pH, solvent nature, seeds nature (solid or in suspension), etc.).

- A future study on the effect of these parameters on the crystallization behavior can provide further insight into the process.

(ii) The formation of a crystal structure depends on the conformational preference of the molecules in the chosen solvent. But one should consider that conformational dynamics of molecules may be reduced by the intramolecular hydrogen bonds, and by the rigidity of some of their groups. Moreover, the crystallization of metastable racemic compounds and/or solid solutions cannot be avoided. These situations may arise and may limit the access to a metastable conglomerate.

- The solution may be to model the forces between the molecules in the solvated state (solid-solid and solid-liquid) and to exploit the result to predict the crystal structures. This is hardly envisageable from an experimental point of view (including screening). However, it may be achieved through a theoretical approach first evaluated in simulation.

- Another idea is to study the behavior of intra- and intermolecular hydrogen bonding systems before and after nucleation. These studies may be carried out using spectroscopic methods (IR, Raman, UV-visible).

(iii) Regarding the choice of a racemic compound with a melting point lower than that of the pure enantiomer: the eutectic composition of the system should also be considered. The closer it is to the racemic compound, the higher the chance of detecting a metastable conglomerate.

- The identification of other conditions which enable nucleation blockage can be an attractive subject for future work.

The application of PC on a conglomerate cocrystal is a significant contribution to the PC field. This may be the first work where cocrystallization is used to achieve enantioseparation by PC. These results enable the future development of a robust process in this context. Nevertheless, the optimization of such a system is still required. It should be also noted that these tests were run at a small scale. Further trials should be extended to larger scales. The PC process enhanced by co-crystallization should be further studied since the obtained yield and productivity were higher than envisaged. Understanding the role of the co-former in the crystallization behavior (*i.e.* the presence of the co-former may avoid the simultaneous crystallization of the two enantiomers?) is an attractive subject for future research.

ANNEX A: EXPERIMENTAL SET-UP AND MATERIALS

Chemicals, materials and experimental techniques employed in this work are reported in the present chapter.

A.1 Chemical materials

Racemic PXL was purchased from TCI EUROPE (Zwijndrecht-Belgium) with a chemical purity higher than 98.0 % and used as received without any further purification.

The stable **pure enantiomer of PXL** (PE I hereafter, Figure A.1) was synthesized by analogy with a published procedure.[121] A mixture of anhydrous theophylline (chemical purity: 99%) (5 g, 27.75 mmol), (*R*)-propylene oxide (chemical purity 99 %, ee 97%) (5 g, 86.08 mmol, 6 mL) and a catalytic amount of triethylamine (1 g, 7.17 mmol, 1 mL) in methanol (40 mL) was stirred for 3 h at reflux until complete dissolution. After cooling the mixture, the solvent was evaporated under reduced pressure. Then, 20 mL of methanol were added, and the flask was stored in the fridge (-18 °C) for 4 h until crystallization. The obtained solid was filtered off and washed with cold ethanol (15 mL) yielding the desired product (*S*)-7-(2-Hydroxypropyl) theophylline, PE I (S), as a white crystalline solid (4 g, 16.78 mmol, yield = 61%) - mp 149.5 °C {Ref.[129] 142-150 °C and Ref.[130] 150.5-151.5 °C}; $[\alpha]_D^{20}$ = – 53° (*c* = 1.00 mg/mL, $CHCl_3$) {Ref.[121] : $[\alpha]_D^{20}$ = – 54° (*c* = 1.00 mg/mL, $CHCl_3$), 98% *ee*}. ee $_{HPLC}$ = (-) 99.9 %.

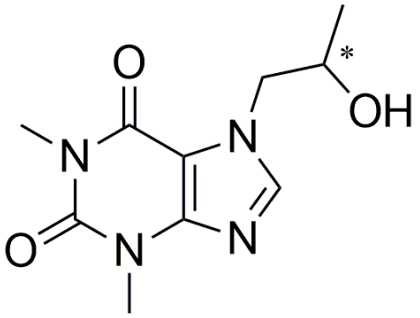

Figure A.1 Chemical structure of (*RS*)-PXL.

The stable racemic and enantiopure form of 3-(2-propylphenoxy)-propane-1,2-diol (P3D) (Figure A.2), were synthesized according to a published procedure.[131] The racemic 3-chloropropane-1,2-diol (chemical purity: 98%) and (*R*)-(-)- 3-chloropropane-1,2-diol (chemical purity: 97% and optical purity: 98%)

and 2-propylphenol (chemical purity: 98%) were purchased from Sigma-Aldrich and used without any further purification.

A solution of NaOH (2 g, 50 mmol) in 7 mL water was added drop by drop to a mixture of 2-propylphenol (4.2 g, 30 mmol) in ethanol (18 mL) and the medium was stirred and heated under reflux for 60 min. Then a solution of racemic or scalemic 3-chloropropane-1,2-diol (4 g, 40 mmol) in 6 mL ethanol was added drop by drop to the reactional medium, and the mixture was left under reflux for 3h. the solvent was evaporated under reduced pressure followed by addition of 20 mL water and extraction with chloroform (3 X 100 mL). the organic phase was concentrated and purified by recrystallization from a mixture of solvent (pentane: diethyl ether 95:5 v:v). Racemic P3D was obtained with a 70% yield, mp 52.3-52.8 °C (Ref [132]: mp = 52.5-53.5 °C). ^{1}H NMR, δ = 0.94-0.99 (3H, t, **CH$_3$**-CH$_2$), 1.56-1.68 (2H, m, **CH$_2$**-CH$_3$), 2.52 (2H, OH, s), 2.58-2.63 (2H, t, **CH$_2$**-CH$_2$), 3.76-3.89 (2H, m, O-**CH$_2$**), 4.05 (1H, m, **CH**-O), 4.14 (2H, m, **CH$_2$**-O), 6.84-6.95 (2H, m, **CH$_{2Ar}$**), 7.14-7.19 (2H, m, **CH$_{2Ar}$**). In the other hand, (*R*)-P3D was prepared with 75% yield, mp 66-67 °C (Ref [132]: mp = 67-69 °C), $[\alpha]^{D}_{20}$ = +12.9 (*c* 10.0, MTBE).

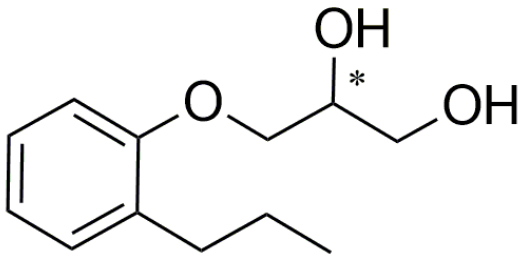

Figure A.2 Chemical structure of (*RS*)-P3D.

Seventeen chiral racemic compounds and twenty coformers were used in this research, purity and suppliers list are presented in Table A.1.

A list of solvent was used in this work: acetone, chloroform, 1,4-dioxane, propan-1-ol, n-butyl acetate, dimethyl sulfoxide, N,N-dimethyl formamide, tetrahydrofuran, t-butyl methyl ether, methanol, acetonitrile, toluene, ethyl acetate, ethanol, water, dichloromethane, butan-2-ol, cyclohexane, n-heptane, isopropyl alcohol, methyl isobutyl ketone, isobutyl alcohol. All solvents are analytical grade and purchased from Sigma Aldrich and were used as received.

Table A.1 Purity and suppliers list of the used chemicals.

Chiral racemic compound	Purity	Supplier
Malic acid	> 99%	Acros Organics
Phenyl alanine	> 99%	Sigma Aldrich
Methionine	> 99%	Acros Organics
Parahydroxy phenylglycine	> 99%	Sigma Aldrich
Norleucine	> 98%	Sigma Aldrich
Arginine	> 95%	Sigma Aldrich
Tyrosine	> 99%	Sigma Aldrich
Tryptophan	> 99%	Sigma Aldrich
Menthol	> 99%	Alfa Aesar
Alanine	> 99%	Sigma Aldrich
Modafinil	/	Non-commercial
2-amino pimelic acid	> 99%	Sigma Aldrich
2-amino adipic acid	> 99%	Merck
Phenylsuccinic acid	> 99%	Acros Organics
Leucine	> 99%	Merck
Histidine	> 98%	Acros Organics
Tartaric acid	> 98%	Lancaster

Coformer	Purity	Supplier
4-methoxybenzoic acid	> 98%	Alfa Aesar
3-chlorobenzoic acid	> 99%	Acros Organics
4-dimethylaminobenzoic acid	> 98%	Acros organics
3-hydroxy-4-nitrobenzoic acid	> 98%	Acros organics
3,4-dichlorobenzoic acid	> 99%	Acros organics
2,6-dichlorobenzoic acid	> 98%	Acros organics
Benzamide	> 98%	Alfa Aesar
Urea	> 98%	VWR Chemicals
Adipic acid	> 99%	Alfa Aesar
Saccharin	> 98%	Acros organics
Stearic acid	> 97%	Acros organics
Methyl urea	> 97%	Acros organics
Citric acid	> 98%	Acros organics
Salicylic acid	> 99%	Acros organics
Acetylsalicylic acid	> 99%	Acros organics
Anthranilic acid	> 99%	Merck
Oxalic acid	> 98%	Alfa Aesar
3,4-dimethoxycinnamic acid	> 99%	Alfa Aesar
2,5-dichlorobenzoic acid	> 97%	Acros Organics
3-hydroxybenzoic acid	> 99%	Acros organics

A.2 Analytical methods assisting chiral characterization and chiral resolution

All crystallization experiments performed in this work were monitored by off-line methods, allowing analysis of solid or liquid phase. They will be described in the next sections.

A.2.1 Powder X-ray diffraction and Single crystal X-ray diffraction

X-ray Powder Diffraction (XRPD) is a non-destructive method employed to study the solid state of crystalline samples from phase identification from the diffraction patterns to the determination of unit cell dimensions. These X-rays are collimated and directed onto the sample; the intensity of the reflected X-rays is recorded. When the geometry of the incident X-rays impinging the sample satisfies Bragg's law, constructive interference occurs and a peak in intensity occurs. A detector records and processes this X-ray signal and converts the signal to a count rate which is then output to a device such as a computer monitor.

$$d = \lambda / (2\sin\theta)$$

d is the interplanar distance, *λ* is the wavelength of the incident wave and *θ* is the diffraction angle

In this work, the analyzed materials were finely ground and homogenized before analysis. Analyses of these samples were performed at room temperature using a D8 Discover diffractometer (Bruker analytic X-ray Systems, Germany) with Bragg-Brentano geometry. The instrument is equipped with a copper anticathode (40 kV, 40 mA, Kα radiation (λ =1.5418 Å)), and a Lynx Eye linear detector. The diffraction patterns were recorded with a scan rate of 0.04° (2*θ*) in the angular range of 3-30° 2*θ*, with a counting time of 4s per step with no rotation applied to the sample.

The X-ray single crystal experiments were carried out on a Bruker SMART APEX diffractometer equipped with a CCD area detector with a Molybdenum cathode-ray tube (Kα1 λ=0.71071 Å). The cell parameters and the orientation matrix of the crystal were preliminary determined by using SMART Software.[133] Data integration and global cell refinement were performed with SAINT Software.[133] Intensities were corrected for Lorentz, polarisation, decay and absorption effects (SAINT and SADABS Software) and reduced to F_O. The Program package WinGX[134] was used for space group determination, structure solution and refinement.

A.2.2 Thermal and thermogravimetry analysis

Differential scanning calorimetry (DSC) is a powerful thermo-analytical technique to determine the thermal behavior and the solid properties of a material as a function of temperature: melting point, heat of fusion, phase transition, glass transition, etc... DSC analysis measures the amount of energy absorbed or released by a sample when it is heated or cooled, providing quantitative and qualitative data on endothermic (heat absorption) and exothermic (heat evolution) processes.

All thermal investigations were performed on a Netzsch DSC 214 Polyma apparatus in sealed or pierced aluminum pans. DSC runs were performed with ~ 4-5 mg of solid sample and using heating rates of 5 and 10 $K.min^{-1}$. The atmosphere of the analyses was regulated by a nitrogen flux (40 mL/min). The Netzsch Proteus Software was used for data Processing.

Thermal gravimetric analysis (TGA) was performed with a Netzsch STA 449 C instrument. Approximately 4-5 mg of solid was used. The samples were heated at a constant heating rate of 10 $K.min^{-1}$. The measurement cell was continuously purged with a stream of flowing helium throughout the experiment. Proteus® Software (Netzsch) was used for data treatment. This analysis allows us to determine simultaneously the weight and the enthalpy changes of a solid sample, more precisely to determine the existence of a solvate/hydrate, detect evaporation, decomposition, oxidation and other effects of temperature change that cause mass changes.

A.2.3 Dynamic Vapor Sorption

Dynamic Vapor Sorption (DVS) is a gravimetric sorption technique that measures how quickly and how much of a solvent is absorbed by a solid sample upon varying the vapor concentration surrounding the sample (e.g., such as a dry powder absorbing water). Mass change using an ultra-sensitive microbalance is recorded during the analysis.

The behavior of the obtained solvate under variable relative humidity (RH) was studied by gravimetric measurements using a DVS apparatus (DVS vacuum, Surface Measurements System, UK). This equipment consists of a microbalance (precision 0.1 μg) set under reduced pressure in an incubator accurately regulated in terms of temperature (precision 0.1 °C) and partial vapor pressure of water. Cocrystal samples were subjected to increasing or decreasing humidity (RH) at room temperature.

A.2.4 Chiral HPLC

The enantiomeric purity of the samples was determined with a chiral high-performance liquid chromatography (C-HPLC) using a CHIRALPAK IC column (DAICEL group, Chiral Technologies Europe), 250 × 4.6 mm. The mobile phase was a heptane:ethanol mixture (7.5:2.5, v:v), and the flow rate was 1 mL/min. The used wavelength for UV detection was 273 nm at 20 °C. Under these conditions, retention times of 15 and 18 min were obtained for PE I (R) and PE I (S) respectively. An offline C-HPLC analysis was used to monitor the enantiomeric excess (*ee*) of the liquid phase and of the solid phase as function of time during the preferential crystallization (PC) processes.

A.2.5 ^{1}H NMR Spectroscopy

NMR or nuclear magnetic resonance spectroscopy is a technique used to determine a compound’s molecular structure. It identifies the carbon-hydrogen framework of an organic compound. Using this method, it is possible to determine

the entire structure of a molecule. Even though there are many other types of NMR including ^{13}C-NMR and ^{15}N-NMR, ^{1}H-NMR is the method used hereafter to characterize the structure of the compounds after syntheses. The ^{1}H NMR spectra (300 MHz) were recorded on a Bruker Spectro spin apparatus in $CDCl_3$ with the solvent as the internal standard.

A.2.6 Second Harmonic Generation

SHG technique is used to verify the formation of non-centrosymmetric crystals,[135] and thus used as a prescreening method for conglomerate detection. A Nd:YAG Q-switched laser (Quantel) operating at 1.06 *μm* was used to deliver 360 *mJ* pulses of 5 ns duration with a repetition rate of 10 Hz. An energy adjustment device made up of two polarizers (P) and a halfwave plate (*λ*/2) allowed the incident energy to be varied from 0 to ca. 200 mJ per pulse. An RG1000 filter was used after the energy adjustment device to remove light from the laser flash lamps. According to Kurtz and Perry's SHG powder method,[136] the SHG signal intensities of the samples were compared to the signal of a reference compound (α-quartz, 45 *μm* average size). In order to qualitatively compare the samples among each other, an equivalent mass of each solid was used for every analysis (*ca.* 200 mg).

A.2.7 Solubility measurements

Solubility of solute according to IUPAC "Gold Book" is defined as the analytical composition of a saturated solution, expressed in terms of the proportion of a designated solute in a designated solvent.[137] In other word, solubility is the property of a chemical substance to dissolve in a solvent or mixture of solvents to form a homogeneous solution depending on temperature and pressure. The solubilities of the solid in different solvents were measured at a constant temperature by the standard gravimetric method.[138]

A suspension of the solid was prepared in a chosen solvent and stirred at 700 rpm. Temperature was controlled using a thermostated double-jacket glass vessels. After equilibration for more than 2 hours, the suspension was filtered, the solid phase in equilibrium with the solution was verified by XRPD and the saturated liquid phase was weighed before and after evaporation. The solubility *s** was calculated in weight percent (*w*%) with *m* the mass of the dissolved solid and m_s the mass of the saturated solution:

$$s^* = \frac{m}{m_s} \times 100 \ (w\%)$$

A.2.8 Induction time measurements

The induction time (t_i) *i.e.* the time required to detect spontaneous crystallization in a supersaturated solution, was determined at different supersaturation ratios and in different solvents. For each solvent/supersaturation couple, a suitable mass of racemic compound was dissolved in a suitable mass of solvent by heating. The solution was then introduced in 4 different 1.5 mL glass vials equipped with magnetic stirrers. The vials were then placed in a Crystal16 (Technobis, The

Netherlands)[116] and stirred (800 rpm) 10 °C above their saturation temperature for at least 90 min. The clear solutions were then cooled down to 20 °C with a cooling rate of 5 °C/min. The moment at which the set temperature (20 °C) was reached is taken as time zero (t_0). The vials were kept at 20 °C until spontaneous crystallization was detected *via* the decrease of light transmission through the sample. The difference between the moment when the transmissivity started to decrease and t_0 was taken as t_i. Once the different samples crystallized, the vials were reheated above their clear point and the procedure was repeated to ensure statistical reproduction.

The solvents that gave the longest t_i values were also tested at a larger scale of 10-20 mL. For this purpose, a suitable amount of solvent was added to a known amount of racemic compound and the mixture was stirred for at least 1h at high temperature to ensure complete dissolution. Then the solution was cooled down to the crystallization temperature T_c (10 or 20 °C) and the t_i value was taken as the time lapse between the moment at which the solution reached T_c and the moment at which spontaneous crystallization occurred, detected visually. Each measurement was repeated at least three times using the same solution.

A.2.9 Infrared and Raman spectroscopy

Infrared and Raman spectra could be used for identifying the polymorphic form of an API. The molecular interaction in the crystal unit cell between polymorphs is different, which leads to changes in the observed spectra including changes in the frequencies, relative intensities and the wavenumber. Vibrations of one or many molecules will change from one polymorph to the other and thus can change the number of bands and shift their frequencies.[139] Each polymorph is characterized and identified by his recognizable vibrational spectrum. These experiments were done during a secondment at Max Planch Institute in Magdeburg.

ATR FT-IR-spectra in the frequency range 4000-400 cm^{-1} at 4 cm^{-1} resolution measures in the transmittance mode using an FT-IR spectrometer with a platinum-ATR diamond and a RT-DLATGS detector. The spectra were averaged over 24 scans. The Raman spectra were recorded in the range 30-3500 cm^{-1} at 4 cm^{-1} resolution using FT-Raman spectrometer. The excitation source was at power level of 1000 mW.

A.2.10 Polarimeter

Polarimeter is used to measure the angle of rotation caused by passing a monochromatic polarized light through an optically active substance loaded in a measurement cell (a 10 cm long cylinder). Opposite optical properties are used to differentiate between enantiomers. When deviate light to the right (clockwise), they are called dextrogyre and noted (+). When light is deviated to the left (anticlockwise), they are levogyre and noted (-).

A deviation of the plane of this light occurs at an angle α_λ^T The enantiomeric excess can be deduced by this equation:

$$ee = \frac{\alpha_\lambda^T}{[\alpha_\lambda^T]^\circ . c . l}$$

l is the length of the cell and c is the concentration (g.L^{-1}) of the sample and $[\alpha_\lambda^T]^\circ$ is the specific optical rotation of the sample.

Optical rotations of the pure enantiomers of PXL and P3D after synthesis were measured on a JASCO P2000 polarimeter. Value of specific rotation is given in deg.mL.g^{-1}.dm^{-1}, and the concentration of solutions c appears in g.L^{-1}.

A.2.11 Hot stage microscopy (HSM)

HSM measurements were performed in a THMS 600 hot-stage (Linkham) coupled with a Nikon Eclipse LV100 microscope (maximum magnification: ×1000) connected to a computer for image capture via a CCD camera. The temperature was regulated via the Linksys32 software.

A.2.12 Grinding experiments

Cocrystals were prepared by grinding or by dissolution/evaporation. All experiments were carried out with a 1:1 stoichiometric ratio of PXL and coformer. Grinding (in dry conditions or by liquid assisted grinding (LAG) was performed at room temperature using a Retsch Mixer Mill model MM400 with 10 mL zirconium oxide grinding jars containing one 12 mm zircon grinding ball at a rate of 20 Hz for 20 min. LAG experiments were performed by adding *ca*. 10-20 *µl* of a selected solvent to the solid mixture prior to grinding. Water, acetone, ethanol, methanol, isopropanol (IPA), n-hexane, dichloromethane (DCM), and chloroform ($CHCl_3$) were used for the LAG experiments. For the same stoichiometric mixture, a dry grinding was also performed.

A.2.13 Binary phase diagram

Binary phase diagrams between enantiomers were constructed using data collected during DSC measurements. The samples (pure compounds or mixtures) were prepared by manual grinding to obtain a fine powder loaded into the DSC aluminum pan and subjected to a heating/cooling program with a heating rate of 5^{o}C/min. For PXL and P3D molecules, the samples were first heated to 200 and 80^{o}C respectively then cooled down to -20 ^{o}C followed with a second heat to 200 and 80^{o}C respectively. The liquidus of the binary phase diagrams were also theoretically calculated by Schröder-Van Laar[24] and Prigogine–Defay equations.[24]

A.2.14 Determination of ternary isotherms between (*R*)-PXL, (*S*)-PXL and isobutyl alcohol

In order to determine isothermal ternary phase diagrams, the solubility values were determined in isobutyl alcohol at 25 and 10 °C using the regular gravimetric method for (i) the stable racemic compound of PXL (Mod I), (ii) the pure enantiomer (*R*)-PXL, (iii) the doubly saturated solution containing (*R*)-PXL and Mod I, and (iv) the equimolar mixture of (*R*)- and (*S*)-PXL (*i.e.,* the metastable conglomerate (Mod II)). Concerning (iii), the enantiomeric composition of the dry extract was measured

by chiral HPLC. For (iv), the solubility of the metastable conglomerate was determined by stirring an equimolar mixture of (*R*) and (*S*)-PXL (prepared manually) in a small volume of isobutyl alcohol for a few minutes under a controlled constant temperature. The solid phase in equilibrium with the saturated solution was verified systematically by XRPD.

A.3 Preferential crystallization

A.3.1 Experimental Set-Up

All PC experiments were performed in 30 mL glass tube crystallizers. Magnetic stirring was set at 800 rpm. For each PC process, a known amount of the racemic solid was dissolved in 10 mL of pure solvent or solvent mixture. Prior to entrainment (*i.e.* cycles of temperature), the prepared racemic solutions were heated above their saturation temperatures to make sure all solid is dissolved. The clear solutions were then cooled down to T_F for SIPC and T_{homo} for S3PC and seeded to start the entrainment. For SIPC, the temperature was kept constant at T_F. For S3PC, a cooling profile from T_{homo} to T_F was adopted immediately. For AS3PC, the initial system contains an enantiomeric excess of one of the two enantiomers. The solution is heated at a calculated temperature T_B so that only the counter enantiomer in default is completely dissolved. Thus, the slurry is composed of crystals of the enantiomer in excess and in thermodynamic equilibrium with its saturated solution. The system is thus self-seeded by crystals of the pure enantiomer. The temperature was decreased from T_B to T_F using a suitable cooling program and stirring mode without any additional seeds so that the crystal growth is favored over secondary nucleation (Figure 1.11).

The monitoring of the entrainment was performed by sampling the liquor at different time intervals to determine the evolution of the enantiomeric excess of the liquid phase and to evaluate the nucleation kinetics of the counter enantiomer. During the processes, the experiment was stopped before crystallization of the counter enantiomer and the solid was filtered and washed with pure cold solvent (heptane or water). C-HPLC was used to monitor the evolution of the enantiomeric excess (ee %) of the liquid phases and the purity of the collected solid.

To quantify the processes (SIPC, S3PC and AS3PC), the process productivity "*Pr"* expressed in $g.h^{-1}.L^{-1}$, was calculated using the following equation:

$$\mathrm{Pr} = \frac{\left(m\ (collected\ solid) * ee\ (\%)\right) - m\ (seeds)}{t\ (process) * V\ (solvnt)}$$

With "*m*" the mass in gram (g), "*t*" the process time in hours (h) (the dead time including the time needed for preparation, filtration and cleaning was not taken into account in this case) and "*V"* the volume of the solvent in litters (L).

ANNEX B: SOLID-STATE LANDSCAPE OF 3-(2-PROPYLPHENOXY)-PROPANE-1,2-DIOL (P3D)

B.1 Introduction and state of the art of the compound

The terminal aryl glycerol ether is rather common in the family of lipids.[140] Many physiologically active substances, including registered drugs like fungicide chlorphenesin, expectorant guaifenesin, muscle relaxant mephenesin, belong to the series of aryl glycerol ethers.[132] The solid state landscape of 3-(2-propylphenoxy)-propane-1,2-diol (P3D) was already investigated by Bredikhin *et al.* showing that P3D belongs to the racemic forming system group representing only one stable racemic compound and one enantiopure forms.[141] During this study, the solid-state characteristics of P3D (Figure A.2) will be re-investigated by a combination of suitable experimental techniques (thermal study, single crystal and powder X-ray diffraction, FTIR, Raman and solubility measurements). To the best of our knowledge, the occurrence of polymorphism of this molecule was not mentioned before in literature.

B.2 Identification and characterization of the different forms in the binary system

The stable racemic form (Form I) and the stable enantiopure form (EI) of P3D, were synthesized as described in Annex A. A metastable racemic form (Form II) was obtained by crystallization experiments from different solvents (propan-1-ol, n-butyl acetate, THF, methanol, acetonitrile, ethyl acetate, dichloromethane, butan-2-ol, isopropanol). This form is thermodynamically less stable than Form I. In the other hand, the recrystallization of the enantiopure form and regardless of the used solvent or condition, always leads to the formation of the stable form EI. A metastable enantiopure form (EII) can be produced by cooling down the melt of EI to room temperature or to 4 °C.

B.2.1 Characterization by X-ray powder diffraction

Form I and Form II of the racemic P3D were identified by XRPD (Figure B.1- a). XRPD pattern of Form I is similar to the one reported by Bredikhin *et al.* (ref. ZOCNUC).[141] Diffractograms of EI, EII and the one reported in literature (ref. ZOCPEO)[141] are represented in Figure B.1- b. A shifting of XRD peaks is seen between the patterns of EI and ZOCPEO between 3° and 15°, the difference between the two patterns become more obvious at higher angles (>20°).

The pattern of the metastable form EII was obtained by melting the stable form EI directly on an XRD sample plate holder and recording the solid pattern once the liquid phase recrystallizes at room temperature. However, leaving the solid for few

minutes at room temperature after its formation will lead to a phase transition into the more stable form EI.

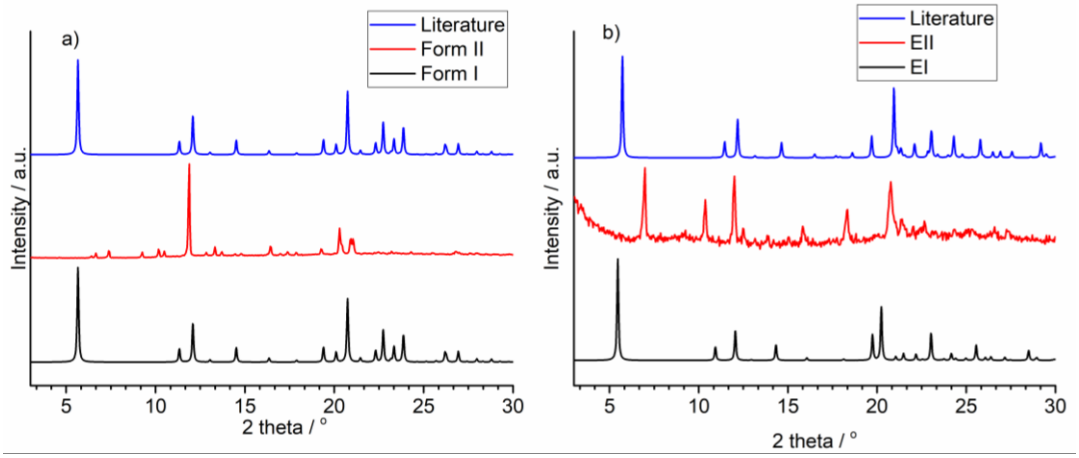

Figure B.1 Experimental XRPD patterns of a) Form I, Form II and the calculated pattern from literature and b) EI, EII and and the calculated pattern from literature.

B.2.2 FTIR and FT-Raman spectroscopy

The polymorphs of the racemic form can be clearly detected by FTIR measurements (Figure B.2). It is easy to differentiate the polymorphic forms in the fingerprint region of OH. The infrared band at 3180 cm^{-1} characterize the most stable racemic form (Form I), whereas this band is shifted to 3370 cm^{-1} after the formation of Form II. There are many small pattern differences in the IR spectra below 1500 cm^{-1}.

The Raman spectra for Form I and Form II of the racemic form have similarities, but also shows differences in the frequency of the bands in the range between 1700 and 400 cm^{-1} and in the intensity in almost all the spectral range (Figure B.2).

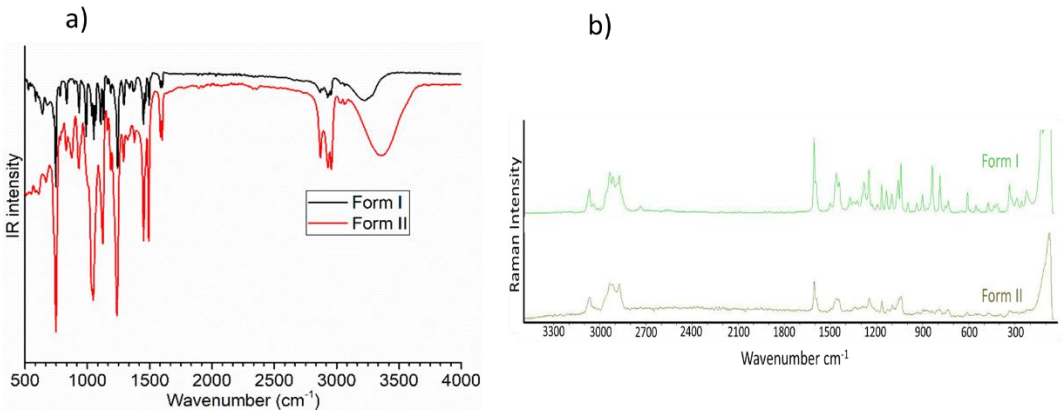

Figure B.2 a) Infrared spectra and b) Raman spectra of Form I and Form II.

The spectra of EI and EII exhibit a difference in the OH stretching bands (Figure B.3 - a) (3220 cm^{-1} for EI and 3420 cm^{-1} for EII). There are several relative intensity differences in the C=C infrared fingerprint region bellow 1700 cm^{-1}.

The Raman spectrum (Figure B.3 - b) of the two polymorphs EI and EII are different in the CH stretching region at around 3000 cm^{-1} and many pattern differences in the Raman spectra below 1400 cm^{-1}.

These observations indicate that the alcohol group participates in hydrogen bonding in the crystal lattice of the racemic and enantiopure forms.

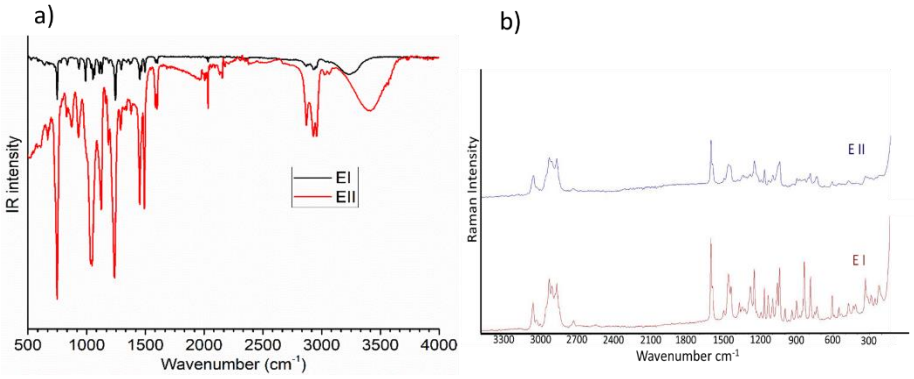

Figure B.3 a) Infrared spectra and b) Raman spectra of EI and EII.

B.2.3 Thermal characterization

Data concerning calorimetric properties of the different forms of P3D using DSC are summarized in Table B.1. Thermogram of the pure stable racemic form Form I (Figure B.4 - a) obtained at a heating rate of 5 K/min shows only one endothermic event ($\Delta_{fus}H$ = 32.4 KJ/mol), corresponding to the melting of this form at T_{onset}=53.0

°C, which confirms that the substance is stable and do not decompose under these conditions.

After recrystallization in the DSC pan, the sample is re-heated and a small exothermic event ($\Delta_{fus}H$ = 1.8 KJ/mol) is detected at 46.3 °C, rapidly followed by the melting of Form I (Figure B.4 - b). It is confirmed that the supercooled melt (SCM) give rises to the crystallization of Form II but this form converts into Form I upon heating at 5 K/min. For this reason, a quantity of racemic Form II was prepared directly in the DSC crucible pan using a Koffler bench and was heated at 20 K/min, it gave a melting temperature at T_{onset}=49.5 °C with a $\Delta_{fus}H$ of 22.2 KJ/mol (Figure B.4 - c).

The same thermal experiments were performed with the pure enantiomer EI, the first run shows a single melting endotherm at T_{onset}=66.6 °C with $\Delta_{fus}H$ = 32.0 kJ.mol^{-1} (Figure B.5 - a). While heating the SCM, a melting endotherm at T_{onset}=58.6 °C indicates the melt of a metastable enantiopure form (EII) with an $\Delta_{fus}H$ = 23.4 kJ.mol^{-1} (Figure B.5 - b).

Based on Burger and Ramberger's[142] heat of fusion rule, if the higher melting point form has the higher heat of fusion, the two forms are usually monotropic.

Table B.1 Thermochemical Data Obtained for the Different Forms by DSC.

	Racemic forms		Enantiopure forms	
	Form I	Form II	EI	EII
Thermodynamic stability	Stable	Metastable	Stable	Metastable
T_{onset} (°C)	53.0	49.5	66.6	58.6
$\Delta_{fus}H$ (KJ/mol)	32.4	22.2	32.0	23.4

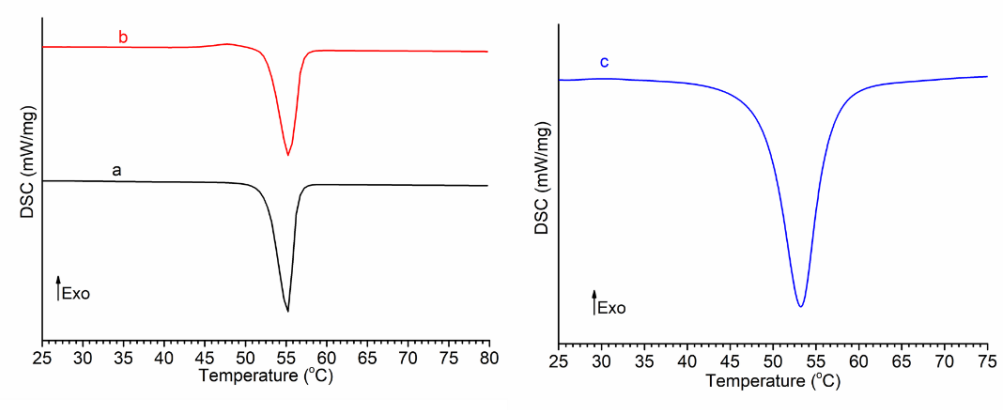

Figure B.4 Differential scanning calorimetry (DSC) study of a) Form I, (b) heating the super cooled melt of (*RS*)-P3D and c) Form II. All runs were performed at 5 K/min.

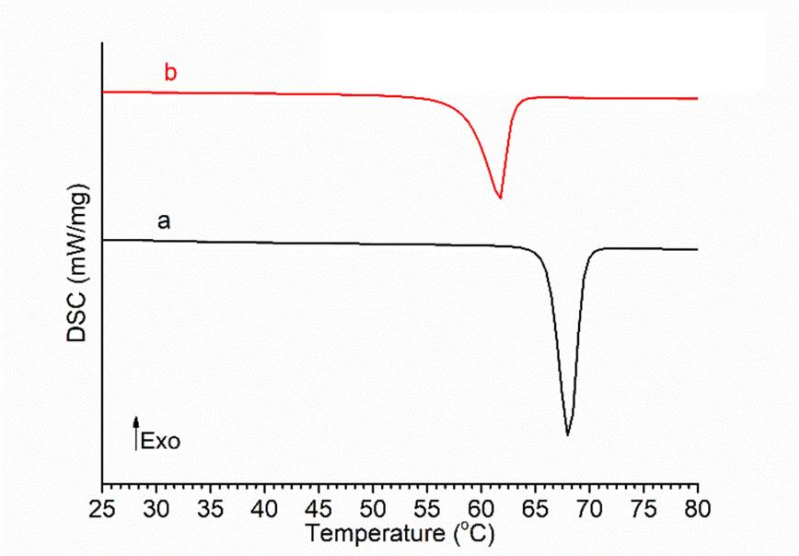

Figure B.5 Differential scanning calorimetry (DSC) study of E-P3D: a) melting endotherm of EI, (b) heating the super cooled melt of E-P3D. All runs were performed at 5 K/min.

B.2.4 Crystal structure of the different forms of P3D

Single crystals of Form I were obtained by slow evaporation of a racemic solution in pentane at room temperature. Single crystals of EI were obtained by a similar procedure using enantiopure P3D. Attempts to grow single crystal of the metastable forms failed.

The single crystal of the racemic Form I shows the same crystal structure as the one published in literature[141] in 2014 (Ref. ZOCNUC), the solid crystallizes in the space group $P2_1/n$. On the other hand, diffraction analysis of EI at room

temperature shows the structure to be orthorhombic $P2_12_12_1$. A monoclinic structure of the pure enantiomer calculated at low temperature (150 K) was reported in another publication (Ref. ZOCPEO) which indicates the presence of a phase transition upon cooling.[141] The difference in the crystallographic data and refinement parameters between the crystal form at 300 K and 150 K are summarized in the table below (Table B.2).

The change in the cell parameters upon cooling shows a small expansion along *a* and a small contraction along *c*, the most significant change even though it is not very big is the contraction along *b*. In the other hand, the symmetry changes from orthorhombic to monoclinic coincide with a reduction in the cell volume. Whereas there are two molecules of P3D in the asymmetric unit of the monoclinic structure, there is only one in the orthorhombic structure. The three independent molecules differ almost insignificantly, mainly in the propyl moiety (Figure B.6).

Hydrogen bonds in the orthorhombic structure are established along *b* axis, wrapping molecules around 2_1 screw axes (Figure B.7 - a). This first type of hydrogen bonds gives rise to molecular chains spreading along *c*. A second type of Hydrogen bonds ensured the cohesion between adjacent molecular bond chains. Along *a*, some $\pi\pi$ interactions (d~3.7Å) are reinforcing this second type of hydrogen bonds (Figure B.7 – b) (Table B.3).

Table B.2 Crystallographic data and refinement parameters for EI, ZOCPEO and ZOCNUC in CSD.

Solid nature	Enantiopure form		Racemic form
	This work (EI)	ZOCPEO	ZOCNUC
Chemical Formula	$C_{12}H_{18}O_3$	$C_{12}H_{18}O_3$	$C_{12}H_{18}O_3$
Temperature / K	300	150	150
Crystal System	Orthorhombic	Monoclinic	Monoclinic
Space Group	$P2_12_12_1$	$P2_1$	$P2_1/n$
Z , Z' (asymmetric units per unit cell)	4,1	4, 2	4, 1
a / *Å*	4.9427(8)	5.0077(9)	4.984(4)
b / *Å*	32.342(5)	30.877(6)	7.525(5)
c / *Å*	7.5348(12)	7.468(1)	31.24(2)
α / °	90	90	90
β / °	90	90.117(2)	92.61(1)
γ / °	90	90	90
V / $Å^3$	1204.5(3)	1154.79	1170.4(14)
d_{calc} / $g.cm^{-3}$	1.160	1.209	1.193
F(000) / e^-	456	456	456

Table B.3 Hydrogen bond table.

D-H...A	d(D-H)	d(H...A)	d(D...A)	<(DHA)
O(1)-H(1)...O(2)#2	0.82	1.9	2.716(2)	170.4
O(2)-H(2A)...O(1)#1	0.82	1.89	2.711(2)	176.2

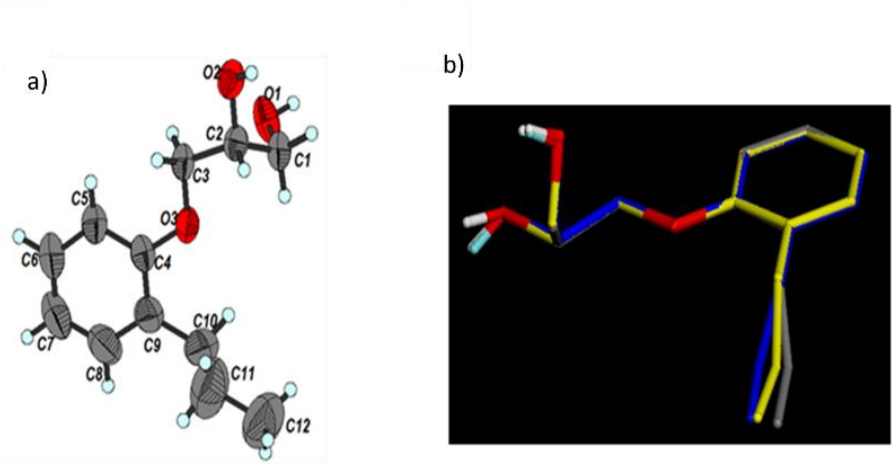

Figure B.6 a) Asymmetric unit in thermal ellipsoidal representation of the orthorhombic structure, with atom labels and b) superimposition with the two molecules from the asymmetric unit of ZOCPEO (yellow and blue).

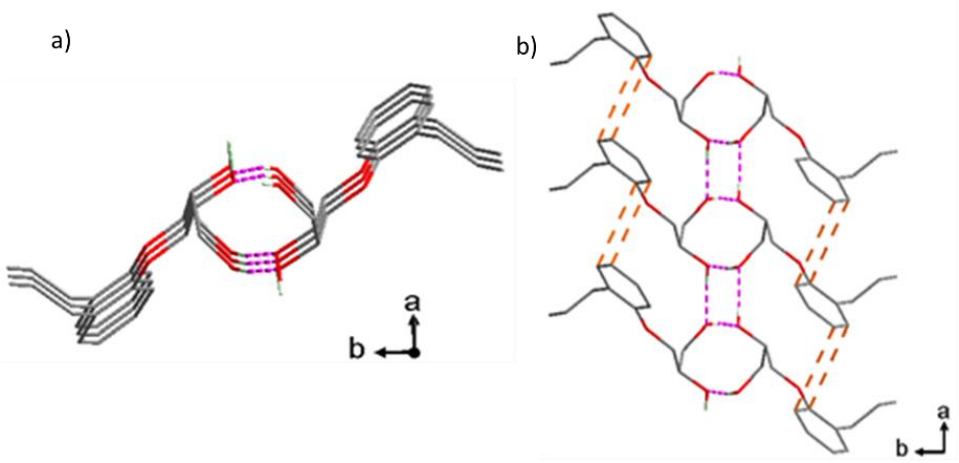

Figure B.7 a) First type of hydrogen bonds (dashed pink lines) established between O(1)-H..O2 generates molecular chains wrapping around 2_1 screw axis, spreading along c and b) A second type of Hydrogen bonds (pink dashed lines) interconnects the molecular chains along a, that leads to molecular layers, in this direction some $\pi\pi$ interactions (orange dashed lines) reinforced the cohesion (d~3.7Å).

Intermolecular interactions give rise to channels in both cases. But there is one type of unidirectional channel in the orthorhombic structure rather than two in the monoclinic model. In both cases a first link connects the same asymmetric units between themselves (linker 1 Figure B.8). Only in monoclinic structure a second type of linker binds the independent molecules together. (Linker 2 in Figure B.8).

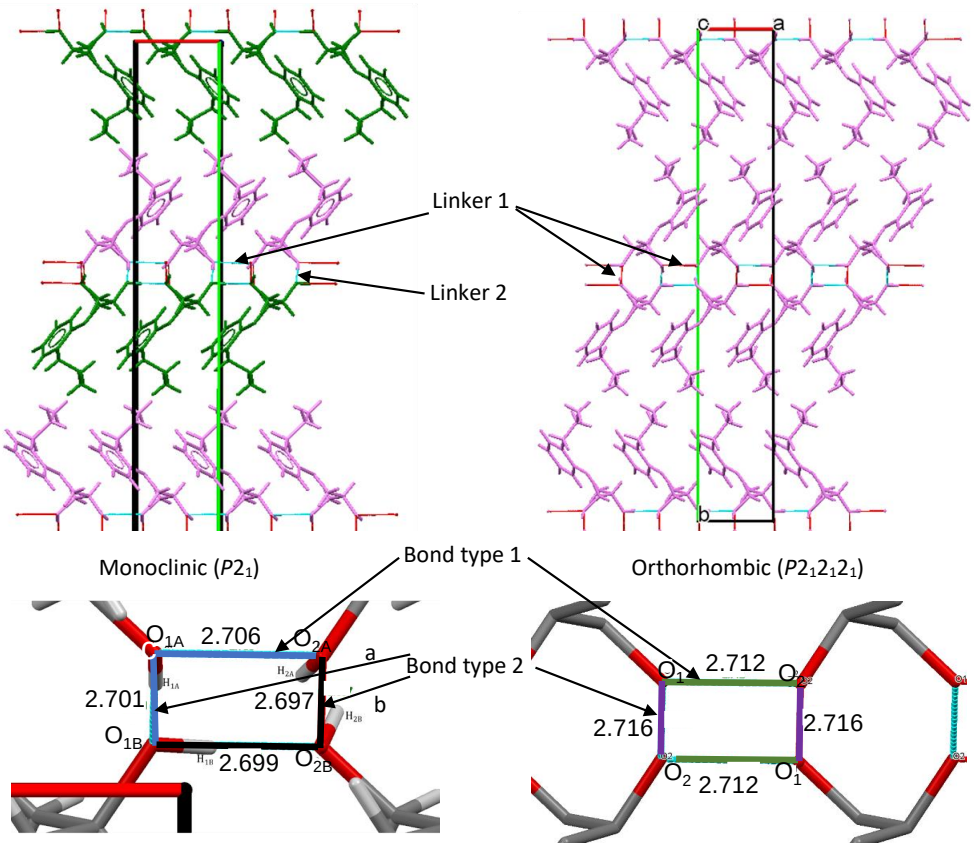

Figure B.8 Comparison of the monoclinic and orthorhombic structures for pure enantiomer of P3D (EI) with the independent molecules identified by colors (monoclinic model is taken from literature single-crystal diffraction experiments: ZOCPEO).

B.2.5 Construction of the binary phase diagram between P3D enantiomers

As a preliminary step, the theoretical binary phase diagram between P3D enantiomers was constructed using the Schröder-Van Laar (to establish the liquidus of EI and EII) and Prigogine–Defay (to establish the liquidus of Form I and Form II) equations.[24] The equations were parametrized with the thermochemical data shown in Table B.1.

The binary phase diagram was experimentally investigated by characterizing the stable equilibrium between the stable Form I and EI. Physical mixtures between the relevant forms were prepared and analyzed by DSC (Figure B.9). The results are presented by blue crosses (for the stable equilibrium) in Figure B.10. These data are in good agreement with the theoretical predictions which suggest that the system behave ideally.

The observation of two forms for the racemic compound as well as for pure enantiomers depicts a situation of double polymorphism similar to diprophylline case and raises the question about the type of the phase relationship between the different solid forms. Experiments did not provide any evidence of the existence of a relationship between Form II and EI nor between Form I and EII. But theoretically speaking we can depict a possibility of a metastable equilibrium between these phases. An extrapolation of the liquidus line of EI and EII can give an idea of the melting point of two metastable conglomerate (round black dot and round purple dot in Figure B.10), but these points were never detected experimentally, thus the presence of a metastable conglomerate was not proved which would explain the reason why PC could not be applied successfully on this system.

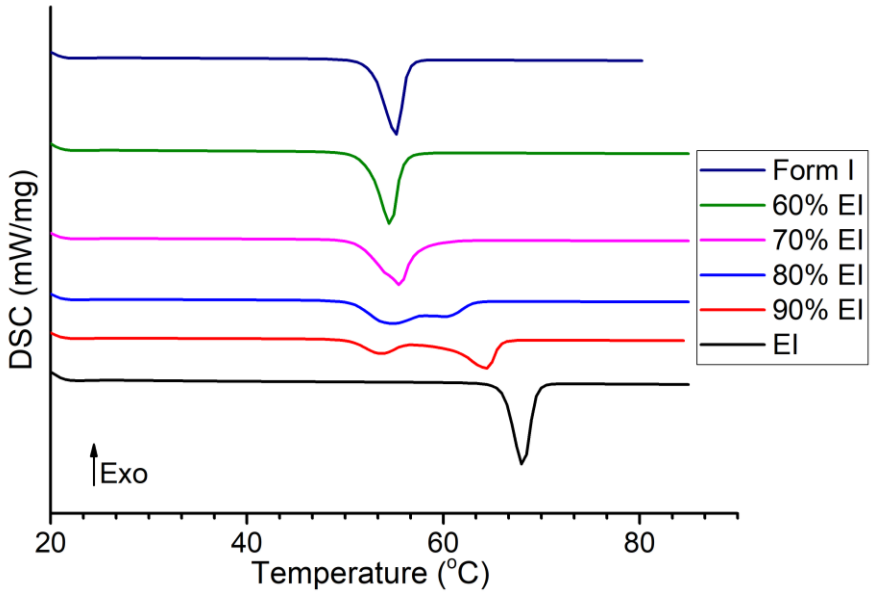

Figure B.9 DSC curves of different mole percent of EI. Heating rate: 5K/min.

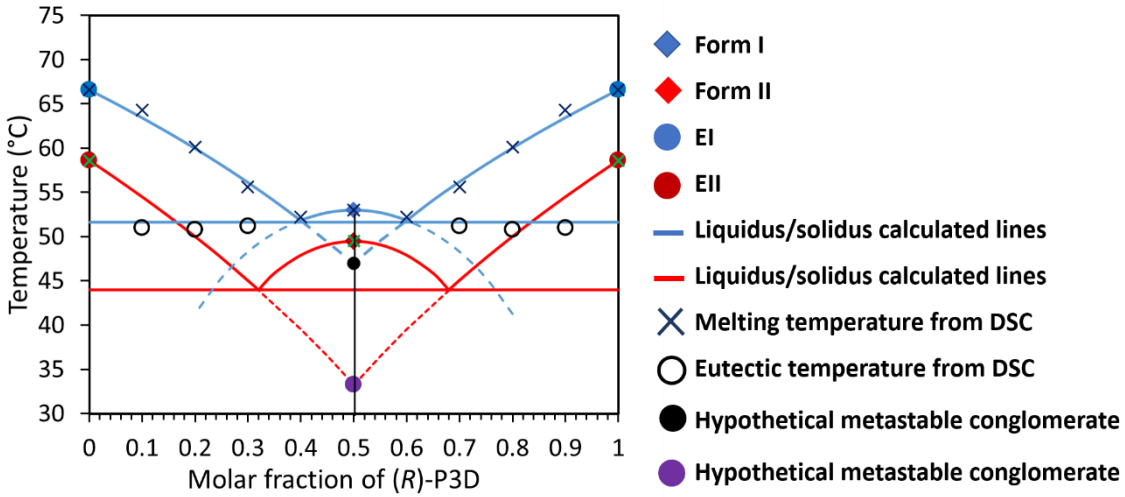

Figure B.10 Binary phase diagram for the stable and metastable equilibrium between the pure enantiomers of P3D.

ANNEX C: CHARACTERIZATIONS OF COCRYSTALS BETWEEN PXL AND DIFFERENT COFORMERS

XRPD and DSC of the different new cocrystals obtained between PXL and the different coformers can be found from Figure C.1 to Figure C.6.

The ^{1}H NMR for these solid phases including the cocrystal between PXL and SA can be found in Figure C.7 to Figure C.13.

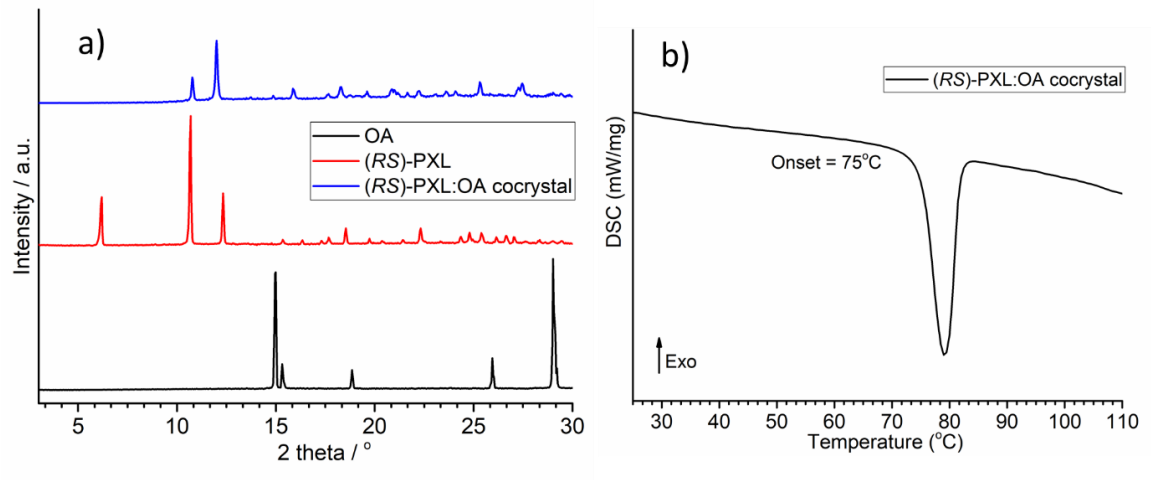

Figure C.1 a) XRPD for racemic PXL, oxalic acid (OA) and PXL-coformer crystal and b) DSC melting curve of the obtained cocrystal.

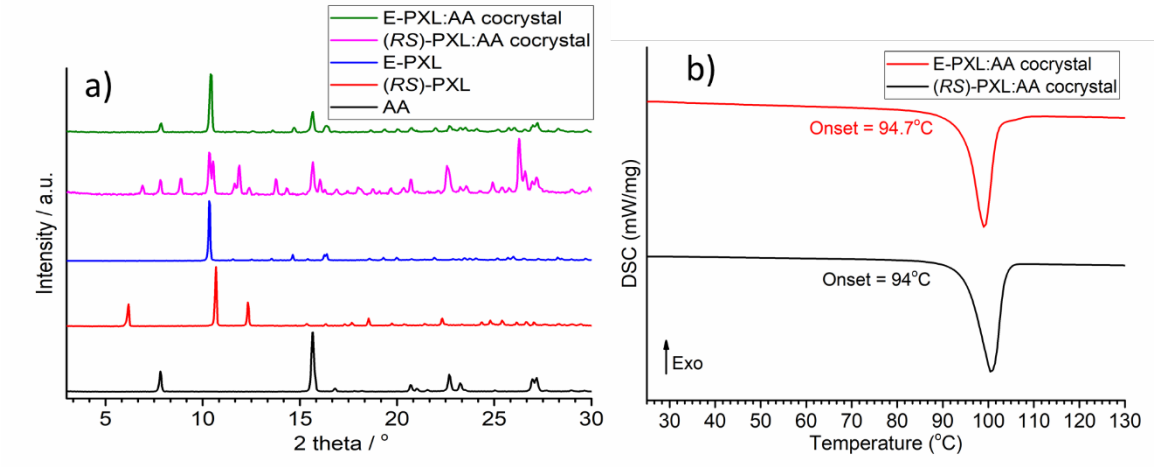

Figure C.2 a) XRPD for racemic PXL, pure enantiomer of PXL, acetyl salicylic acid (AA) and PXL-coformer crystal and b) DSC melting curve of the obtained cocrystal.

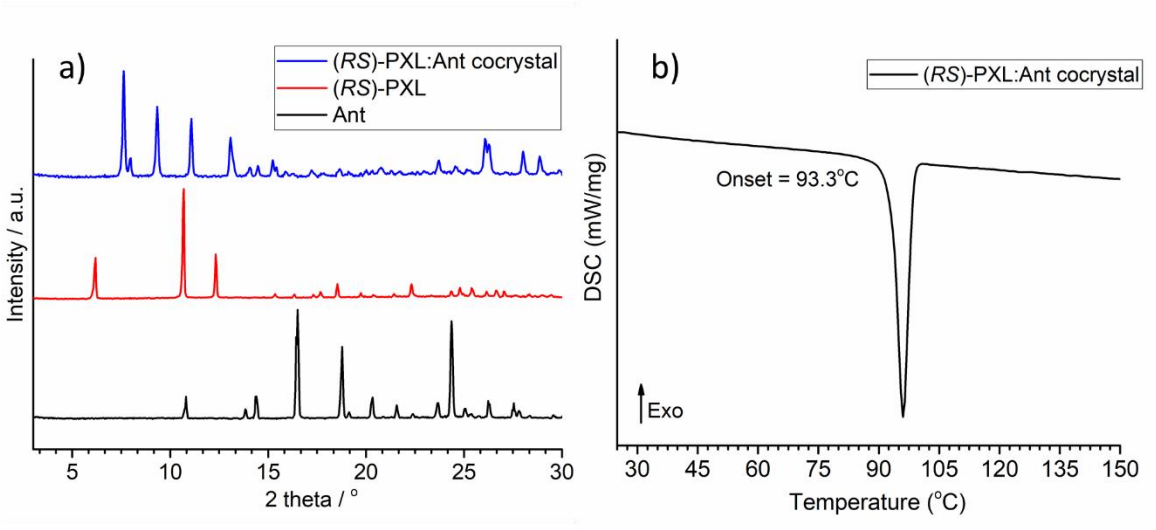

Figure C.3 a) XRPD for racemic PXL, anthranilic acid (Ant) and PXL-coformer crystal and b) DSC melting curve of the obtained cocrystal.

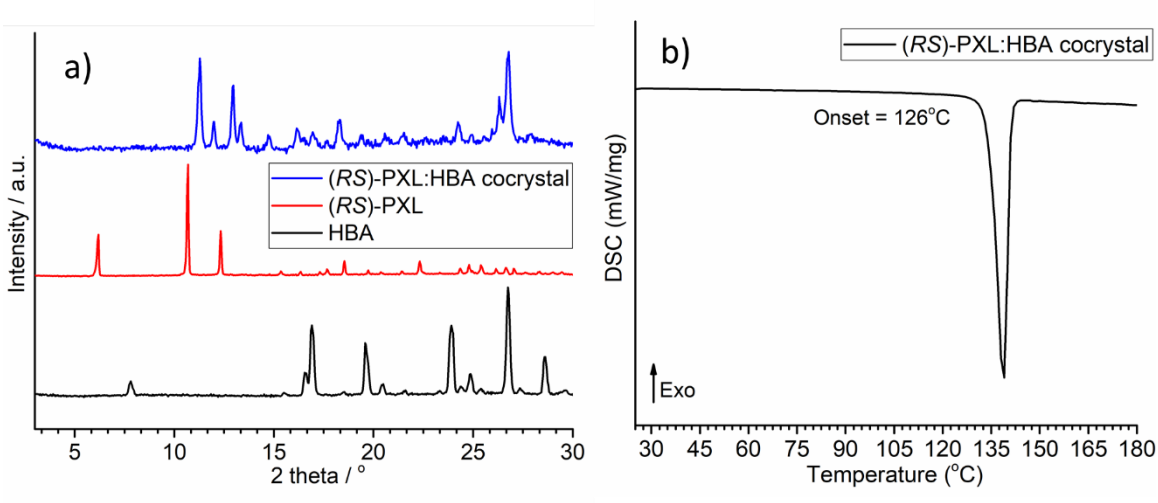

Figure C.4 a) XRPD for racemic PXL, hydroxybenzoic acid (HBA) and PXL-coformer crystal and b) DSC melting curve of the obtained cocrystal.

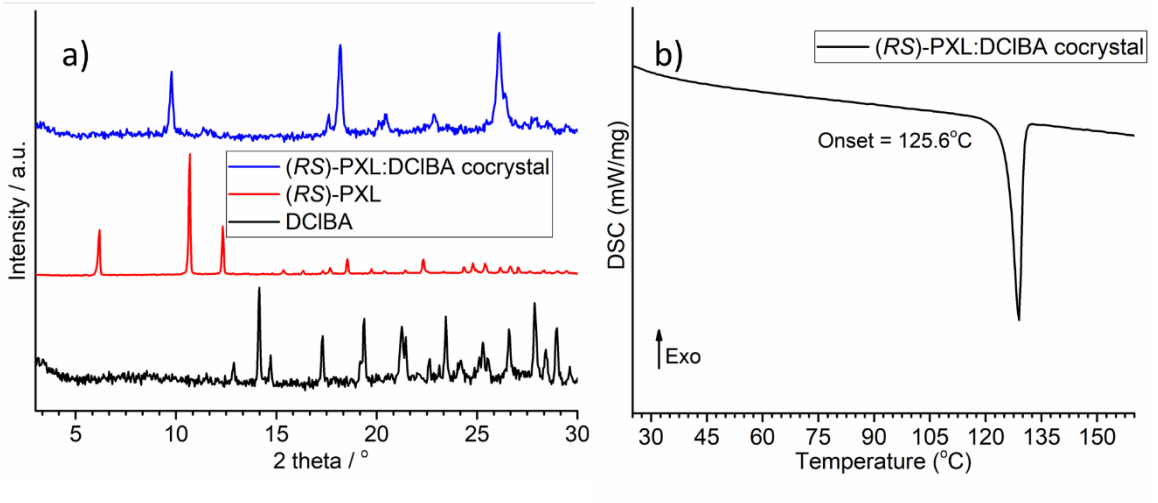

Figure C.5 a) XRPD for racemic PXL, dichlorobenzoic acid (DClBA) and PXL-coformer crystal and b) DSC melting curve of the obtained cocrystal.

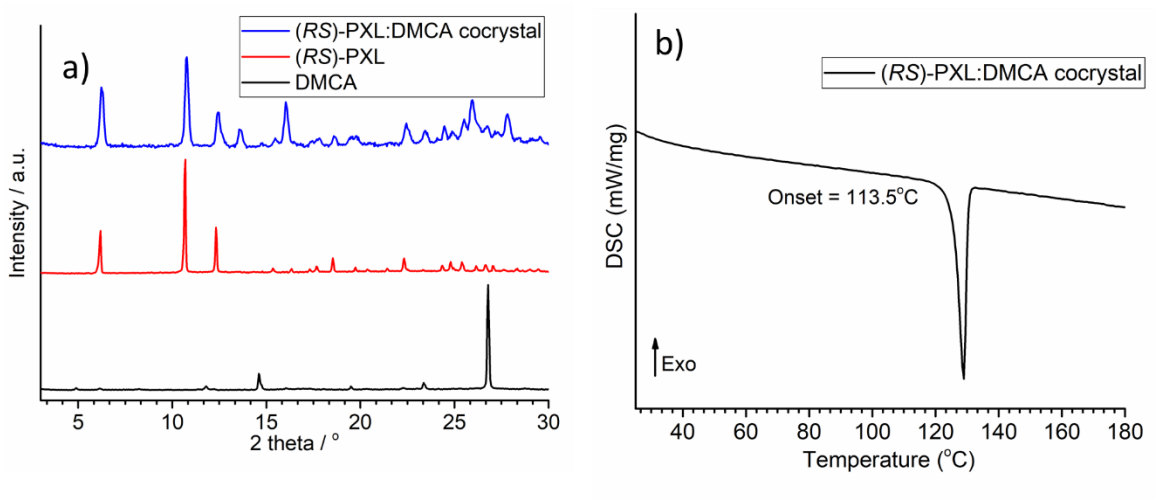

Figure C.6 a) XRPD for racemic PXL, dimethoxy cinnamic acid (DMCA) and PXL-coformer crystal and b) DSC melting curve of the obtained cocrystal.

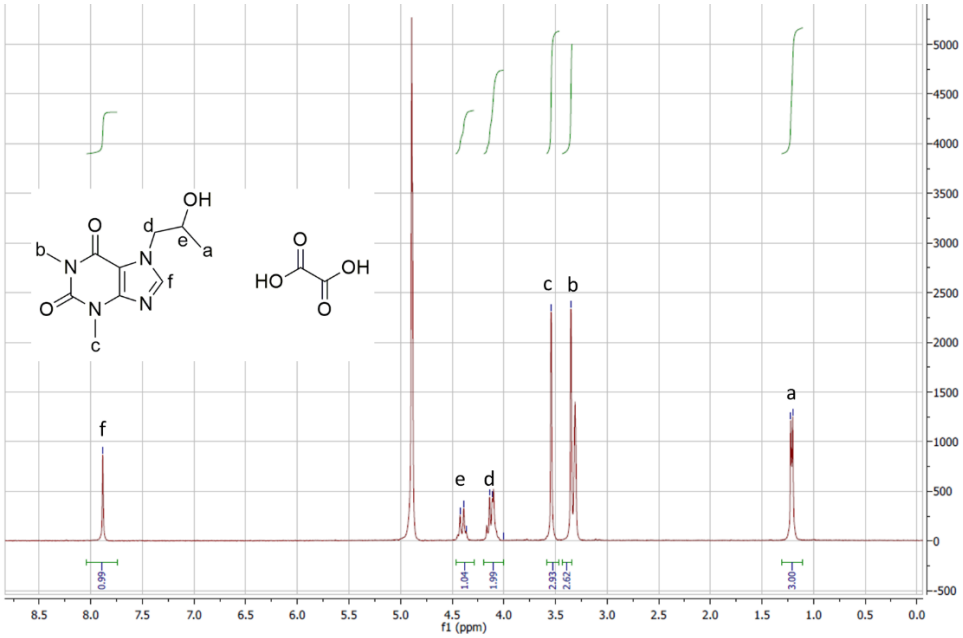

Figure C.7 ^{1}H NMR of the cocrystal obtained between PXL and OA in MeOD. Hydrogens of OA were not detected by NMR in MeOD.

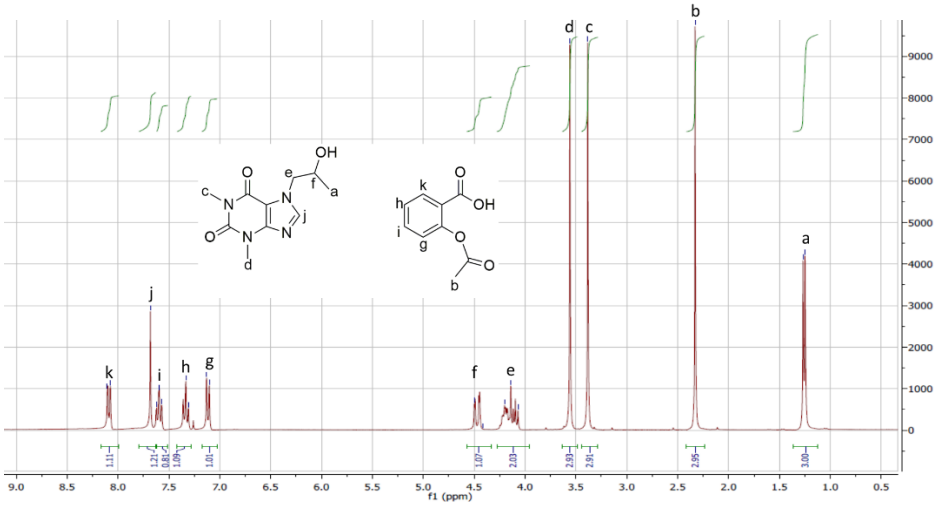

Figure C.8 ^{1}H NMR of the cocrystal between PXL and AA in $CDCl_3$.

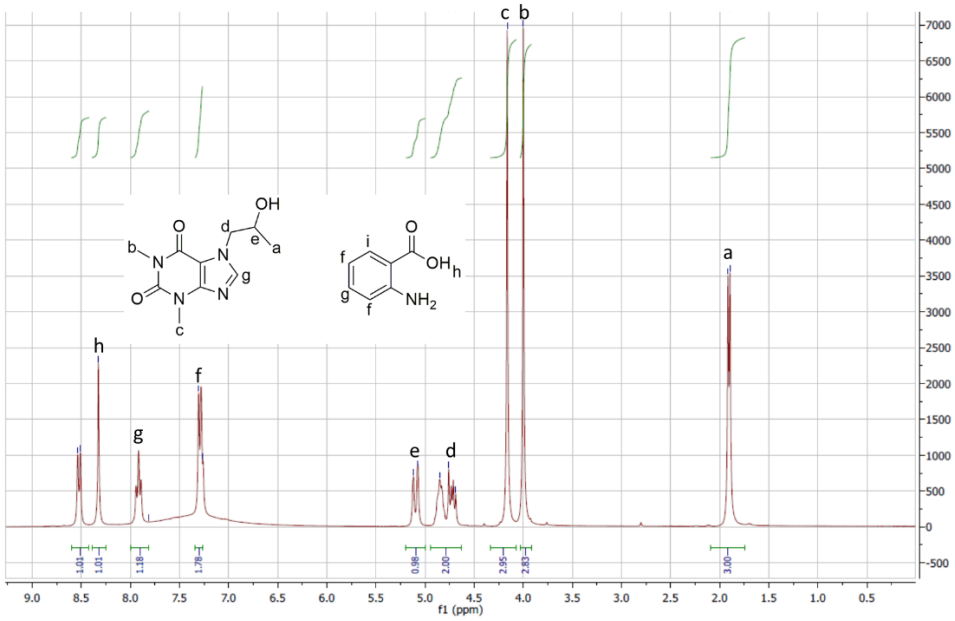

Figure C.9 ^{1}H NMR of the cocrystal between PXL and Ant in $CDCl_3$.

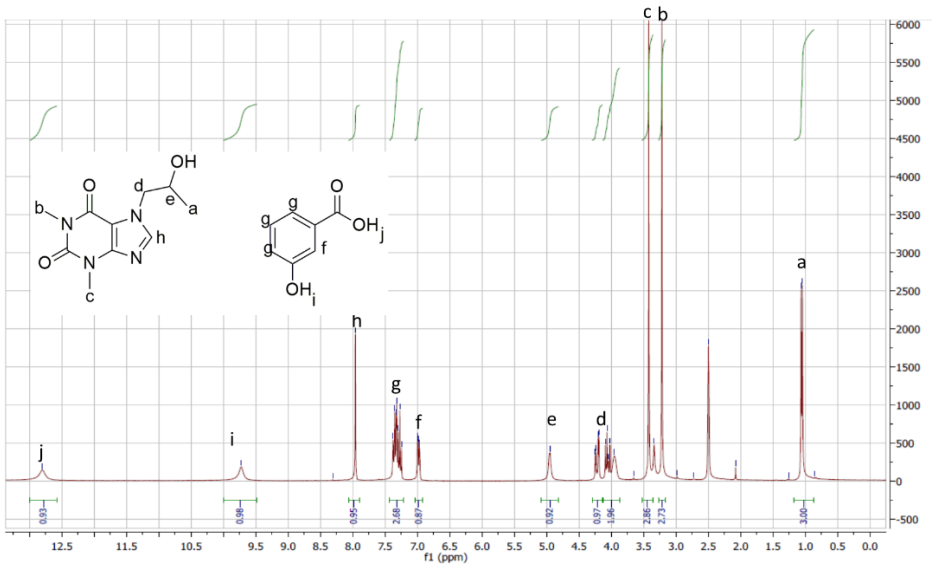

Figure C.10 ^{1}H NMR of the cocrystal between PXL and HBA in $(CD_3)_2SO$.

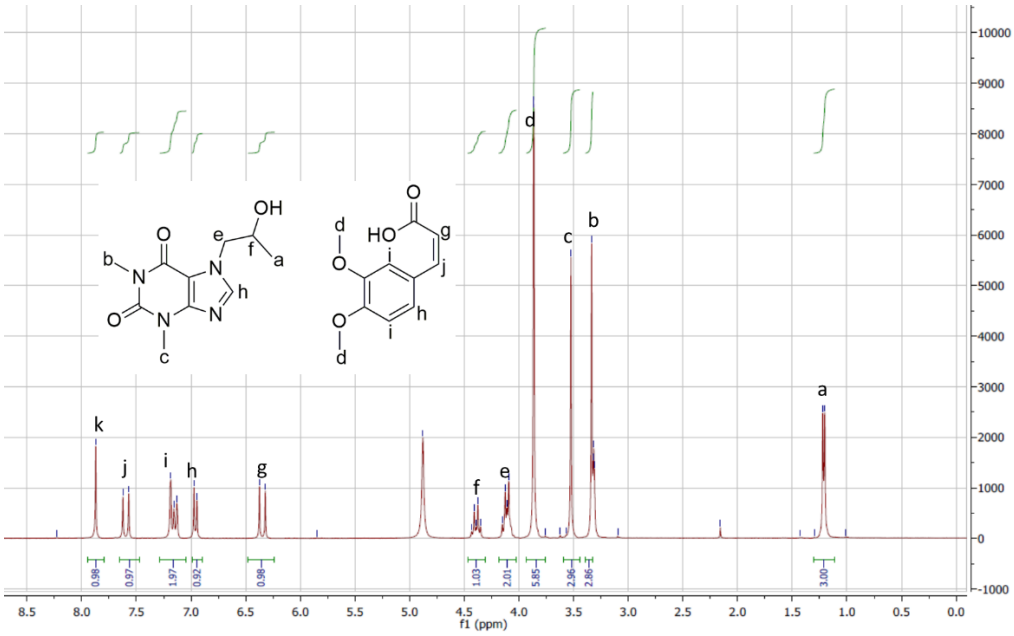

Figure C.11 ^{1}H NMR of the cocrystal between PXL and DMCA in MeOD.

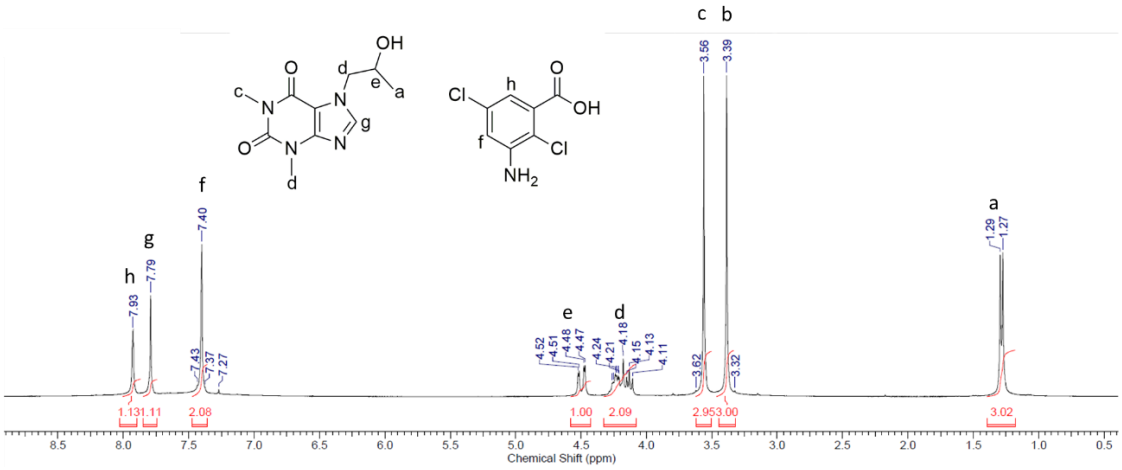

Figure C.12 ^{1}H NMR of the cocrystal obtained between PXL and DClBA.

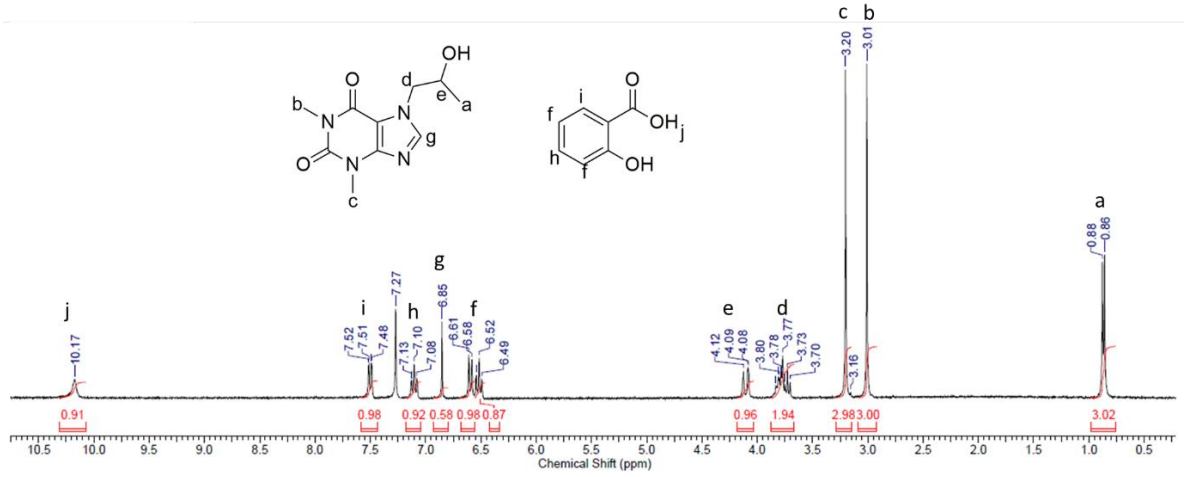

Figure C.13 ^{1}H NMR of the cocrystal obtained between PXL and SA in $CDCl_3$.

ANNEX D: INDUCTION TIME STUDY

We report the nucleation rates of (*RS*)-PXL in different solvents using Crystal16 apparatus during a secondment at Strathclyde university-Glasgow. These rates are determined from cumulative probability distributions of induction times in many measurements at a constant supersaturation at a given constant temperature (20 °C) in 1 mL agitated solution.

The probability P(t) to detect crystals at time t can be determined by this equation:

$$P(t) = 1 - \exp(-JV(t_i - t_g))$$

To detect the formed nuclei, it should grow to appreciable sizes before they can be detected, this causes a delay t_g (the growth time). The induction time "t_i" is the period of time between the achievement of a constant supersaturation and the detection of crystals. V is volume and J is the stationary nucleation rate.

For M isolated experiments, the probability P(t) to measure an induction time between zero and time t is defined in:

$$P(t) = \frac{M+(t)}{M}$$

$M^+(t)$ is the number of experiments in which crystals are detected at time t. The experimentally determined probability distribution P(t) of the induction time can be described by the cumulative probability distribution function, leading to the determination of nucleation rate J and growth time t_g.

D.1 Proxyphylline (PXL)

t_i measurements were performed at 20 °C for β = 1.5, 2, 2.3, and 3 in 1mL scale in different solvents. At each supersaturation ratio, several numbers of t_i measurements were done in 1 mL vials (Table D.1 and Table D.2). The empty boxes in the tables refer to no crystal nucleation occurring.

As expected, the t_i values show a large variation at one supersaturation. In case of small samples, the stochastic aspect of nucleation is usually observed, because a single crystal or a small number of crystals are used as a detection criterion of nucleation. The different solvents presented in Table D.1 and Table D.2 were also investigated on larger scale to study the effect of sample volume on t_i results (Table 3.1). For large samples, the stochastic aspect was not observed in actual experiments because a small number of crystals are rather difficult to detect when the sample is large.

It should be noted that t_i of PXL was not measured in some solvents, like, acetone, chloroform, n-butyl acetate, dimethyl sulfoxide, water, DCM, IBA due to the high solubility of PXL in the solvent or to the low evaporation temperature of the solvent or its unavailability in the laboratory during the time of experiments.

Table D.1 Induction time data for Proxyphylline in different solvents at a) β = 1.5 and b) β = 2.

a)

1,4-dioxane	THF	MeOH	Acetonitrile	EtOH	Butan-2-ol	MIBK	Ethyl acetate
131	113	153	72	63	95	170	70
51	91	237	25	83	104	70	186
230	73	252	59	284	198	70	178
	87		219	157	24	186	
	295		105		126	178	
	46		27		146	131	
	40				45		
					94		
					101		
					276		

b)

1,4-dioxane	THF	Acetonitrile	Propan-1-ol	EtOH	Butan-2-ol	Ethyl acetate
57	25	303	202	42	29	50
18	26	135	59	11	38	
27	40	244	216	15	222	
		75				
		169				

Table D.2 Induction time data for Proxyphylline in different solvents at a) β = 2.3 and b) β = 3.

a)

Propan-1-ol	Butan-2-ol	Ethyl acetate
41	52	520
353	136	56
61	33	47
76	24	27
	157	11
	186	60
	483	71
	189	10
	195	82
		24
		19
		110
		56

b)

MeOH	Propan-1-ol	EtOH	Butan-2-ol
262	52	123	45
183	43	163	94
101	149	235	101
	263	306	276
	176	136	16
			239

For a supersaturation β = 3, nucleation of PXL was hindered in ethanol for an average of 3 hours. Ethanol was then chosen for further study. With the total number of M = 192 induction times, only in 114 samples crystals were detected. The probability distribution P(t) of the induction time can be determined (Figure D.1).

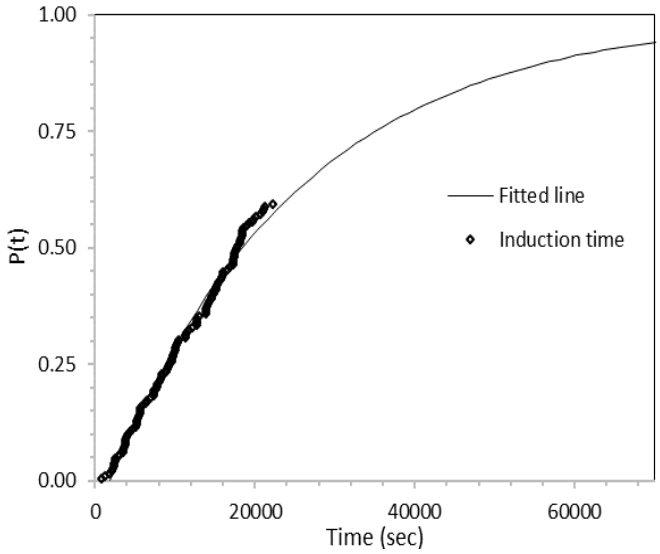

Figure D.1 Probability distribution of the induction times of 192 experimental data points for PXL in ethanol at β = 3.

From the fitted line in Figure D.1, we can calculate a nucleation rate J = 41.8 ± 0.45 m^{-3} s^{-1} and a growth time t_g = 1874.2 ± 91 s.

BIBLIOGRAPHY

(1) Sanganyado, E.; Lu, Z.; Fu, Q.; Schlenk, D.; Gan, J. Chiral Pharmaceuticals: A Review on Their Environmental Occurrence and Fate Processes. *Water Res.* **2017**, *124*, 527–542.

(2) Gu, C. H.; Grant, D. J. W. Physical Properties and Crystal Structures of Chiral Drugs. In *Handbook of Experimental Pharmacology: Stereochemical Aspects of Drug Action and Disposition.*; Springer, Berlin., 2003; Vol. 153, pp 113–139.

(3) Smith, S. W. Chiral Toxicology: It's the Same Thing Only Different. *Toxicol. Sci.* **2009**, *110* (1), 4–30.

(4) Liu, J. T.; Liu, R. H. Enantiomeric Composition of Abused Amine Drugs: Chromatographic Methods of Analysis and Data Interpretation. *J. Biochem. Biophys. Methods* **2002**, *54* (1–3), 115–146.

(5) Lin, G.Q.; Zhang, J.G.; Cheng, J.F. *Chiral Drugs: Chemitry and Biological Action*; John Wiley & Sons: New Jersey, 2011.

(6) Carvalho, P. O.; Cass, Q. B.; Calafatti, S. A.; Contesini, J. F.; Bizaco, R. Review—Alternatives for the Separation of Drug Enantiomers: Ibuprofen as a Model Compound. *Braz. J. Chem. Eng.* **2006**, *23* (3), 291–300.

(7) Takemura, T.; Saito, K.; Nakazawa, S.; Mori, N. Separation and Characterization of All Configurational Isomers by Enzymatic Discrimination of Each Chiral Function. *Tetrahedron Lett.* **1992**, *33* (42), 6335–6338.

(8) Armstrong, D. W.; Liu, Y.; Ekborgott, K. H. A Covalently Bonded Teicoplanin Chiral Stationary Phase for HPLC Enantioseparations. *Chirality* **1995**, *7* (6), 474–497.

(9) Casas, J.; Engqvist, M.; Ibrahem, I.; Kaynak, B.; Córdova, A. Direct Amino Acid Catalyzed Asymmetric Synthesis of Polyketide Sugars. *Angew. Chem. Int. Ed* **2005**, *44* (9), 1343–1345.

(10) Sögütoglu, L. C.; Steendam, R. R. E.; Meekes, H.; Vlieg, E.; Rutjes, F. P. J. T. Viedma Ripening: A Reliable Crystallisation Method to Reach Single Chirality. *Chem. Soc. Rev.* **2015**, *44* (19), 6723–6732.

(11) Coquerel, G. Preferential Crystallization. In *Topics in Current Chemistry*; Springer: Berlin-Heidelberg, 2007; pp 1–50.

(12) Brandel, C.; Amharar, Y.; Rollinger, J. M.; Griesser, U. J.; Cartigny, Y.; Petit, S.; Coquerel, G. Impact of Molecular Flexibility on Double Polymorphism, Solid Solutions and Chiral Discrimination during Crystallization of Diprophylline Enantiomers. *Mol. Pharmaceutics* **2013**, *10* (10), 3850–3861.

(13) Rosaxoff, M. A. On Fischer's Classification of Stereo-Isomers. *J. Am. Chem.*

Soc. **1906**, *28* (1), 114–121.

(14) Cahn, R. S.; Ingold, C.; Prelog, V. Specification of Molecular Chirality. *Angew. Chem. Int. Ed.* **1966**, *5* (4), 385–415.

(15) Willia, K.; Lee, E. Importance of Drug Enantiomers in Clinical Pharmacology. *Drugs* **1985**, *30* (4), 333–354.

(16) Katzung, B. G.; Trevor, A. J. *Basic and Clinical Pharmacology*, 14th ed.; McGraw Hill Education: New York, 2015.

(17) Sheldon, R. A. *Chirotechnology: Industrial Synthesis of Optically Active Compounds*; CRC Press, 1993.

(18) Agranat, I.; Caner, H.; Caldwell, J. Putting Chirality to Work: The Strategy of Chiral Switches. *Nat. Rev. Drug Discov.* **2002**, *1* (10), 753–768.

(19) Mansfield, P.; Henry, D.; Tonkin, A. Single-Enantiomer Drugs. *Clin. Pharmacokinet.* **2004**, *43* (5), 287–290.

(20) Grasedyck, K. D-Penicillamine-Side Effects, Pathogenesis and Decreasing the Risks. *Z. Rheumatol.* **1988**, *47*, 17–19.

(21) Kahana, L. M. Toxic Ocular Effects of Ethambutol. *Can. Med. Assoc. J.* **1987**, *137* (3), 213–216.

(22) Powell, J. R.; Ambre, J. J.; Ruo, T. I. The Efficacy and Toxicity of Drug Stereoisomerism. In *Drug stereochemistry*; Wainer, I. W., Drayer, D. E., Eds.; Marcel Dekker: New York, 1988; pp 245–270.

(23) Administration, U. S. F. & D. *Development of New Stereoisomeric Drugs*; Washington, DC, 1992.

(24) Jacques, J.; Collet, A.; Wilen, S. H. *Enantiomers, Racemates and Resolutions*; John Wiley & Sons, Inc.: New York, 1981.

(25) Lorenz, H.; Perlberg, A.; Sapoundjiev, D.; Elsner, M. P.; Seidel-Morgenstern, A. Crystallization of Enantiomers. *Chem. Eng. Process* **2006**, *45* (10), 863–873.

(26) Lachman, L.; Lieberman, H. A.; Kanig, J. L. *The Theory and Practice of Industrial Pharmacy*; Lea & Febiger, 1986.

(27) Pangarkar, P. A.; Tayade, A. M.; Uttarwar, S. G.; Wanare, R. S. Drug Polymorphism: An Overview. *Int. J. Pharm. Technol.* **2012**, *5*, 2374–2402.

(28) Purohit, R.; Venugopalan, P. Polymorphism : An Overview. *Reson.* **2009**, *14* (9), 882–893.

(29) Raza, K.; Kumar, P.; Ratan, S.; Malik, R.; Arora, S. Polymorphism : The Phenomenon Affecting the Performance of Drugs. *SOJ Pharm. Pharm. Sci.* **2014**, *1* (2), 1–10.

(30) Kristl, A.; Srčič, S.; Vrečer, F.; Šuštar, B.; Vojnovic, D. Polymorphism and Pseudopolymorphism: Influencing the Dissolution Properties of the Guanine

Derivative Acyclovir. *Int. J. Pharm.* **1996**, *139* (1–2), 231–235.

(31) Haleblian, J.; McCrone, W. Pharmaceutical Applications of Polymorphism. *J. Pharm. Sci.* **1969**, *58* (8), 911–929.

(32) Brittain, H. G. *Polymorphism in Pharmaceutical Solids*; Marcel Dekker, Inc.: New York, USA, 1999.

(33) Cruz-Cabeza, A. J.; Bernstein, J. Conformational Polymorphism. *Chem. Rev.* **2014**, *114* (4), 2170–2191.

(34) Buerger, M. J. Polymorphism and Phase Transformations. *Fortschritte Der Mineralogie* **1961**, *39* (1), 9–24.

(35) Thiruvengadam, E.; Vellaisamy, G. Polymorphism in Pharmaceutical Ingredients. *Int. J. Pharm. Pharm. Sci.* **2014**, *3* (3), 621–633.

(36) Bauer, J.; Spanton, S.; Henry, R.; Quick, J.; Dziki, W.; Porter, W.; Morris, J. Ritonavir: An Extraordinary Example of Conformational Polymorphism. *Pharm. Res.* **2001**, *18* (6), 859–866.

(37) Kasuga, N. C.; Saito, Y.; Sato, H.; Yamaguchi, K.; Ishida, H. Packing Polymorphism in the Crystal Structure of 4,5-Dimethoxy-2-Nitrobenzyl Acetate. *Acta Cryst. Sect. E. Struct. Reports Online* **2015**, *71* (5), 483–486.

(38) Henck, J. O.; Kuhnert-Brandstatter, M. Demonstration of the Terms Enantiotropy and Monotropy in Polymorphism Research Exemplified by Flurbiprofen. *J. Pharm. Sci.* **1999**, *88* (1), 103–108.

(39) Yu, L. Inferring Thermodynamic Stability Relationship of Polymorphs from Melting Data. *J. Pharm. Sci.* **1995**, *84* (8), 966–974.

(40) Lohani, S.; Grant, D. J. W. Thermodynamics of Polymorphs. In *Polymorphism in the Pharmaceutical Industry*; Wiley-VCH: Weinheim, Germany, 2006; pp 21–42.

(41) Barbas, R.; Martí, F.; Prohens, R.; Puigjaner, C. Polymorphism of Norfloxacin: Evidence of the Enantiotropic Relationship between Polymorphs A and B. *Cryst. Growth Des.* **2006**, *6* (6), 1463–1467.

(42) Yang, L.; Yin, Q.; Hou, B.; Wang, Y.; Bao, Y.; Wang, J.; Hao, H. Solubility and Thermodynamic Stability of the Enantiotropic Polymorphs of 2,3,5-Trimethyl-1,4-Diacetoxybenzene. *Ind. Eng. Chem. Res.* **2013**, *52* (7), 2477–2485.

(43) Riesco, M. R.; Martı, F. J.; Lo, S.; Torres, M. R.; Garrido, L.; Rodrı, J. A. Monotropic Polymorphism in Copper (II). *Cryst. Growth Des.* **2008**, *8* (7), 2547–2554.

(44) Rietveld, I. B.; Céolin, R. Rotigotine: Unexpected Polymorphism with Predictable Overall Monotropic Behavior. *J. Pharm. Sci.* **2015**, *104* (12), 4117–4122.

(45) Brog, J. P.; Chanez, C. L.; Crochet, A.; Fromm, K. M. Polymorphism, What It Is and How to Identify It: A Systematic Review. *RSC Adv.* **2013**, *3* (38), 16905–16931.

(46) Chieng, N.; Rades, T.; Aaltonen, J. An Overview of Recent Studies on the Analysis of Pharmaceutical Polymorphs. *J. Pharm. Biomed. Anal.* **2011**, *55* (4), 618–644.

(47) Danesh, A.; Chen, X.; Davies, M. C.; Roberts, C. J.; Sanders, G. H. W.; Tendler, S. J. B.; Williams, P. M.; Wilkins, M. J. The Discrimination of Drug Polymorphic Forms from Single Crystals Using Atomic Force Microscopy. *Pharm. Res.* **2000**, *17* (7), 887–890.

(48) Yu, L.; Reutzel, S. M.; Stephenson, G. A. Physical Characterization of Polymorphic Drugs: An Integrated Characterization Strategy. *Pharm. Sci. Technolo. Today* **1998**, *1* (3), 118–127.

(49) Danesh, A.; Chen, X.; Davies, M. C.; Roberts, C. J.; Sanders, G. H. W.; Tendler, S. J. B.; Williams, P. M.; Wilkins, M. J. Polymorphic Discrimination Using Atomic Force Microscopy: Distinguishing between Two Polymorphs of the Drug Cimetidine. *Langmuir* **2000**, *16* (2), 866–870.

(50) Carrer, H.; Cortez, J.; Frare, L. M.; Costa, M. B.; Bittencourt, P. R. S. Thermal Characterization of the Bromopride Recrystallized from Different Solvents and at Different Temperature Conditions. *J. Therm. Anal. Calorim.* **2016**, *123* (2), 927–931.

(51) Giron, D. Thermochimica Acta Thermal Analysis Characterisation and Calorimetric of Polymorphs Methods in the and Solvates. *Thermochim. Acta* **1995**, *248* (94), 1–59.

(52) Braga, D.; Palladino, G.; Polito, M.; Rubini, K.; Grepioni, F.; Chierotti, M. R.; Gobetto, R. Three Polymorphic Forms of the Co-Crystal 4,4′-Bipyridine/Pimelic Acid and Their Structural, Thermal, and Spectroscopic Characterization. *Chem. Eur. J.* **2008**, *14* (32), 10149–10159.

(53) Vrecer, F.; Srcic, S.; Smid-Korbar, J. Investigation of Piroxicam Polymorphism. *Int. J. Pharm.* **1991**, *68*, 35–41.

(54) Li, J.; Bourne, S. A.; Caira, M. R. New Polymorphs of Isonicotinamide and Nicotinamide. *Chem. Commun.* **2011**, *47* (5), 1530–1532.

(55) Sacchetti, M. Thermodynamic Analysis of DSC Data for Acetominophen Polymorphs. *J. Therm. Anal. Calorim.* **2001**, *63*, 345–350.

(56) Aaltonen, J.; Strachan, C. J.; Pöllänen, K.; Yliruusi, J.; Rantanen, J. Hyphenated Spectroscopy as a Polymorph Screening Tool. *J. Pharm. Biomed. Anal.* **2007**, *44* (2), 477–483.

(57) Aaltonen, J.; Rantanen, J.; Siiriä, S.; Karjalainen, M.; Jørgensen, A.; Laitinen, N.; Savolainen, M.; Seitavuopio, P.; Louhi-Kultanen, M.; Yliruusi, J. Polymorph Screening Using Near-Infrared Spectroscopy. *Anal. Chem.* **2003**,

75 (19), 5267–5273.

(58) Dandeu, A.; Humbert, B.; Carteret, C.; Muhr, H.; Plasari, E.; Bossoutrot, J. M. Raman Spectroscopy - A Powerful Tool for the Quantitative Determination of the Composition of Polymorph Mixtures: Application to CaCO3 Polymorph Mixtures. *Chem. Eng. Technol.* **2006**, *29* (2), 221–225.

(59) Isogai, A.; Usuda, M.; Kato, T.; Uryu, T.; Atalla, R. H. Solid-State CP/MAS 13C NMR Study of Cellulose Polymorphs. *Macromolecules* **1989**, *22* (7), 3168–3172.

(60) Brittain, H. G.; Morris, K. R.; Bugay, D. E.; Thakur, A. B.; Serajuddin, A. T. M. Solid-State NMR and IR for the Analysis of Pharmaceutical Solids: Polymorphs of Fosinopril Sodium. *J. Pharm. Biomed. Anal.* **1993**, *11* (11–12), 1063–1069.

(61) Duer, M. J. *Solid-State NMR Spectroscopy: Principles and Applications*; Blackwell Science: Oxford, 2002.

(62) Yu, Z. B.; Han, Y.; Zhao, L.; Huang, S.; Zheng, Q. Y.; Lin, S.; Córdova, A.; Zou, X.; Sun, J. Intergrown New Zeolite Beta Polymorphs with Interconnected 12-Ring Channels Solved by Combining Electron Crystallography and Single-Crystal X-Ray Diffraction. *Chem. Mater.* **2012**, *24* (19), 3701–3706.

(63) Dinnebier, R. E.; Sieger, P.; Nar, H.; Shankland, K.; David, W. I. F. Structural Characterization of Three Crystalline Modifications of Telmisartan by Single Crystal and High-Resolution X-Ray Powder Diffraction. *J. Pharm. Sci.* **2000**, *89* (11), 1465–1479.

(64) Drebushchak, T. N.; Boldyreva, E. V. Variable Temperature (100-360 K) Single-Crystal X-Ray Diffraction Study of the Orthorhombic Polymorph of Paracetamol (p-Hydroxyacetanilide). *Z. Kristallogr.* **2004**, *219* (8), 506–512.

(65) Rodríguez-Spong, B.; Price, C. P.; Jayasankar, A.; Matzger, A. J.; Rodríguez-Hornedo, N. General Principles of Pharmaceutical Solid Polymorphism: A Supramolecular Perspective. *Adv. Drug Deliv. Rev.* **2004**, *56* (3), 241–274.

(66) Khankari, R. K.; Grant, D. J. W. Pharmaceutical Hydrates. *Thermochim. Acta* **1995**, *248*, 61–79.

(67) Giron, D.; Goldbronn, C.; Mutz, M.; Pfeffer, S.; Piechon, P.; Schwab, P. Solid State Characterizations of Pharmaceutical Hydrates. *J. Therm. Anal. Calorim.* **2002**, *68* (2), 453–465.

(68) Stephenson, G. A.; Groleau, E. G.; Kleemann, R. L.; Xu, W.; Rigsbee, D. R. Formation of Isomorphic Desolvates: Creating a Molecular Vacuum. *J. Pharm. Sci.* **1998**, *87* (5), 536–542.

(69) Zhu, H.; Yuen, C.; Grant, D. J. W. Influence of Water Activity in Organic Solvent + Water Mixtures on the Nature of the Crystallizing Drug Phase. 2.

Ampicillin. *Int. J. Pharm.* **1996**, *139* (1–2), 33–43.

(70) Chen, L. R.; Young, V. G.; Lechuga-Ballesteros, D.; Grant, D. J. W. Solid-State Behavior of Cromolyn Sodium Hydrates. *J. Pharm. Sci.* **1999**, *88* (11), 1191–1200.

(71) Morris, K. R. Structural Aspects of Hydrates and Solvates. In *Drugs and the pharmaceutical sciences*; Marcel Dekker: New York, 1999; pp 125–182.

(72) Rajput, L.; Biradha, K. Crystalline Forms of 1,3,5-Benzene-Tri(Pyridinyl)Carboxamides: Isolated Site Hydrates as Polymorphs and Solvates. *J. Mol. Struct.* **2011**, *991* (1–3), 97–102.

(73) Kennedy, A. R.; Okoth, M. O.; Sheen, D. B.; Sherwood, J. N.; Teat, S. J.; Vrcelj, R. M. Cephalexin: A Channel Hydrate. *Acta Crystallogr. Sect. C Cryst. Struct. Commun.* **2003**, *59* (11), 650–652.

(74) Redman-Furey, N.; Dicks, M.; Bigalow-Kern, A.; Cambron, R. T.; Lubey, G.; Lester, C.; Vaughn, D. Structural and Analytical Characterization of Three Hydrates and an Anhydrate Form of Risedronate. *J. Pharm. Sci.* **2005**, *94* (4), 893–911.

(75) Petit, S.; Coquerel, G. Mechanism of Several Solid-Solid Transformations between Dihydrated and Anhydrous Copper(II) 8-Hydroxyquinolinates. Proposition for a Unified Model for the Dehydration of Molecular Crystals. *Chem. Mater.* **1996**, *8* (9), 2247–2258.

(76) Aitipamula, S.; Banerjee, R.; Bansal, A. K.; Biradha, K.; Cheney, M. L.; Choudhury, A. R.; Desiraju, G. R.; Dikundwar, A. G.; Dubey, R.; Duggirala, N.; et al. Polymorphs, Salts, and Cocrystals: What's in a Name? *Cryst. Growth Des.* **2012**, *12* (5), 2147–2152.

(77) Porter, W. W.; Elie, S. C.; Matzger, A. J. Polymorphism in Carbamazepine Cocrystals. *Cryst. Growth Des.* **2008**, *8* (1), 14–16.

(78) Limwikrant, W.; Nagai, A.; Hagiwara, Y.; Higashi, K.; Yamamoto, K.; Moribe, K. Formation Mechanism of a New Carbamazepine/Malonic Acid Cocrystal Polymorph. *Int. J. Pharm.* **2012**, *431* (1–2), 237–240.

(79) Ter Horst, J. H.; Cains, P. W. Co-Crystal Polymorphs from a Solvent-Mediated Transformation. *Cryst. Growth Des.* **2008**, *8* (7), 2537–2542.

(80) Nauha, E.; Nissinen, M. Co-Crystals of an Agrochemical Active - A Pyridine-Amine Synthon for a Thioamide Group. *J. Mol. Struct.* **2011**, *1006* (1–3), 566–569.

(81) Zhu, W.; Zheng, R.; Fu, X.; Fu, H.; Shi, Q.; Zhen, Y.; Dong, H.; Hu, W. Revealing the Charge-Transfer Interactions in Self-Assembled Organic Cocrystals: Two-Dimensional Photonic Applications. *Angew. Chem. Int. Ed* **2015**, *54* (23), 6785–6789.

(82) Zhang, J.; Xu, W.; Sheng, P.; Zhao, G.; Zhu, D. Organic Donor-Acceptor

Complexes as Novel Organic Semiconductors. *Acc. Chem. Res.* **2017**, *50* (7), 1654–1662.

(83) Bolton, O.; Simke, L. R.; Pagoria, P. F.; Matzger, A. J. High Power Explosive with Good Sensitivity: A 2:1 Cocrystal of CL-20:HMX. *Cryst. Growth Des.* **2012**, *12* (9), 4311–4314.

(84) Landenberger, K. B.; Bolton, O.; Matzger, A. J. Two Isostructural Explosive Cocrystals with Significantly Different Thermodynamic Stabilities. *Angew. Chem. Int. Ed* **2013**, *52* (25), 6468–6471.

(85) Trask, A. V. An Overview of Pharmaceutical Cocrystals as Intellectual Property. *Mol. Pharm.* **2007**, *4* (3), 301–309.

(86) Rodríguez-Hornedo, N. Cocrystals: Molecular Design of Pharmaceutical Materials. *Mol. Pharm.* **2007**, *4* (3), 299–300.

(87) Vishweshwar, P.; McMahon, J. A.; Peterson, M. L.; Hickey, M. B.; Shattock, T. R.; Zaworotko, M. J. Crystal Engineering of Pharmaceutical Co-Crystals from Polymorphic Active Pharmaceutical Ingredients. *Chem. Commun.* **2005**, *10* (36), 4601–4603.

(88) Karki, S.; Friščić, T.; Fabián, L.; Laity, P. R.; Day, G. M.; Jones, W. Improving Mechanical Properties of Crystalline Solids by Cocrystal Formation: New Compressible Forms of Paracetamol. *Adv. Mater.* **2009**, *21* (38–39), 3905–3909.

(89) Shevchenko, A.; Bimbo, L. M.; Miroshnyk, I.; Haarala, J.; Jelínková, K.; Syrjänen, K.; Van Veen, B.; Kiesvaara, J.; Santos, H. A.; Yliruusi, J. A New Cocrystal and Salts of Itraconazole: Comparison of Solid-State Properties, Stability and Dissolution Behavior. *Int. J. Pharm.* **2012**, *436* (1–2), 403–409.

(90) Stanton, M. K.; Bak, A. Physicochemical Properties of Pharmaceutical Co-Crystals: A Case Study of Ten AMG 517 Co-Crystals. *Cryst. Growth Des.* **2008**, *8* (10), 3856–3862.

(91) Yan, D.; Delori, A.; Lloyd, G. O.; Friščić, T.; Day, G. M.; Jones, W.; Lu, J.; Wei, M.; Evans, D. G.; Duan, X. A Cocrystal Strategy to Tune the Luminescent Properties of Stilbene-Type Organic Solid-State Materials. *Angew. Chem. Int. Ed* **2011**, *50* (52), 12483–12486.

(92) Desiraju, G. R. Hydration in Organic Crystals: Prediction from Molecular Structure. *J. Chem. Soc. Chem. Commun.* **1991**, No. 6, 426–428.

(93) Seyden-Penne, J. *Chiral Auxilaries and Ligands in Asymmetric Synthesis*; Wiley: New York, 1995.

(94) Kagan, H. B.; Fiaud, J. C. Kinetic Resolution. In *Topics in Stereochemistry*; Eliel, E. L., Wilen, S. H., Eds.; John Wiley & Sons, Inc., 1988.

(95) El Gihani, M. T.; Williams, J. M. J. Dynamic Kinetic Resolution. *Curr. Opin. Chem. Biol.* **1999**, *3* (1), 11–15. https://doi.org/10.1016/S1367-

5931(99)80003-9.

(96) Leusen, F. J. J.; Noordik, J. H.; Karfunkel, H. R. Racemate Resolution via Crystallization of Diastereomeric Salts: Thermodynamic Considerations and Molecular Mechanics Calculations. *Tetrahedron* **1993**, *49* (24), 5377–5396.

(97) Beesley, T. E.; Scott, R. P. W. *Chiral Chromatography*; John Wiley & Sons, 1998.

(98) Levilain, G.; Coquerel, G. Pitfalls and Rewards of Preferential Crystallization. *Cryst. Eng. Comm.* **2010**, *12* (7), 1983–1992.

(99) Ojima, I. *Catalytic Asymmetric Synthesis*, 2nd ed.; Ojima, I., Ed.; John Wiley & Sons: New York, 2004.

(100) Gotor, V.; Alfonso, I.; Garcia-Urdiales, E. *Aymmetric Organic Synthesis with Enzymes*; John Wiley & Sons, 2008.

(101) Vogl, E. M.; Groger, H.; Shibasaki, M. Towards Perfect Asymmetric Catalysis: Additives and Cocatalysts. *Angew. Chem. Int. Ed.* **1999**, *38* (11), 1570–1577.

(102) Rekoske, J. E. Chiral Separations. *AlChE Journal* **2001**, *47* (1), 2–5.

(103) Jozwiak, K.; Moaddel, R.; Ravichandran, S.; Plazinska, A.; Kozak, J.; Patel, S.; Yamaguchi, R.; Wainer, I. W. Exploring Enantiospecific Ligand-Protein Interactions Using Cellular Membrane Affinity Chromatography: Chiral Recognition as a Dynamic Process. *J. Chromatogr. B Anal. Technol. Biomed. Life Sci.* **2008**, *875* (1), 200–207.

(104) Däppen, R.; Arm, H.; Meyer, V. R. Applications and Limitations of Commercially Available Chiral Stationary Phases for High-Performance Liquid Chromatography. *J. Chromatogr. A* **1986**, *373*, 1–20.

(105) *Novel Optical Resolution Technologies*; Sakai, K., Hirayama, N., Tamura, R., Eds.; Springer, 2007; Vol. 269.

(106) Alvarez Rodrigo, A.; Lorenz, H.; Seidel-Morgenstern, A. Online Monitoring of Preferential Crystallization of Enantiomers. *Chirality* **2004**, *16* (8), 499–508.

(107) Myerson, A. *Handbook of Industrial Crystallization*; Butterworth-Heinemann: USA, 2002.

(108) Mersmann, A.; Bartosch, K. How to Predict the Metastable Zone Width. *J. Cryst. Growth* **1998**, *183* (1–2), 240–250.

(109) Kubota, N. A New Interpretation of Metastable Zone Widths Measured for Unseeded Solutions. *J. Cryst. Growth* **2008**, *310* (3), 629–634.

(110) O'Grady, D.; Barrett, M.; Casey, E.; Glennon, B. The Effect of Mixing on the Metastable Zone Width and Nucleation Kinetics in the Anti-Solvent Crystallization of Benzoic Acid. *Chem. Eng. Res. Des.* **2007**, *85* (7 A), 945–

952.

(111) Sayan, P.; Ulrich, J. Effect of Various Impurities on the Metastable Zone Width of Boric Acid. *Cryst. Res. Technol* **2001**, *36* (4–5), 411–417.

(112) Nagy, Z. K.; Fujiwara, M.; Woo, X. Y.; Braatz, R. D. Determination of the Kinetic Parameters for the Crystallization of Paracetamol from Water Using Metastable Zone Width Experiments. *Ind. Eng. Chem. Res.* **2008**, *47* (4), 1245–1252.

(113) Bensouissi, A.; Roge, B.; Mathlouthi, M. Effect of Conformation and Water Interactions of Sucrose, Maltitol, Mannitol and Xylitol on Their Metastable Zone Width and Ease of Nucleation. *Food Chem.* **2010**, *122* (2), 443–446.

(114) Nordström, F. L.; Svärd, M.; Rasmuson, Å. C. Primary Nucleation of Salicylamide: The Influence of Process Conditions and Solvent on the Metastable Zone Width. *CrystEngComm* **2013**, *15* (36), 7285–7297.

(115) Coquerel, G. Preferential Crystallization. In *Novel Optical Resolution Technologies*; Sakai, K., Hirayama, N., Tamura, R., Eds.; Topics in Current Chemistry-Springer: Berlin, Heidelberg, 2007; pp 1–51.

(116) Brandel, C.; ter Horst, J. H. Measuring Induction Times and Crystal Nucleation Rates. *Faraday Discuss.* **2015**, *179*, 199–214.

(117) *U.S. Department of Health & Human Services. National Center for Advancing Translational Sciences Inxight:Drugs.*

(118) Kuhnert-Brandstätter, M.; Kofler, A.; Kramer, G. Beitrag Zur Mikroskopischen Charakterisierung Und Identifizierung von Arzneimitteln Unter Einbeziehung Der UV-Spektrophotometrie. *Sci. Pharm.* **1974**, *42*, 234–248.

(119) Eckert, T.; Miiller, J. Über Polymorphe Modifikationen Des Nifedipine Aus Unterkühlten Schmelzen. *Arch. Pharm.* **1977**, *310*, 116–118.

(120) Griesser, U. J.; Auer, M. E.; Burger, A. Micro-Thermal Analysis, FTIR- and Raman-Microscopy of (R,S) -Proxyphylline Crystal Forms. *Microchem. J.* **2000**, *65*, 283–292.

(121) Borowiecki, P.; Paprocki, D.; Dudzik, A.; Plenkiewicz, J. Chemoenzymatic Synthesis of Proxyphylline Enantiomers. *J. Org. Chem.* **2016**, *81* (2), 380–395.

(122) Kadam, S. S.; Kramer, H. J. M.; Ter Horst, J. H. Combination of a Single Primary Nucleation Event and Secondary Nucleation in Crystallization Processes. *Cryst. Growth Des.* **2011**, *11* (4), 1271–1277.

(123) Gonella, S.; Mahieux, J.; Sanselme, M.; Coquerel, G. Spotting a Conglomerate Is Just Halfway to Achieving a Preparative Resolution by Preferential Crystallization. *Org. Process Res. Dev.* **2012**, *16* (2), 286–293.

(124) Renou, L.; Coste, S.; Cartigny, Y.; Petit, M. N.; Vincent, C.; Schneider, J. M.;

Coquerel, G. Mechanism of Hydration and Dehydration of Ciclopirox Ethanolamine (1:1). *Cryst. Growth Des.* **2009**, *9* (9), 3918–3927.

(125) Fours, B.; Cartigny, Y.; Petit, S.; Coquerel, G. Formation of New Polymorphs Without Any Nucleation Step Desolvation of the Rimonabant Monohydrate: Directional Crystallisation Concomitant to Smooth Dehydration. *Faraday Discuss.* **2015**, *179*, 475–488.

(126) Coquerel, G. Solubility of Chiral Species as Function of the Enantiomeric Excess. *J. Pharm. Pharmacol.* **2015**, *67* (6), 869–878.

(127) Lorenz, H.; Sapoundjiev, D.; Seidel-Morgenstern, A. Solubility Equilibria in Chiral Systems and Their Importance for Enantioseparation. *Eng. Life Sci.* **2003**, *3* (3), 132–136.

(128) Mahieux, J.; Gonella, S.; Sanselme, M.; Coquerel, G. Crystal Structure of a Hybrid Salt-Cocrystal and Its Resolution by Preferential Crystallization: ((±)Trans-N,N′- Dibenzyldiaminocyclohexane)(2,3-Dichlorophenylacetic Acid)4. *CrystEngComm* **2012**, *14* (1), 103–111.

(129) Ruud-Christensen, M.; Skjetne, T.; Krane, J.; Aasen, A. J. Synthesis of (R)- and (S)-Proxyphylline. *Acta Chem. Scand. B* **1984**, *38*, 331–333.

(130) Selvig, K.; Ruud-Christensen, M.; Aasen, A. J. Optical Resolution, Absolute Configuration, And Activity of the Enantiomers of Proxyphylline. *J. Med. Chem.* **1983**, *26* (10), 1514–1518.

(131) Egri, G.; Kolbert, A.; Balint, J.; Fogassy, E.; Novak, L.; Poppe, L. Baker's Yeast Mediated Stereoselective Biotransformation of 1-Acetoxy-3-Aryloxypropan-2-Ones. *Tetrahedron: Asymmetry* **1998**, *9* (2), 271–283.

(132) Bredikhin, A.; Bredikhin, Z.; Novikova, V.; Zakharychev, P.; Gubaidullin, A. Three Different Types of Chirality-Driven Crystallization within the Series of Uniformly Substitued Phenyl Glycerol Ethers. *Chirality* **2008**, *20*, 1092–1103.

(133) Bruker AXS Inc., Bruker SMART (5.059) and SAINT (6.01), 1997, Madison, Wisconin.

(134) Farrugia, L. J. WinGX: Version 1.70.01: An Integrated System of Windows Programs for the Solution, Refinement and Analysis of Single Crystal X-Ray Diffraction Data. *J. Appl. Cryst.* **1999**, *32*, 837–838.

(135) Simon, F.; Clevers, S.; Dupray, V.; Coquerel, G. Relevance of the Second Harmonic Generation to Characterize Crystalline Samples. *Chem. Eng. Technol.* **2015**, *38* (6), 971–983.

(136) Kurtz, S. K.; Perry, T. T. A Powder Technique for the Evaluation of Nonlinear Optical Materials. *J. Appl. Phys.* **1968**, *39* (8), 3798–3813.

(137) McNaught, A. D.; Wilkinson, A. *IUPAC Compendium of Chemical Terminology, 2nd Ed.*; Blackwell Science: Oxford, U.K., 1997.

(138) Polenske, D.; Lorenz, H.; Seidel-Morgenstern, A. Separation of Propranolol

Hydrochloride Enantiomers by Preferential Crystallization: Thermodynamic Basis and Experimental Verification. *Cryst. Growth Des.* **2007**, *7* (9), 1628–1634.

(139) Fateley, W. G.; McDevitt, N. T.; Bentley, F. F. Infrared and Raman Selection Rules for Lattice Vibrations: The Correlation Method. *Appl. Spectrosc.* **1971**, *25* (2), 155–173.

(140) Avalos, M.; Babiano, R.; Cintas, P.; Jimenez, J. L.; Palacios, J. C. Symmetry Breaking by Spontaneous Crystallization—Is It the Most Plausible Source of Terrestrial Handedness We Have Long Been Looking for?—A Reappraisal. *Orig. Life Evol. Biospheres* **2004**, *34*, 391–405.

(141) Gubaidullin, A. T.; Samigullina, A. I.; Bredikhina, Z. A.; Bredikhin, A. A. Crystal Structure of Chiral Ortho-Alkyl Phenyl Ethers of Glycerol: True Racemic Compound, Normal, False and Anomalous Conglomerates within the Single Five-Membered Family. *Cryst. Eng. Comm.* **2014**, *16* (29), 6716.

(142) Burger, A.; Ramberger, R. On the Polymorphism of Pharmaceuticals and Other Molecular Crystals. *Mikrochim. Acta.* **1979**, *72* (3–4), 259–271.

PRESENTATIONS LIST

- October 2019: Applying Cyclic Preferential Crystallization on Stable Racemic Systems. Oral presentation, **Friedrich–Alexander University Erlangen–Nürnberg**, Erlangen, **Germany.**

- August 2019: Non-Classical Studies for Cyclic Preferential Crystallization of a Stable Racemic Compound. Oral presentation, **BIWIC**, VISTEC, **Thailand.**

- May 2019: Resolution of the racemic compound via innovative ways. Oral presentation, **Cristal9**, Nancy, **France.**

- May 2019: Chiral resolution of proxyphylline via its metastable conglomerate and its conglomerate co-crystal. Oral presentation**, SYNCOM company**, Groningen, **The Netherlands.**

- September 2018: Polymorphism & Enantiomeric Resolution of Stable Racemic Systems. Oral presentation, **University of Rouen**, Rouen, **France.**

- September 2018: Implementation of preferential crystallization in unfavorable cases: Detection of the metastable conglomerate. Poster presentation, **BIWIC**, Rouen, **France.**

- April 2018: Resolving of stable racemic systems by means of preferential crystallization. Oral presentation, **University of Manchester**, Manchester, **UK.**

- November 2017: Concept of coupling kinetic data and thermodynamic aspects to resolve stable racemic systems by means of preferential crystallization. Oral presentation, **TeraCrystal company**, Cluj Napoca, **Romania.**

- July 2017: Chiral Resolution of Pharmaceutical Racemic Compounds: Implementation of Preferential Crystallization in Unfavorable Cases. Poster presentation, **Radboud University**, Nijmegen, **The Netherlands**

PUBLICATIONS LIST

- Harfouche L. C., Cartigny Y., Brandel C., ter Horst J., Petit S., Coquerel G. Enabling Direct Preferential Crystallization in a Stable Racemic Compound System, Molecular Pharmaceutics, 16 (11), **2019**, 4670-4676. https://doi.org/10.1021/acs.molpharmaceut.9b00805

- Harfouche L. C., Cartigny Y., Brandel C., Petit S., Coquerel G. (2020). Resolution by Preferential Crystallization of Proxyphylline by using its Salicylic Acid Monohydrate Co-crystal. Chemical Engineering & Technology, **2020**. https://doi.org/10.1002/ceat.202000040

- Harfouche L. C., Couvrat N., Sanselme M., Cartigny Y., Brandel C., Petit S., Coquerel G. Discovery of New Proxyphylline Based Chiral Cocrystals: Solid State Landscape and Dehydration Mechanism. Crystal Growth and Design, **2020**. https://doi.org/10.1021/acs.cgd.0c00149

Abstract: Many active pharmaceutical ingredients are chiral compounds. The two enantiomers of the corresponding molecules exhibit identical chemical and physical properties, but the desired biological activity is often provided by only one enantiomer. The strict regulations forced the pharmaceutical industry to develop new ways to produce pure enantiomers. Among separation methods, Preferential Crystallization (PC), is a technique with relatively high productivity and low cost. It consists of the out-of-equilibrium alternative crystallization of both enantiomers. It is thought that the application of PC is only possible when the enantiomers crystallize as a conglomerate, *i.e.* a physical mixture of homochiral particles. Yet, only ca 5-10% of the racemic species crystallize as a conglomerate, which strongly limits the applicability of PC. The work investigates how to perform PC in the remaining 90-95% of cases, for enantiomers crystallizing as racemic compounds, *i.e.* a 1:1 stoichiometric compound made with both enantiomers. Following an adequate screening procedure based on physico chemical and molecular considerations, one racemic chiral molecule was selected as model compound, namely “proxyphylline” (PXL). After the construction of the binary phase diagram between the enantiomer of PXL reveals a rich polymorphism (double polymorphism for enantiomer and racemic), PXL has been resolved by two approaches:

(a) *via* an unforeseen metastable conglomerate, by inhibiting the spontaneous crystallization and growth of the undesired forms and by achieving a wide metastable zone width due to the selection of a suitable solvent. The obtained results extend the applicability of PC to the racemic forming system with specific thermodynamic (melting temperature) and kinetic (wide metastability) characteristics.

(b) *via* a stable monohydrated conglomerate prepared by cocrystallization with salicylic acid. It was resolved by PC from a water/ethanol mixture with high productivity. This may be the first report of PC applied to such a cocrystal system.

Keywords: chirality, preferential crystallization, nucleation inhibition, enantiomeric resolution, racemic compounds, chiral cocrystal, phase diagram.

Resumé: De nombreux principes actifs pharmaceutiques sont des composés chiraux. Les deux énantiomères des molécules correspondantes présentent des propriétés chimiques et physiques identiques mais l’activité biologique est souvent associée à un seul des deux. Les réglementations strictes ont obligé l'industrie pharmaceutique à développer de nouvelles méthodes pour produire des énantiomères purs. Parmi les méthodes de séparation, la cristallisation préférentielle (CP) est une technique ayant une productivité relativement élevée et un faible coût. Elle consiste en une cristallisation alternative hors équilibre des deux énantiomères. Il est communément admis que la CP peut uniquement être appliquée lorsque les deux énantiomères cristallisent sous forme d’'un conglomérat, *i.e.* un mélange physique de particules homochirales. Pourtant, seulement 5-10% des espèces racémiques cristallisent sous forme de conglomérat ce qui limite fortement l'applicabilité de la CP. Le travail de cette thèse vise à étudier comment réaliser la CP dans les 90-95% restants, pour les énantiomères cristallisants sous forme de composés racémiques, i.e. un composé défini stœchiométrique (1 :1). À la suite de l’identification de critères spécifiques (physico-chimique et moléculaires) la « Proxyphylline » (PXL) a été sélectionnée comme molécule chirale modèle pour cette étude. Après une construction du diagramme de phase entre énantiomères de la PXL, laissant apparaître un riche paysage polymorphique, la PXL a été résolue par selon approches :

(a) *via* la présence d’un conglomérat métastable et en inhibant la nucléation et la croissance du composé racémique (qui présente une large zone de métastabilité dans un solvant donné). Les résultats obtenus étendent l’efficacité de la CP aux systèmes présentant des composés racémiques et qui ont des caractéristiques thermodynamiques (température de fusion) et cinétiques (large zone de métastabilité) particulières.

(b) *via* un conglomérat monohydraté préparé par cocristallisation avec l’acide salicylique. La résolution par CP a été effectuée dans un mélange eau/éthanol avec une certaine efficacité. Cette étude est une des premières à rapporter la mise en place de la CP appliqué à des cocristaux chiraux.

Mots-clés : chiralité, cristallisation préférentielle, inhibition de la nucléation, résolution énantiomérique, composés racémiques, cocristal chiral, diagramme de phases.